In Situ Laser Raman Studies of the Mechanism of Ethanol Oxidation over Supported Molybdenum Oxide

by

Weimin Zhang

Dissertation submitted to the Faculty of the Virginia Polytechnic Institute and State University in partial fulfillment of the requirements for the degree of

DOCTOR OF PHILOSOPHY

IN

MATERIALS ENGINEERING AND SCIENCE

APPROVED:

S. Ted Oyama, Chair

Robert J. Bodnar

David F. Cox

Seshu B. Desu

Joseph S. Merola

September 1995

Blacksburg, Virginia

Key words: Ethanol oxidation, Molybdenum oxide, Mechanism, Laser Raman

ABSTRACT

Ethanol oxidation over supported molybdenum oxide was studied by *in situ* laser Raman spectroscopy, deuterium isotopic substitution, together with steady-state and transient reactivity and kinetic measurements. The combination of techniques allows a complete description of the mechanism of ethanol oxidation on MoO_3 supported on SiO_2, Al_2O_3, and TiO_2, including the quantification of adsorbed ethoxide species. Very interestingly, on the SiO_2-supported catalysts two types of adsorbed ethoxide species were observed. One, associated with Mo=O bonds, was a true reactive intermediate, while the other, associated with Mo-O-Mo bonds, was an unreactive spectator on the surface.

Isotopic substitution experiments established that the same mechanism with two stages occurred over MoO_3 on SiO_2, Al_2O_3 and TiO_2: an equilibrated adsorption step to form adsorbed ethoxide intermediates, followed by either of two rate-determining steps, α-hydrogen abstraction from the ethoxide intermediates to form acetaldehyde or β-hydrogen abstraction to form ethylene.

The activation energy was found to be the same for the different supports at the similar loading levels. The link to reducibility and the existence of a common ethoxide intermediate indicated that the rate was controlled by a term in the preexponential factor. From the similarity in the isotope effect the controlling factor was deduced to be the electronic partition function associated with the density of electron-accepting levels in the molybdate-support complex.

Analysis of the reaction isotherms showed that activation energy decreased with increasing coverage, suggesting a non-uniform surface. Consistent with this, the kinetics could be described by an extended treatment of Temkin's theory of rates. A full derivation of the theory, which was expanded to accommodate two types of sites, is presented.

Propylene oxidation was studied on MoO_3 on SiO_2, Al_2O_3 and TiO_2. Oxygen chemisorption and temperature programmed reduction (TPR) results indicated that the molybdenum oxide - support interaction decreased in the order: $TiO_2 > Al_2O_3 > SiO_2$. Temperature programmed surface reaction (TPSR) of adsorbed ethanol was used to characterize the acid-base properties of the catalysts, which played an important role in the formation of oxidation products.

A comparative study of ethanol oxidation over MoO_3 on SiO_2, Al_2O_3, and TiO_2 by O_3/O_2 and O_2 was carried out in a flow reactor. The effect of ozone appeared below a transition temperature which differed according to the support (523 K on SiO_2, 448 K on Al_2O_3 and 443 K on TiO_2). The reactivity below the transition temperature followed the order $SiO_2 > TiO_2 > Al_2O_3$, while above it the reactivity followed the order $TiO_2 > Al_2O_3 > SiO_2$. It appeared that the ozone decomposition activity of the catalysts played an important role in ethanol oxidation by O_3/O_2.

Acknowledgments

I would like to thank my colleagues: Anantha Desikan, Bala Dhandapani, Sasangan Ramanathan, Victor L. S. da Silva, Rajat Kapoor, Charles C. Yu, Todd St. Clair, Wei Li, Anil Prahu and Toby E. Lucy for their support and encouragement through these years.

I would like to extend my gratitude to my Ph. D. committee members, professors Robert J. Bodnar, David F. Cox, Seshu B. Desu, and Joseph S. Merola, for their suggestions and guidance.

I wish to express my sincere gratitude to Prof. S. Ted Oyama for his perceptive guidance and remarkable patience during my Ph. D. study.

I would like to thank my family and my parents for their support and encouragement. This dissertation is dedicated to my wife, Jia, for her constant support and sacrifice through these years.

Table of Contents

List of Figures

List of Tables

Chapter 1

Introduction

Selective oxidation by heterogeneous catalysis refers to the conversion of organic compounds on solid phase catalysts to oxygen-containing products. Catalytic oxidation is a complex phenomenon with several steps occurring consecutively on the surface of catalysts. The combination of reactants with a catalyst produces intermediates that are critical in promoting the formation of desired products.[1]

Selective oxidative transformations of organic compounds on complex oxide catalysts are currently the main method of synthesis of a series of important chemical products such as aldehydes, acids, nitriles, etc. Selective oxidations account for 86% of the oxidation processes used in the production of the top 25 organic chemicals (Table 1).[2]

Numerous techniques such as Auger electron spectroscopy (AES), electron spin resonance (ESR), X-ray photoelectron spectroscopy (XPS), laser Raman spectroscopy (LRS), infrared spectroscopy (IR), nuclear magnetic resonance (NMR) have been used to study the physical properties of catalysts. They provide information on the surface structure of catalysts and the nature of chemical species present on the surfaces. However, detailed spectroscopic studies under *in situ* conditions are lacking.

Among these spectroscopies, LRS and IR are suitable techniques for studying adsorbed intermediates at *in situ* reaction conditions because they can be used at high

Table 1.1. Major Chemicals produced by catalytic oxidation in the United States in 1991.[2]

Chemical	Production[a]	Process	Catalyst
Sulfuric Acid	88.56	Heterogeneous Oxidation	V_2O_5
Nitric Acid	15.50	Heterogeneous Oxidation	Pt/Rh
Terepthalic Acid	13.30	Homogeneous Oxidation	Bromides of Heavy Metals and Salt of Co & Mn
Formaldehyde	6.41	Heterogeneous Oxidation	Mo, Fe and V Oxides
Ethylene Oxide	5.58	Heterogeneous Epoxidation	Ag
Acylonitrile	3.20	Heterogeneous Ammoxidation	Bi-P-Mo
Propylene Oxide	3.20	Homogeneous Oxidation	Mo-Napthenate
Vinyl Acetate	2.55	Heterogeneous Oxidation	Pt Salts
Adipic Acid	1.64	Homogeneous Oxidation	Co-Napthenate and NH_4VO_3 - Cu

[a] Billions of lbs.

temperature and pressure. IR is valuable for studying vibrations associated with adsorbed species but cannot be used for vibrational frequencies below 1300 cm^{-1} because most catalytic supports absorb strongly in the infrared spectrum in that region. Thus, some important chemical bonds such as metal-oxygen and metal-carbon bonds cannot be examined. LRS, on the other hand, does not suffer from this disadvantage and works very well below 1300 cm^{-1}.[3]

LRS is a powerful tool in the characterization of oxide catalysts, and has been used to establish the structure of a series of oxide catalyst systems.[4-7] In contrast, due to the low throughput with conventional dispersive laser Raman spectroscopy, few LRS studies of adsorbed organic species have been reported in the past twenty years.[3] It will shown in this dissertation that this problem can be solved by combining a short monochromator equipped with a charge-coupled-device (CCD) multichannel detector and a holographic super notch-plus filter.

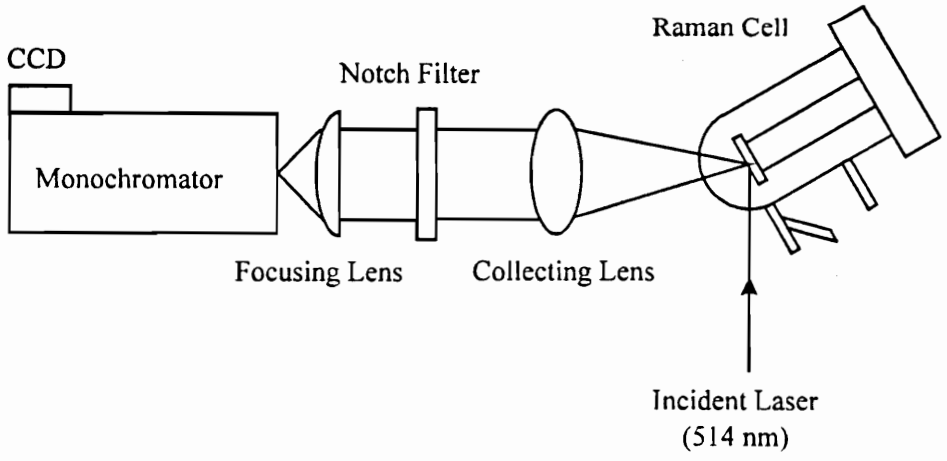

Schematic of Laser Raman Spectroscopy

Various researchers have made great efforts to elucidate the nature of solid surfaces in a static manner in different experimental atmospheres such as air for microscopy and ultra-high vacuum for surface measurements. However, in heterogeneous catalysis the reaction takes place predominantly on catalyst surfaces with adsorbed species present to various extents, which influence the properties of the surfaces. Moreover, the surface may be reconstructed to a state very much different from the clean well-defined surfaces present in the absence of reactants or preceding the reaction. The observed adsorbed species under adsorption conditions far from the reaction conditions may not be the true reaction intermediates. Therefore, it is very important to study the catalyst surfaces while the reaction is occurring.

Although alcohol oxidations over MoO_3 based catalysts have been extensively studied,[8-35] the reactions are still not completely understood. Controversy about the effect of structure and the nature of the active sites still remain, and the cause of the reactivity dependence on support has not yet been clarified. Ethanol oxidation has been less studied than methanol oxidation. The roles of Mo-O-Mo and Mo-O-M (M = support) structures and details of the reaction steps of ethanol oxidation over supported MoO_3 catalysts have not been investigated. Importantly, the reaction intermediates for this reaction have not been identified. The work in this dissertation seeks to shed light on these important topics.

Molybdenum oxide is a major component in catalysts for allylic[36,37] and alcohol oxidation,[8-35] and a minor component in many other oxidation catalysts such as those used for

olefin dehydrogenation[38] and for aromatic[39] and paraffin[40] oxidation. The different supports to be used interact with molybdenum oxide to different degrees ($SiO_2 << Al_2O_3 < TiO_2$),[7] allowing systematic studies of reducibility, dispersion, and acidity/basicity to be carried out.

In this dissertation, we will study the reactive intermediates in the selective oxidation of ethanol on molybdenum oxide by laser Raman spectroscopy (LRS) under *in situ* reaction conditions. Combination of this information with data from reactivity, isotopic substitution kinetics and acidity-basicity measurements, thermodynamics calculations will give a complete description of the mechanism of this selective oxidation reaction.

Chapter 2 deals with the effects of support, structure and active sites on ethanol oxidation over supported molybdenum catalysts, the measurements of adsorbed species under *in situ* reaction conditions by laser Raman spectroscopy, and the origin of the support effects.

Chapter 3 deals with the identification of the true reactive intermediates by laser Raman spectroscopy under actual reaction conditions, and the kinetics and mechanism of ethanol oxidation on supported molybdenum oxide.

Chapter 4 shows a non-uniform surface analysis of the kinetics of ethanol oxidation over SiO_2-supported molybdenum oxide based on Temkin's theory of rates on non-uniform surfaces.

Chapter 5 presents a study of acid-base properties of supported molybdenum oxide by temperature-programmed surface reaction (TPSR) of adsorbed ethanol, and their effects on propylene oxidation.

Chapter 6 summarizes the effects of ozone, as an alternative oxidant, on reactivity and selectivity in ethanol oxidation over supported molybdenum oxide.

References:

(1). Oyama, S. T.; Desikan, A. N.; and Zhang, W. in "*Catalytic Selective Oxidation*" (Oyama, S. T.; and Hightower, J. W. eds.), ACS Series 523, pp. 16, 1992.

(2). *Current Industrial Reports*, U. S. Dept. of Commerce, Bureau of Census, Washington D. C., 1991.

(3). Cooney, R. P.; Gurthoys, G.; and Tam, N. T. *Adv. Catal.* 1975, 24, 293.

(4). Delgass, W. H.; Haller, G. L.; Kellerman. R.; and Lunsford, J. H. "*Spectroscopy in Heterogeneous Catalysis*", Academic Press, New York, 1979.

(5). Chan, S. S.; Wachs, I. E.; Murrell, L. L.; and Hall, W. K. *J. Phys. Chem.* 1984, 88, 5831.

(6). Vuurman, M. A., and Wachs, I. E. *J. Phys. Chem.* 1992, 96, 5008.

(7). Desikan, A. N.; Huang, L.; and Oyama, S. T. *J. Phys. Chem.* 1991, 95, 10050. Desikan, A. N.; Huang, L.; and Oyama, S. T. *J. Chem. Soc. Faraday Trans. I*, 1992, 88, 3357.

(8). Pernicone, N.; Altering, F.; Liberti, G.; and Lanzavecchia, G. *J. Catal.* 1969, 14, 293.

(9). Edwards, J.; Nicollaidis, J.; Cutlip, M. B.; and Bennett, C. O. *J. Catal.* 1977, 50, 24.

(10). Chung, J. S.; and Bennett, C. O. *J. Catal.* 1985, 92, 173.

(11). Chung, J. S.; Miranda, R.; and Bennett, C. O. *J. Chem. Soc. Faraday Trans. I*, 1985, 81, 19.

(12). Chung, J. S.; and Bennett, C. O. *J. Chem. Soc. Trans. Faraday Trans. I*, 1986, 82, 2155.

(13). Chung, J. S.; Miranda, R.; and Bennett, C. O. *J. Catal.* 1988, 114, 398.

(14). Farneth, W. E.; Ohuchi, F.; Staley, R. H.; Chowdhry, U.; and Sleight, A. W. *J. Phys. Chem.* 1985, 89, 2493.

(15). Tatibouët, J. M.; and Germain, J. E. *J. Catal.* 1981, 72, 375.

(16). Tatibouët, J. M.; Germain, J. E.; and Volta, J. C. *J. Catal.* 1983, 82, 240.

(17). Ohuchi, F.; Firment, L. E.; Chowdhry, U.; and Ferretti, A. *J. Vac. Sci. Technol.* 1984, A2, 1022.

(18). Chowdhry, U.; Ferretti, A.; Firment, L. E.; Machiels, C. J.; Ohuchi, F.; Sleight, A. W.; and Stakey, R. H. *Appl. Surf. Sci.* 1984, 25, 249.

(19). Machiels, C. J.; Cheng, W. H.; Chowdhry, U.; Farneth, W. E.; Hong, F.; McCarron, E. M.; and Sleight, A. W. *Appl. Catal.* 1986, 25, 249.

(20). Machiels, C. J.; and Sleight, A. W. *J. Catal.* 1982, 76, 238.

(21). Yang, T. J.; and Lunsford, J. H. *J. Catal.* 1987, 103, 55.

(22). Nováková, J.; Jíru, P.; and Zavadil, V. *J. Catal.* 1970, 17, 93.

(23). Cheng, W. H.; Chowdhry, U.; Ferretti, A.; Firment, L.; Groff, R. P.; Machiels, C. J.; McCarron, E. M.; Staley, R. H.; and Sleight, A. W. in"*Heterogeneous Catalysis*" (Shapiro, B. L. eds.), pp. 165, Texas A&M Univ. Press, College Station, Texas, 1984.

(24). Allison, J. N.; and Goddard III, W. A. *J. Catal.* 1985, 92, 127.

(25). Niwa, M.; Mizutani, M.; Takahashi, M.; and Murakami, Y. *J. Catal.* 1981, 70, 14.

(26). Niwa, M.; Yamada, H.; and Murakami, Y. *J. Catal.* 1992, 134, 331.

(27). Matsuoka, Y; Niwa, M.; and Murakami, Y. *J. Chem. Phys.* 1990, 94, 1477.

(28). Tatibouët, J. M.; and Germain, J. E. *J. Chem. Res.* 1981, (S) 268; 1981, (M) 3070.

(29). Iwasawa, Y.; Nakano, Y.; and Ogasawara, S. *J. Chem. Soc. Faraday Trans. I*, 1978, 74, 2986.

(30). Ono, T.; Kamisuki, H.; Hisashi, H.; and Miyata, H. *J. Catal.* 1989, 116, 303.

(31). Ono, T.; Nakagawa, Y.; Miyata, H.; and Kubokawa, Y. *Bull. Chem. Soc. Jpn.* 1984, 57, 1205.

(32). Iwasawa, Y.; and Tanaka, H. *Proc. Int. Congr. Catal.*, 8th Berlin, IV-381, 1984.

(33). Iwasawa, Y.; Asakura, K.; Ishii, H.; and Kuroda, H. *Z. Phys. Chem.* 1985, 144, 105.

(34). Alyea, E. C.; Brown, K. F.; Durham, L.; and Svazic, T. in "*Progress in Catalysis*" (Smith, K. J.; and Sanford, E. C. eds.), Elsevier Sci. Pub. B. V., pp. 309, 1992.

(35). Farneth, W. E.; Staley, R. H.; and Sleight, A. W. *J. Am. Chem. Soc.* 1986, 108, 2327.

(36). Adams, C. R.; and Jennings, T. S. *J. Catal.* 1963, 2, 63.

(37). Krenze, J. D.; and Keulks, J. *J. Catal.* 1980, 61, 316.

(38). Doroshenko, V. A.; Shapovalova, L. P.; Zrelenina, A.; Tmennov, D. N.; Taranukha, O. M.; and Lushnik, I. S. *Kinet. Katal.* 1983, 24, 749.

(39). Ai, M. in"*New Development in Selective Oxidation*" (Centi, G.; and Trifiro, F. eds.), pp. 257, Eleseiver, Amsterdam, 1990.

(40). Ai, M.; and Ikawa, T. *J. Catal.* 1975, 40, 20.

Chapter 2

Effect of Support in Ethanol Oxidation on Molybdenum Oxide

2.1. Introduction

In this chapter, recently developed titration techniques for counting surface metal centers on oxide catalysts[1,2] are used to determine accurate turnover rates of ethanol oxidation. This is coupled with *in situ* laser Raman spectroscopy (LRS) measurements at reaction conditions to identify reactive intermediates. The combination allows investigation of the nature of support effects and the overall mechanism of the ethanol oxidation reaction on MoO_3 supported on SiO_2, Al_2O_3, and TiO_2, and the roles of Mo-O-Mo and Mo=O bonds. It will be shown that electronic effects associated with the availability of empty states above the Fermi energy strongly influence the reactivity of the surface molybdenum species.

The main body of literature on alcohol oxidation over MoO_3-containing catalysts is of studies of methanol oxidation to formaldehyde.[3-22] These studies have covered the nature of adsorbed intermediates,[3-9] the effect of structure,[10-14] the measurement of kinetic isotope effects,[15,16] the identity of active sites (e.g. Mo=O, or Mo-O-Mo),[3-14,16,19] the nuclearity of active centers (e.g. Mo monomer, or Mo dimer),[17-21] and the effect of supports.[14,22] Among the various authors, there is general agreement that, a methoxide

type intermediate is responsible for the formation of formaldehyde,[3-9] and that the rate-determining step involves abstraction of a hydrogen atom from the adsorbed methoxy group.[16,17] However, controversy about the effect of structure and support and the nature of the active sites still remains.

In the literature, fewer papers have dealt with ethanol oxidation than methanol oxidation over MoO_3-containing catalysts[11,23-30] In analogy to methanol oxidation, Tatibouët, *et al.*,[11,23] carried out ethanol oxidation over oriented MoO_3 crystallites prepared by sublimation. They showed the formation of acetaldehyde on basal planes (010) containing Mo=O bonds and apical planes (001)+(101) containing both Mo=O and Mo-O-Mo bonds in the presence and absence of oxygen, and suggested that Mo=O sites were responsible for acetaldehyde formation. A similar conclusion was reached by Iwasawa, *et al.*,[24] and Ono, *et al.*[25,26] Iwasawa, *et al.*,[24] used infrared (IR) spectroscopy to show that the Mo=O bond in MoO_3/SiO_2 reacted easily with adsorbed ethanol at 423 K and returned back to its original form after reoxidation at the same temperature. Ono, *et al.*,[25] suggested that the reactivity of MoO_3 highly dispersed on group IV oxide supports for ethanol oxidation was related to its surface structure. Crystalline MoO_3 gave a low reactivity, whereas surface polymolybdates gave a high reactivity. In the case of the polymolybdates, the Mo=O bond strength obtained using LRS and IR data depended on the support, and followed the order of $SiO_2 > TiO_2 > ZrO_2$. The reactivity expressed as turnover rates for ethanol oxidation followed the reverse order $ZrO_2 > TiO_2 > SiO_2$. The turnover rates were calculated based on surface concentration of non-crystalline molybdenum oxide. In another study of ethanol oxidation on different MoO_3 loadings on TiO_2, Ono, *et al.*,[26] further related the reactivity in ethanol

oxidation to the Mo=O bond strength measured by IR spectroscopy. A maximum rate of oxidation of ethanol obtained over a 10 wt% MoO_3/TiO_2 sample was attributed to a weakening of the Mo=O bond strength.

In addition to the role of the Mo=O bond, Iwasawa, *et al.*,[27,28] proposed that Mo dimers were the active centers for ethanol oxidation to acetaldehyde over MoO_3/SiO_2 by demonstrating the high reactivity of SiO_2-attached dioxo Mo dimer species prepared from organometallic precursors. This was supported by a reactivity study of ethanol oxidation over MoO_3/Al_2O_3 and MoO_3/TiO_2 prepared by the metal oxide vapor synthesis (MOVS) method.[29] In this study, Alyea, *et al.*, showed that these catalysts with the Mo dimer structure on the surfaces reached a conversion of 100% at 523 K and a selectivity of 100% to acetaldehyde. Although an ethoxide type intermediate for ethanol oxidation to acetaldehyde over supported MoO_3 catalysts was suggested by Iwasawa, *et al.*,[24] and Farneth, *et al.*,[30] the studies provided little kinetic data, and only limited evidence from IR and temperature-programmed desorption (TPD) measurements. The roles of Mo-O-Mo and Mo-O-M (M = support) structures and details of the reaction steps of ethanol oxidation over supported MoO_3 catalysts have not been touched upon.

In this chapter, the effect of structure is examined by varying the loading of molybdenum on the supports. It will be shown that catalyst structure does not have a strong influence on the rate, but this is due to a compensation between an adsorption equilibrium step and a subsequent rate-determining step. The overall rate is strongly affected by electronic factors associated with the metal oxide-support interaction.

2.2. Experimental

2.2.1. Catalyst preparation and characterization

Samples were prepared by impregnating silica (Cabosil L90, $S_g = 89\ m^2\ g^{-1}$), alumina (Degussa Aluminumoxid C, $S_g = 93\ m^2\ g^{-1}$) and titania (Degussa P25, $S_g = 46\ m^2\ g^{-1}$) with solutions of ammonium molybdate (Aldrich 98%) in distilled water to incipient wetness. These materials and the pure supports were then dried at 393 K for 6 h and calcined at 773 K for 6 h. Sample preparation and characterization using oxygen chemisorption, BET, XRD, and LRS methods have been described in detail elsewhere.[1,2] Surface area and oxygen uptake data for the samples used in the present study are summarized in Table 2.1. Two sets of sample were used: low loading (1% MoO_3/SiO_2, 5% MoO_3/Al_2O_3, and 1% MoO_3/TiO_2) and high loading (9% MoO_3/SiO_2, 15% MoO_3/Al_2O_3, and 9% MoO_3/TiO_2).

2.2.2. Steady-State reactivity studies

The reactor system used for the steady-state reaction study was a conventional flow reactor. Mass flow controllers (Brooks, model 5850E) calibrated for each specific gas employed were used to obtain the desired composition and flow rate of the feed

Table 2.1. O_2 chemisorption data

Samples	O_2 uptake / μmol g^{-1}	SA / m^2 g^{-1}
SiO_2	8±1	89
1% MoO_3/SiO_2	29	61
9% MoO_3/SiO_2	59	73
Al_2O_3	-	93
5% MoO_3/Al_2O_3	120	82
15% MoO_3/Al_2O_3	450	-
TiO_2	-	46
1% MoO_3/TiO_2	34	35
9% MoO_3/TiO_2	250	33
MoO_3	46	5.5

stream. A liquid mixture of ethanol and water was injected through an injection port with a syringe pump (Sage Model 341B). The feed stream was passed through a U-shaped quartz reactor (13 mm ID), and product analysis was performed by an on-line gas chromatograph (SRI Model 8610) equipped with a flame ionization detector (FID) and a thermal conductivity detector (TCD). A Carbosphere column (Alltech, 80/100 mesh) was used with the TCD to separate O_2, CO, CO_2, and H_2O, and a Porapak QS column (Alltech, 80/100 mesh) was used with the FID to separate C_2H_4, CH_3CHO, $(C_2H_5)_2O$, CH_3COOH, and $CH_3COOC_2H_5$. Data processing was carried out by using Peaksimple II software. A six-way valve allowed switching between a calibration gas stream and the reaction feed without disconnecting the sample cell.

Gases used in this study were helium (Linde Ultra High Purity Grade, 99.999%) and oxygen (Linde Ultra High Purity Extra Dry Grade, 99.6%). They were passed through purifiers (Zeolite R3-11 for O_2, and Molsieve SA for He) during use. Ethyl alcohol (Pharmco, 99%) was used without further purification. The standard partial pressures of reactants in the reactivity study were P_{C2H5OH} = 8 kPa, P_{O2} = 8 kPa, P_{H2O} = 4 kPa, and P_{He} = 81 kPa. Typically, sample sizes loaded in the quartz reactor were 1g, and the total flow rate for all experiments was 110 μmol s^{-1} (160 cm^3 min^{-1}). Rates were expressed as turnover rates based on surface sites titrated by high temperature oxygen chemisorption. Briefly, oxygen uptakes were measured by a pulse method on samples prereduced in hydrogen at moderate temperatures (600 - 640 K). The reduction was carried out at a temperature just below that at which bulk reduction occurred, and the

method was independently calibrated by laser Raman spectroscopy at low loadings and by x-ray diffraction at high loadings.[1,2]

Attention was paid to establish steady-states and to ensure that the catalysts were stable during each experiment. Each sample was pretreated for 1h with the O_2, He, and H_2O mixture (without C_2H_5OH) at the highest temperature to be reached in the experiment. Steady-state reactivity data were taken at each desired temperature after maintaining conditions for at least two hours. After each set of measurements, one initial point was repeated to verify catalyst stability. Carbon and oxygen balances closed to 100±5% for most experiments, with just a few points, yielding 100±8%. Nevertheless, catalyst deactivation was observed due to molybdenum oxide sublimation, particularly in the low loading samples. Measurements were carried out for time periods for which catalysts were stable (10 - 30 h).

2.2.3. Raman spectroscopy

Raman spectra were obtained using the 514 nm line of an Ar ion laser (Lexel, Model 95) with a power of 100 mW at the sample. The scattered light was filtered with a holographic super notch-plus filter (Kaser Optical) and directed into a single monochromator (Spex, model 500M) equipped with a liquid nitrogen cooled CCD detector. A slit width of 50 μm was used to achieve a resolution better than 5 cm^{-1}.

The spectra of supported molybdenum oxide catalysts and the adsorbed species were obtained in a cell that allowed *in situ* measurements. The samples (~ 0.3 g of powder) were pressed into thin wafers of 1mm thickness and were spun at 600 - 1000 rpm to avoid local sample heating. The spectroscopic measurements were carried out while simultaneously running the catalytic reaction with 1.6 kPa ethanol and 99.4 kPa oxygen at a total flow rate of 110 μmol s^{-1}. High oxygen partial pressure was chosen so as to keep a bright sample color. Acquisition time for each spectrum was typically 2 hours in order to obtain a desired signal-to-noise ratio.

The 1% MoO_3/SiO_2 sample was chosen for study because with the 9% MoO_3/SiO_2 sample the features from adsorbed ethanol species were covered by the intense Raman bands of crystalline molybdenum oxide. Another reason for the use of the well dispersed sample was that it could be used to study the role of the different surface groups (Mo=O, Mo-O-Mo) in activating ethanol.

2.2.4. Partial pressure effects

The partial pressure effect studies were performed under conditions away from the flammability limit (2-5% ethanol in oxygen).[31] These studies were carried out by varying the concentration of one of the reactants while maintaining the total space velocity constant by adjusting the flow rate of He.

2.3. Results

2.3.1. Steady-state reactivity studies

Figure 2.1 shows the plots of conversion and selectivity versus temperature for low MoO_3 loading samples (1% MoO_3/SiO_2, 5% MoO_3/Al_2O_3, and 1% MoO_3/TiO_2). Figure 2.2 shows the same plot for high MoO_3 loading samples (9% MoO_3/SiO_2, 15% MoO_3/Al_2O_3, and 9% MoO_3/TiO_2) and pure MoO_3. During the reactions, the main products were acetaldehyde, ethylene, diethyl ether, and CO_x at both loading levels. Blank experiments on the pure supports (dashed lines in Fig. 2.1) showed that their activity was considerably lower than the supported samples with SiO_2 being the most inert. SiO_2 produced only a small amount of acetaldehyde at very high temperature (> 570 K), whereas Al_2O_3 produced mainly diethyl ether in the whole temperature range (400 - 525K) and CO_x at very high temperature, while TiO_2 produced mainly acetaldehyde in the whole range and CO_x at high temperature. Unsupported MoO_3 produced mainly acetaldehyde and diethyl ether. Considerable amounts of acetic acid were formed by all samples at high Mo loading. Conversions and selectivities for all samples are summarized in Table 2.2, 2.3, and 2.4. Figures 2.3 and 2.4 present Arrhenius plots of total rates for the low loading and the high loading samples, respectively. Rates are reported as turnover rates based on surface Mo atoms titrated by oxygen chemisorption.[1,2]

The reactivity of both sets (low and high loadings) of samples follows the same

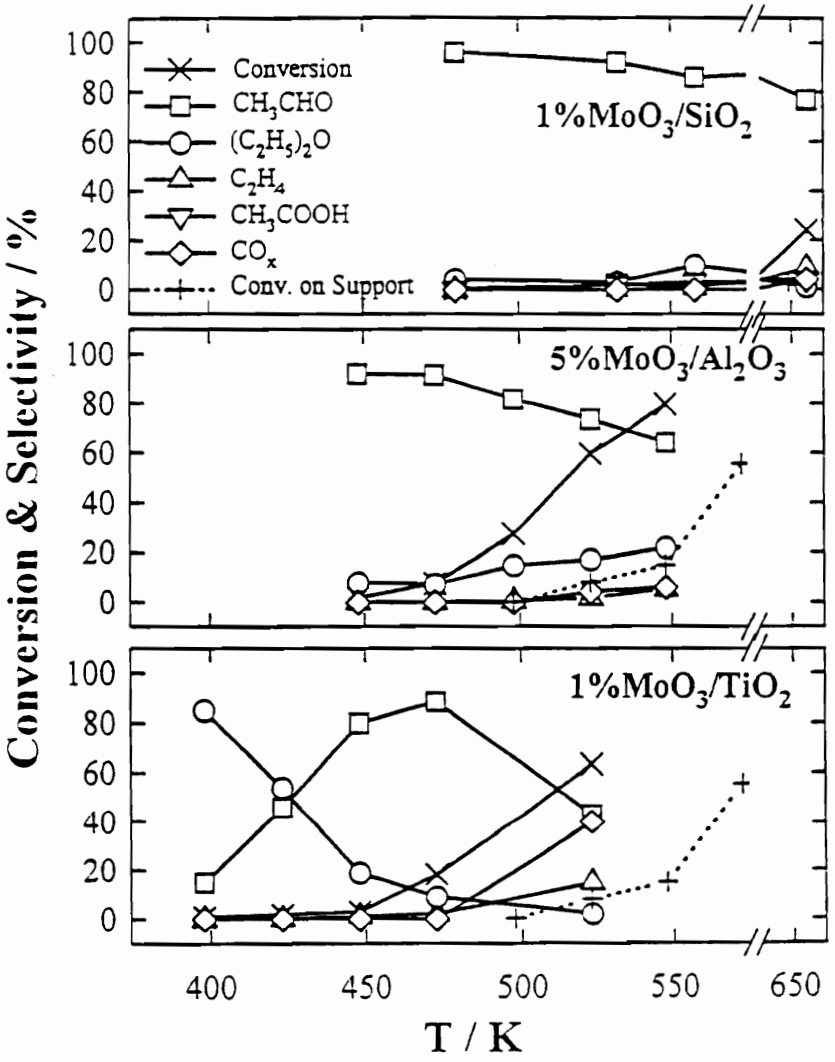

Figure 2.1. Conversion and selctivity for ethanol oxidation at different temperatures over the low loading sample.

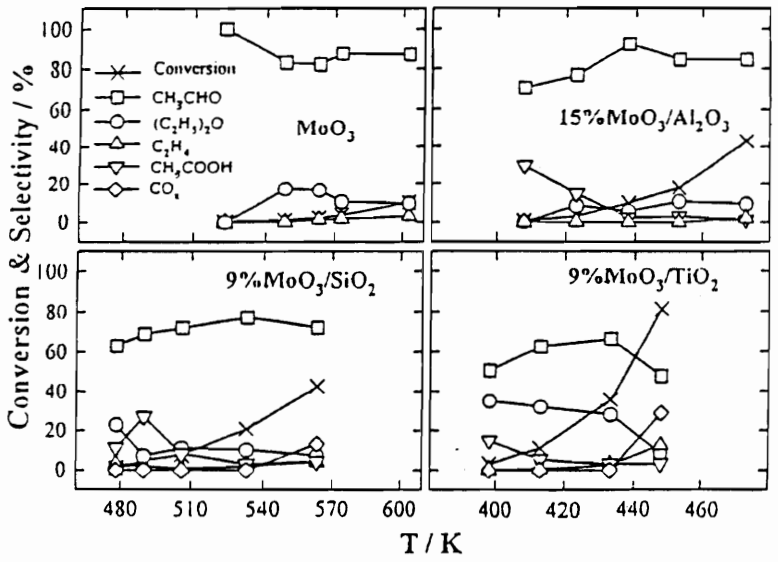

Figure 2.2. Conversion and selectivity for ethanol oxidation at different temperatures over the high loading samples.

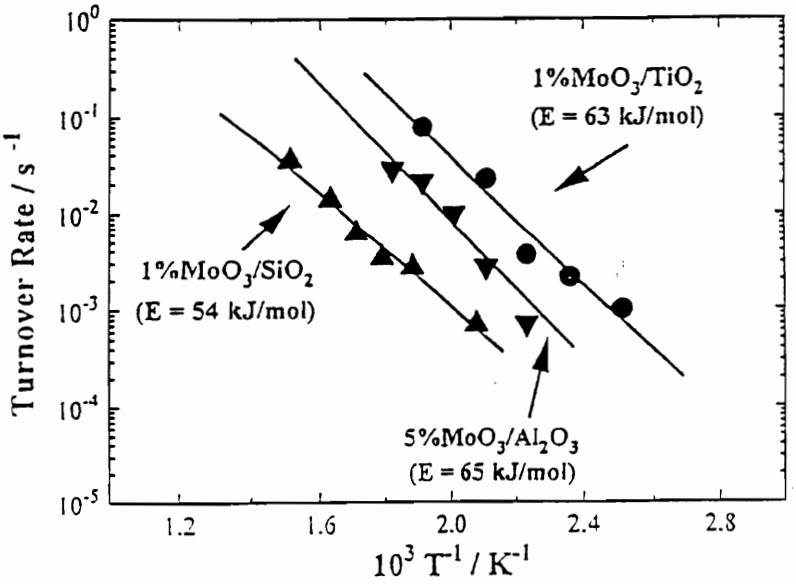

Figure 2.3. Arrhenius plots for ethanol oxidation over the low loading samples.

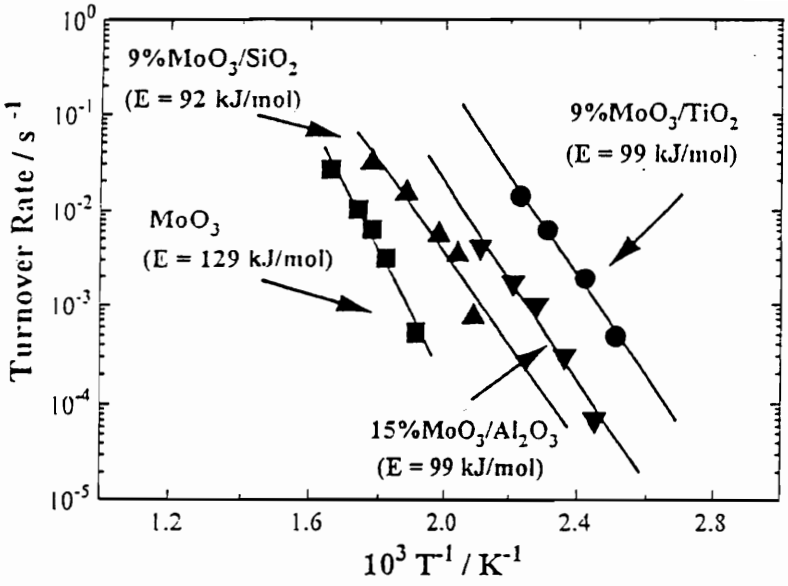

Figure 2.4. Arrhenius plots for ethanol oxidation over the high loading samples.

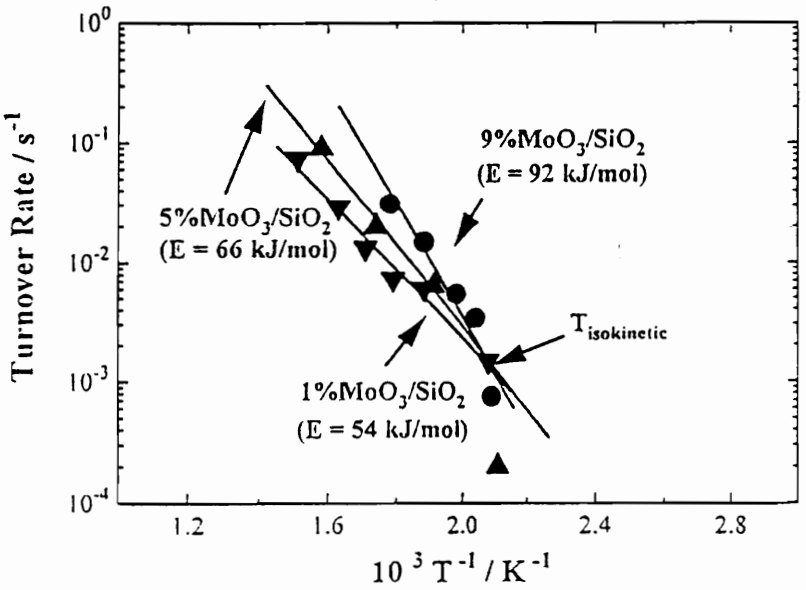

Figure 2.5. Arrhenius plots for ethanol oxidation over different MoO_3 loadings on SiO_2.

Table 2.2. Ethanol oxidation on MoO_3/SiO_2.

Samples	Temp. / K	Selectivity / %						Conv. / %	v_t* / 10^{-3} s^{-1}
		C_2H_4	CH_3CHO	$(C_2H_5)_2O$	CH_3COOH	$CH_3COOC_2H_5$	CO_x		
	480	-	96	4	-	-	-	0.5	0.7
1% MoO_3/SiO_2	532	2	92	3	2	-	-	1.9	2.7
	558	1	86	10	3	-	-	2.3	3.4
	575	3	81	14	2	-	-	2.4	3.5
	585	3	87	7	3	-	-	4.2	6.2
	662	9	78	1	4	4	4	24.3	35.5
	478	3	63	23	11	-	-	1.1	0.8
	490	2	69	7	27	-	-	4.7	3.4
9% MoO_3/SiO_2	506	1	72	11	8	-	-	7.5	5.5
	533	2	77	10	3	6	-	20.7	15.0
	563	4	72	7	4	10	13	42.7	31.0

* v_t is turnover rate.

Table 2.3. Ethanol oxidation on MoO_3/Al_2O_3.

Samples	Temp. / K	Selectivity / %						Conv. / %	v_t / 10^{-3} s^{-1}
		C_2H_4	CH_3CHO	$(C_2H_5)_2O$	CH_3COOH	$CH_3COOC_2H_5$	CO_x		
	448	-	92	8	-	-	-	1.9	0.7
	473	-	92	7	-	1	-	7.6	2.7
5% MoO_3/Al_2O_3	498	1	82	15	-	2	-	27.7	9.9
	523	2	74	17	-	3	4	59.8	21.3
	548	5	64	22	-	3	6	79.8	28.5
	408	-	71	-	29	-	-	0.7	0.1
	423	2	77	7	14	-	-	3.1	0.3
15% MoO_3/Al_2O_3	438	2	90	6	2	-	-	9.9	1.0
	453	3	82	10	3	2	-	17.7	1.7
	473	1	84	10	1	2	2	43.0	4.1

Table 2.4. Ethanol oxidation on MoO_3/TiO_2.

Samples	Temp. / K	Selectivity / %						Conv. / %	v_t / 10^{-3} s^{-1}
		C_2H_4	CH_3CHO	$(C_2H_5)_2O$	CH_3COOH	$CH_3COOC_2H_5$	CO_x		
	398	-	15	85	-	-	-	0.8	1.0
	423	-	46	54	-	-	-	1.7	2.2
1% MoO_3/TiO_2	448	-	81	19	-	-	-	2.9	3.7
	473	2	88	9	-	1	-	18.2	23.0
	523	15	43	2	-	-	40	63.5	80.0
	398	-	50	35	15	-	-	2.8	0.5
9% MoO_3/TiO_2	413	-	63	32	5	-	-	10.9	1.8
	433	3	60	28	3	-	6	35.8	6.2
	448	212	48	8	3	-	29	81.4	14.0

Table 2.5. Activation energies

Sample	E_a / kJ mol^{-1}
1% MoO_3/SiO_2	54
5% MoO_3/Al_2O_3	65
1% MoO_3/TiO_2	63
9% MoO_3/SiO_2	92
15% MoO_3/Al_2O_3	99
9% MoO_3/TiO_2	99
MoO_3	129

order, $TiO_2 > Al_2O_3 > SiO_2$. Apparent activation energies (E_{app}) cluster around 50-60 kJ mol^{-1} for the low loading samples and 90-100 kJ mol^{-1} for the high loading samples (Table 2.5). The Arrhenius plot of pure MoO_3 is shown in Figure 2.4, while those for different MoO_3 loading samples on SiO_2 are shown in Figure 2.5. The plots are very close together, and indicate a slight trend toward higher activity for the high loading samples. Apparent activation energies also increase with loading; 54 kJ mol^{-1} for 1% MoO_3/SiO_2, 66 kJ mol^{-1} for 5% MoO_3/SiO_2, 92 kJ mol^{-1} for 9% MoO_3/SiO_2, and 129 kJ mol^{-1} for pure MoO_3. Selectivities to the main products versus support at a fixed conversion are plotted in Figures 2.6 and 2.7. The selectivity for the low loading samples is independent of support, whereas the selectivity for the high loading samples shows a strong dependence on support.

2.3.2. Raman spectroscopy

Raman results are presented in Figures 2.8 and 2.9. The Raman spectra of SiO_2 and 1% MoO_3/SiO_2 were taken after calcining at 773 K under moisture-free conditions at room temperature in a flow of purified oxygen. The Raman bands at 604, 804, 974 and 1044 cm^{-1} are due to amorphous silica,[32,33] whereas the Raman band at 984 cm^{-1} is due to Mo=O stretching in octahedrally coordinated monomeric molybdenum species.[33] The weak band at 819 cm^{-1} due to Mo-O-Mo stretching indicates that trace amounts of crystalline molybdenum oxide are present on the surface.[1,2,33] The band at 1550 cm^{-1} is

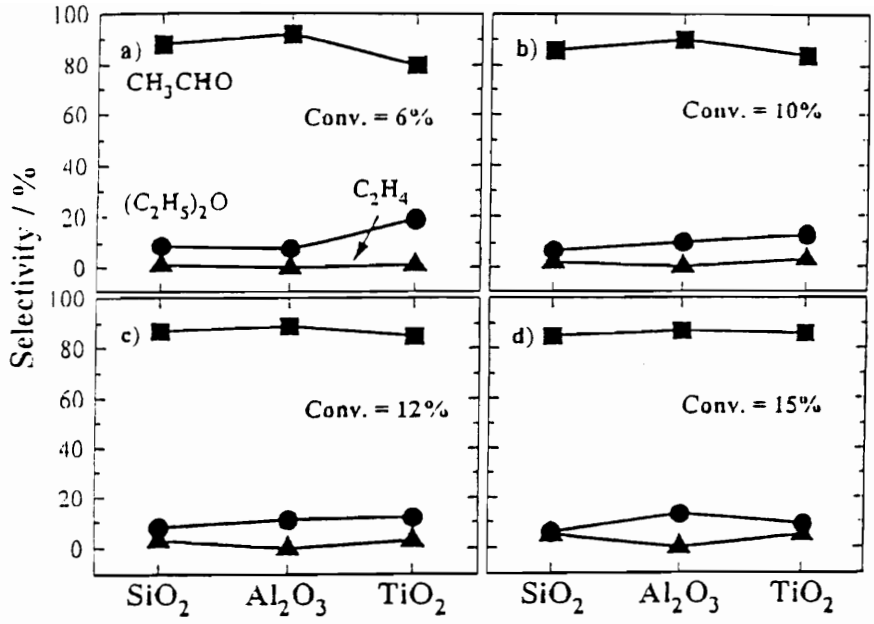

Figure 2.6. Selectivity dependence on support for ethanol oxidation over the low loading samples.

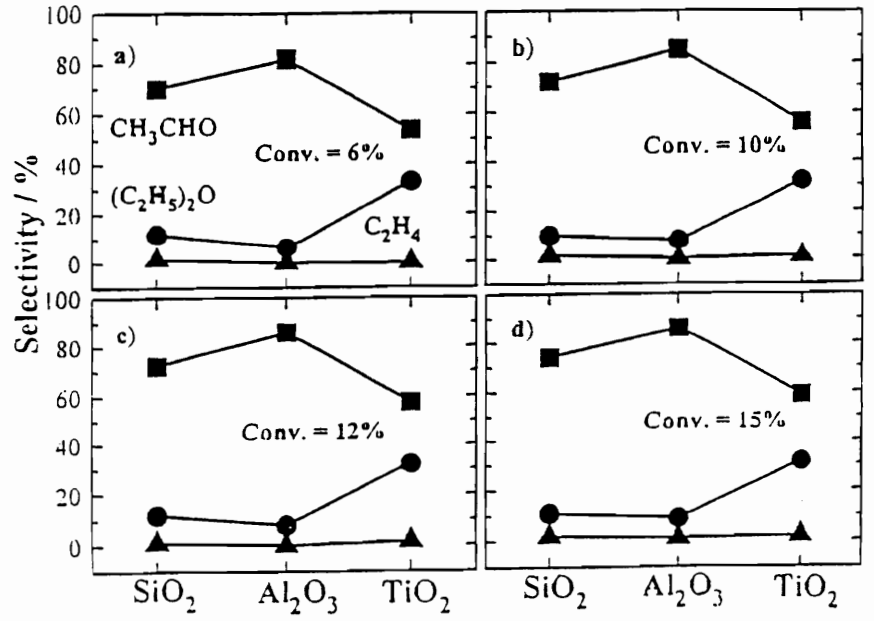

Figure 2.7. Selectivity dependence on support for ethanol oxidation over the high loading samples.

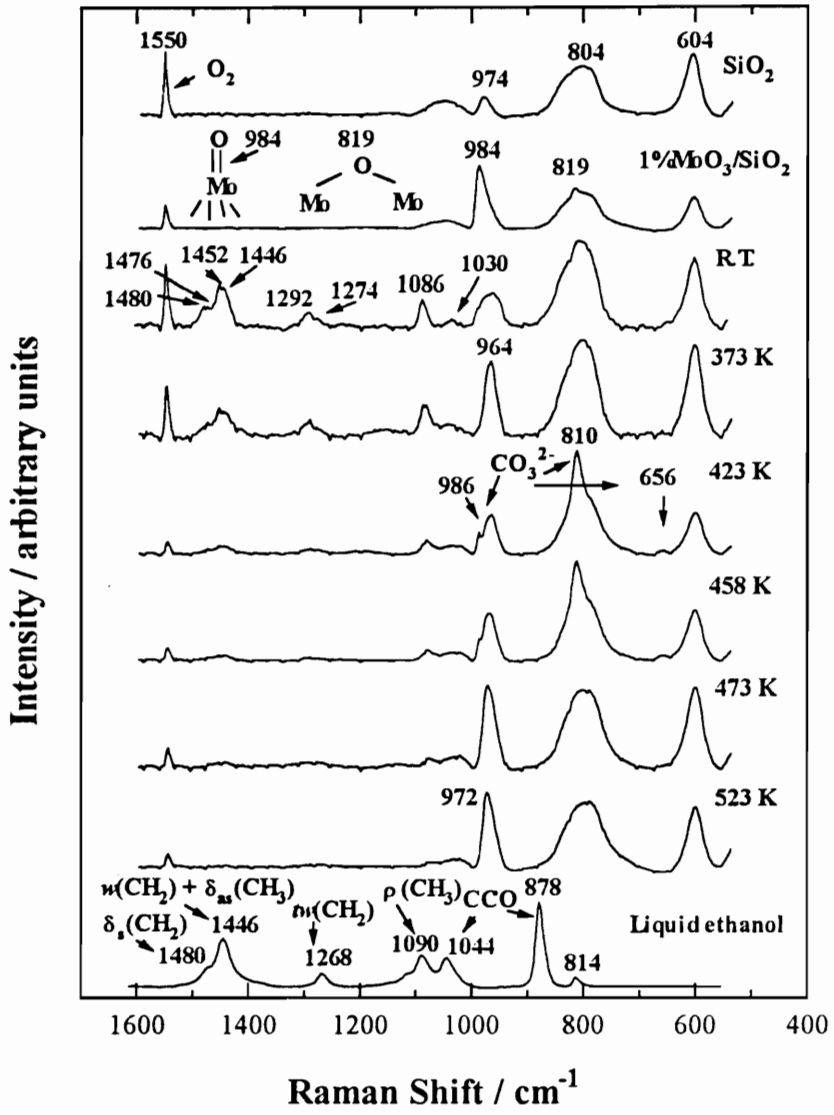

Figure 2.8. Raman spectra of adsorbed species at different reaction temperatures in the low frequency region.

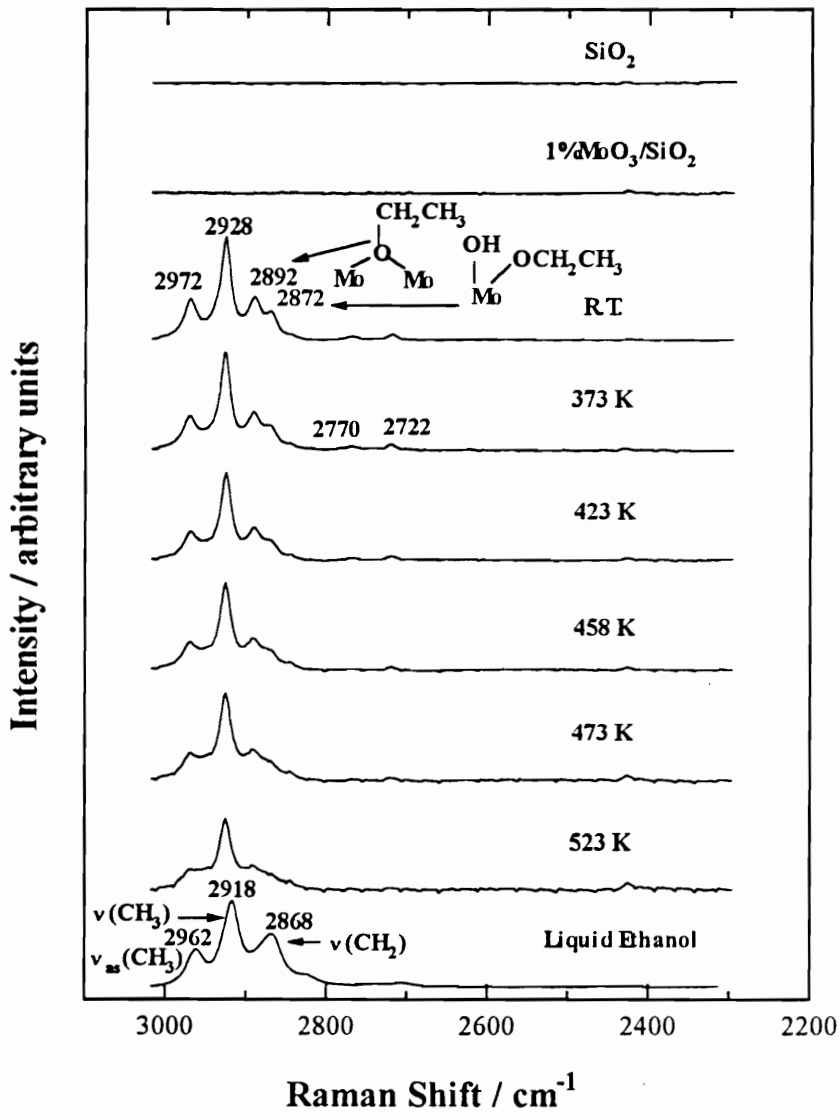

Figure 2.9. Raman spectra of adsorbed species at different reaction temperatures in the high frequency region.

due to gas phase oxygen.[34,35] This was confirmed by the disappearance of the band after switching from oxygen to helium.

All measurements reported below are carried out at steady-state reaction conditions, not temperature-programmed conditions. After introducing the reaction mixture (P_{EtOH} = 1.6 kPa, P_{O2} = 99.4 kPa) at room temperature, the intensity of the band at 984 cm^{-1} drops dramatically, and its position is shifted to ~ 960 cm^{-1} where it appears as a broad feature. At the same time, the Mo-O-Mo stretching feature at 819 cm^{-1} disappears. The drop in the intensity of the Mo=O stretching band is accompanied by a sample color change from white to blue. The intensity of the band increases gradually with increasing temperature while the reaction mixture is flowing through the cell. The sample color changes from blue back to white when the temperature reaches 523 K, while the peak position recovers to 972 cm^{-1} at this point. The band returns to its original form only by heating the sample in O_2 at 773 K for 2 hours after cutting off the reaction mixture supply.

New features with peak positions at 1030, 1086, 1274, 1292, 1446, 1452, 1476, 1480, 2722, 2770, 2872, 2892, 2928, and 2972 cm^{-1} appear with introduction of the reaction mixture at room temperature. The assignment of these features is summarized in Table 2.6. These features can be attributed to ethoxy groups adsorbed on two different type of sites. This will be covered in detail in the discussion section. The decrease of the intensity of these features with increasing temperature indicates the reaction of the two adsorbed species. Interestingly, one of the two types of ethoxy groups, characterized by

Table 2.6. Assignment of laser Raman bands

Frequencies / cm^{-1} (liquid ethanol)	Frequencies / cm^{-1} (adsorbed species)	Assignment ‡	Reference
430 w*		δ(CCO)	46
878 vs		ν(CCO)	45, 46
	1030 vw	ν(CCO)	45
1044 m		ν_{as}(CCO)	46
1090 m	1086 m	$\rho(CH_3)$	45,46
1268 w	1274, 1292 w	*tw*(CH_2)	45, 46
1446 s	1446, 1452 s	*w*$(CH_2) + \delta_{as}(CH_3)$	24, 45, 46
1480 sh	1476, 1480 sh	$\delta_s(CH_2)$	45,46
2868 s	2872, 2892 s	$\nu_s(CH_2)$	24, 45, 46
2918 vs	2928 vs	$\nu_s(CH_3)$	24, 45, 46
2962 vs	2972 vs	$\nu_{as}(CH_3)$	24, 45, 46

* vs = very strong, s = strong, m = medium, w = weak, vw = very weak, sh = shoulder.

‡ ν = stretching, δ = in-plane deformation, *t* = twisting, ρ = rocking.

the band at 2872 cm^{-1}, reacts faster than the other. It is almost invisible when the temperature reaches 458 K. In contrast, the ethoxy group characterized by the band at 2892 cm^{-1} is still visible even when the temperature is raised to 523 K.

As the temperature reaches 423 K, three new bands appear at 656, 810 and 986 cm^{-1}, which corresponds to vibration modes of carbonate.[36] These bands remain at 458 K, but disappear at 473 K and above. The formation of the carbonate species is probably due to the decomposition of the ethoxy groups at intermediate temperatures.

2.3.3. Partial pressure effects

The partial pressure effects for C_2H_5OH, O_2, and H_2O on the three main products, acetaldehyde, ethylene and diethyl ether, are carried out on the 9% MoO_3/SiO_2 sample. Only the results for acetaldehyde formation are reported in this chapter. A detailed kinetic analysis will be given in Chapters 3 and 4.

2.4. Discussion

2.4.1. Steady-state reactivity studies

The dispersion of MoO_3 on SiO_2, Al_2O_3 and TiO_2 has been studied using oxygen chemisorption, x-ray diffraction, and laser Raman spectroscopy in our previous papers.[1,2]

These studies indicated that, under *in situ* conditions, the highly dispersed phases on the low loading samples were isolated monomeric Mo(VI) species, and small crystallites of MoO_3 on the high loading samples. In order to correlate reactivity with surface structure, in the present study, ethanol oxidation was carried out on both low and high loading samples.

Figures 2.3 and 2.4 show that the reactivity of ethanol oxidation over MoO_3 on the various supports follows the trend $TiO_2 > Al_2O_3 > SiO_2$. Our previous results established that the molybdate-support interaction is of an acid-base nature, where the strength of the interaction, with respect to the support, also follows the order $TiO_2 > Al_2O_3 > SiO_2$.[2] TPR[38] results on the low MoO_3 loading samples show that reducibility of surface molybdates on the various supports also follows the same sequence. Clearly, the reactivity for ethanol oxidation over MoO_3 on SiO_2, Al_2O_3, and TiO_2 can be associated with the molybdate-support interaction and the reducibility of the surface molybdate. This finding is in good agreement with a theoretical study by Weber.[39] Based on a molecular orbital study of C-H bond breaking during the oxidative dehydrogenation of methanol catalyzed by metal oxide surfaces, he proposed that the more reducible supports such as TiO_2 and ZrO_2 produce more active catalysts than the refractory supports such as SiO_2 and Al_2O_3 for methanol oxidation, because the more reducible supports have a more accessible set of empty orbitals. This is discussed further at the end.

An interesting aspect of the ethanol oxidation reaction is the effect of structure probed by the reactivity dependence on dispersion. Figure 2.5 shows that there is only a

small increase in reactivity with MoO_3 loading, indicating that ethanol oxidation is apparently not highly dependent on structure. This will be shown to be due to a compensation effect, with rate parameters changing considerably with particle size, actually making the reaction structure-sensitive. The same conclusion can be drawn for ethanol oxidation over MoO_3 on Al_2O_3 and TiO_2 where the high loading samples have only slightly higher rates than the low loading samples (Figs. 2.3 and 2.4). The slight increase of reactivity with Mo loading is consistent with the proposal of Allison and Goddard III, *et al.*,[19] that two neighboring Mo sites are responsible for the formation of formaldehyde in methanol oxidation. Iwasawa, *et al.*,[27,28] also demonstrated the high reactivity of SiO_2-attached dioxo Mo dimer species for ethanol oxidation prepared from organometallic precursors. Mo dimers were also observed on Al_2O_3 and TiO_2.[29] A conversion of 100% in the temperature range of 503 - 523 K and a selectivity of 100% to acetaldehyde in ethanol oxidation over the catalysts prepared by the metal oxide vapor synthesis (MOVS) method were reported by the same authors.

The finding here of an increase in reactivity with Mo loading is consistent with a gradual increase of neighboring molybdenum centers. The effect on the overall rate is small because of a compensation effect. This is indicated by the observation of an isokinetic temperature (Fig. 2.5) for the SiO_2 supported samples and an increase in apparent activation energy with loading (Figs. 2.3 and 2.4) for all samples. As will be discussed further, the compensation is due to the presence of an equilibrated step prior to the rate-determining step.

The role of adsorbate bonding has been extensively discussed in our previous papers.[40,41] We suggested that the existence of two types of intermediates (M-O-R, and M-R) is responsible for selectivity in partial oxidation of hydrocarbons. The M-O-R type intermediate, where the hydrocarbon is bonded through an oxygen atom, produces selective oxidation products, and the M-R type intermediate, where a direct metal-carbon bond exists, produces CO_x. In the case of ethanol oxidation, a simple intermediate, an adsorbed ethoxy group is mainly responsible for the formation of the selective oxidation products. This is supported by the finding of ethoxy groups by the *in situ* laser Raman studies in the present study.

The plots of selectivity of various products versus support shown in Figures 2.6 and 2.7 indicate that the selectivity for the low loading samples is independent of support $SiO_2 \sim Al_2O_3 \sim TiO_2$, but the selectivity for the high loading samples has a strong dependence on support. The selectivity to diethyl ether on 9% MoO_3/TiO_2 increases by a factor of two in comparison to that on 1% MoO_3/TiO_2. This suggests that acetaldehyde, ethylene, and diethyl ether are produced through intermediates adsorbed on different sites.

The *in situ* Raman investigation of ethanol oxidation over 1% MoO_3/SiO_2 in the present study shows that there are at least two types of ethoxy groups present on the surface. These ethoxy groups can be associated with the Mo=O and Mo-O-Mo sites. Clearly, the diethyl ether formation in the present study is not due to Mo-O-Mo sites because an increase in selectivity to diethyl ether with increasing MoO_3 loading on SiO_2 and Al_2O_3 is not observed. A more plausible explanation for our results is that diethyl

ether formation is associated with the Mo-O-M sites (M = Si, Al, and Ti). On the other hand, acetic acid formation occurs through Mo-O-Mo sites, since acetic acid is produced only on the high loading samples. It should be noted that in all cases, the protons associated with the metal-oxygen sites may be important in determining selectivity. However, our results suggest that neighboring Mo centers, as far as selectivity is concerned, play an important role in ethanol oxidation.

On the basis of IR and kinetic studies of ethanol oxidation over SiO_2-attached dioxo Mo monomer and dimer catalysts, Iwasawa, *et al.*,[24,27,28] showed that these catalysts had a selectivity of 97% to acetaldehyde. They proposed that the Mo=O bond was the active site for acetaldehyde formation by showing that this species reacted reversibly with adsorbed ethanol at 423 K. Acetaldehyde was the only product formed at this temperature at steady-state.

Ono, *et al.*,[25] studied the activity of ethanol oxidation over different MoO_3 loadings on TiO_2, and found that acetaldehyde was the major product during reaction. They attributed the maximum reactivity of 10% MoO_3/TiO_2 to the weakening of the Mo=O bond. In a more recent study of ethanol oxidation over highly dispersed MoO_3 on group IV oxide supports, Ono, *et al.*,[26] reported that acetaldehyde was again the major product. They showed that reactivity reported by turnover rates followed the order ZrO_2 > TiO_2 > SiO_2, and the trend could be directly related to Mo=O bond strength as measured by IR and Raman spectroscopy: a weak Mo=O bond gave a high reactivity, and a strong Mo=O bond gave a low reactivity. By comparing the trend of reactivity of the

low loading samples in the present study to the Raman results reported previously,[1,2] we find no direct relation between Mo=O bond strength and reactivity. The same finding was also reported by Wachs's group recently.[42]

2.4.2. Raman spectroscopy

In-depth studies of alcohol adsorption on metal oxides using vibrational spectroscopy were first conducted by Greener.[43] He carried out an IR study of the adsorption of methanol and ethanol on aluminum oxide, and reported the first spectroscopic evidence for the formation of surface methoxide from methanol and surface ethoxide from ethanol at 308 K. Since then, the surface ethoxide species have been reported on iron,[44] vanadium oxide,[32] molybdenum oxide[24] and molybdenum single crystals.[45] Only one study has dealt with the investigation of reaction intermediates in ethanol oxidation over supported molybdenum oxide catalysts. In this paper, Iwasawa, *et al.*,[24] studied ethanol oxidation over silica supported molybdenum oxide catalysts prepared by organometallic processors using IR spectroscopy under *in situ* reaction conditions at 423 K. The IR features originated from adsorbed ethanol species at 1373, 1385, 1446, 2900, 2835, and 2982 cm^{-1} were assigned to the ethoxide structure. A detailed study of ethoxide adsorbed on the Mo (110) surface by HREELS and *ab initio* calculations was reported by Uvdal, *et al.* recently.[45] Due to the poor resolution of the spectrometer (~ 70 cm^{-1}), the HREELS spectra of molybdenum ethoxide in the paper are not useful for the

assignment of the Raman features in the present study, but the *ab initio* calculations for the vibrational frequencies of the normal modes of molybdenum ethoxide in the same work are very helpful.

The major difference of the present study from the previous investigations is that the laser Raman measurements of the reaction intermediates in the present study was carried out at *in situ* continuous reaction conditions over a wide range of temperature (300 K - 523K).

In the present study, the Raman bands developed from ethanol adsorption on 1% MoO_3/SiO_2 are at 1030, 1086, 1274 and 1292 (doublet), 1446 and 1452 (doublet), 1476 and 1480 (doublet), 2770, 2722, 2872 and 2892 (doublet), 2928, and 2972 cm^{-1} (Figs. 2.8 and 2.9). Ethanol adsorption on SiO_2 did not show any significant Raman features. Even though the Raman bands at 1086, 1446, and 2872 cm^{-1} coincide with those of liquid ethanol,[46] all the bands from 1030 to 2972 cm^{-1} can still be assigned to dissociatively adsorbed species because the most intense Raman band due to the CCO stretching mode at 878 cm^{-1} from liquid ethanol does not show up. Instead, this mode appears at 1030 cm^{-1} as a weak and broad feature which is the characteristic evidence for the formation of an adsorbed species.[45] The bands at 1086, 1446, and 2872 cm^{-1} still remain visible even at 423 K, but are very unlikely to be due to molecularly adsorbed ethanol at such a high temperature. Rather they belong to dissociatively adsorbed species.

Other than the bands at 1030, 1086, 1274, 1292, 1476, 1480, 2722 and 2770 cm^{-1}, the rest of the bands at 1446 and 1452, 2892, 2928, and 2972 cm^{-1} are close to the IR

bands reported for the ethoxide structure by Iwasawa, *et al.*,[24] In fact, Iwasawa, *et al.*,[24] did not report any IR bands below 1300 cm^{-1}. The two bands at 2722 and 2770 cm^{-1} observed in the standard liquid ethanol and adsorbed ethanol spectra in Figure 9 are probably due to aldehyde impurities in the ethanol used in the present study.[47] The *ab initio* by Uvdal, *et al.*,[45] calculations for molybdenum ethoxide did predict the existence of the CCO stretching mode at 1020 cm^{-1}, CH_3 rocking mode at 1091 cm^{-1} and CH_2 twist mode at 1274 cm^{-1}, which are very close to the observed modes at 1030, 1086, 1274, and 1292 cm^{-1}. Based on the above discussion, the Raman bands at 1030, 1086, 1274 and 1293 (doublet), 1446 and 1452 (doublet), 1476 and 1480 (doublet), 2872 and 2892 (doublet), 2928, and 2972 cm^{-1} can be assigned to ethoxy groups adsorbed on molybdenum oxide.

The splitting of the Raman bands associated with CH_2 vibrations together with the broad CCO stretching mode at 1030 cm^{-1} strongly suggest the presence of two types of ethoxy groups on molybdenum oxide. The formation of the two types ethoxy groups can be related to the disappearance of the molybdenum oxide features at 984 and 819 cm^{-1}, which correspond the Mo=O and Mo-O-Mo vibrations, respectively. Since this study does not provide information about the Mo-O-Si vibration modes, we cannot rule out the possibility that a third type of ethoxy group adsorbs on the Mo-O-Si sites, and is not distinguishable from the above two ethoxy groups.

According to the present study, the Mo=O bond is more reactive than the Mo-O-Mo bond. After introducing the reaction mixture at room temperature, both the Raman

bands due to the Mo=O stretching mode at 984 cm^{-1} and the Mo-O-Mo stretching mode at 819 cm^{-1} disappear owing to the interaction with ethanol. A change of sample color from white to blue is observed at the same time indicating reduction. With increasing temperature from 373 to 523 K while the reaction mixture is flowing through the Raman cell, the Mo=O bond is easily reoxidized as indicated by the increase in the intensity of this band and the peak position shift from 964 to 972 cm^{-1}. The decrease in the concentration of the ethoxy groups characterized by the 2872 cm^{-1} band in the same temperature range probably suggests that this type of ethoxy group is associated with the Mo=O sites. Furthermore, the selectivity at these conditions suggests that the ethoxide species associated with the Mo=O sites preferentially produces acetaldehyde. Although the Mo=O sites are associated with the ethoxide species, specifics of the bonding arrangement and the reaction pathways are uncertain.

In contrast to the Mo=O functionality, after reduction at room temperature, the Mo-O-Mo feature does not come back with increasing temperature until the sample is reoxidized at 773 K for 2 hours in pure oxygen. Correspondingly, this suggests that the remaining ethoxy group characterized by the band at 2892 cm^{-1} at 523 K is associated with the Mo-O-Mo sites, and is relatively unreactive.

2.4.3. Kinetics

A detailed study of the partial pressure effect on 9% MoO_3/SiO_2 was performed at 523 K to provide further information about the mechanism of ethanol oxidation and will be reported in detail elsewhere.[37] The experimentally-determined ethanol partial pressure dependence for acetaldehyde production was: $v_{CH3CHO} = (L)\ k\ P_{C2H5OH}^{0.86}$. A two-step sequence that is consistent with the obtained kinetics is the following:

$$CH_3CH_2OH + S_1 \underset{}{\overset{K}{\rightleftharpoons}} S_2$$

$$S_2 \xrightarrow{k} CH_3CHO + S_1$$

Where S_1 represents empty sites and S_2 occupied sites (adsorbed ethoxide). The sequence incorporates the key finding from isotopic studies,[37] namely equilibrated adsorption of ethanol to form an ethoxide species (step 1) and rate-determining decomposition of that species to acetaldehyde (step 2). Employing the Temkin theory of rates[47] on non-uniform surfaces, it is possible[37] to derive the following expression for the rate: $v_{CH3CHO} = (L)\ k'\ P_{C2H5OH}^{0.86}$, which agrees with the experimental rate. The rate parameter, k', is a product of the rate constant for the second step and a function of equilibrium constants associated with the adsorption of ethanol, water, and oxygen. For

the simplified sequence above it is just $k' = k K^{1-m}$, where m is the Brønsted transfer coefficient.[48]

The overall apparent activation energy, E_{app}, is seen to be composed of two terms, $E_{app} = E + (1-m)\Delta H$, where E is the activation energy of the rate determining step and ΔH is the heat of adsorption of ethanol. Since adsorption processes are mostly exothermic, ΔH is a negative quantity which results in smaller apparent activation energies. This explains why the observed activation energies are substantially lower than the C-H bond-dissociation energy of $CH_3CH(OH)$-(H) of 389 kJ mol^{-1}. Also the increase in activation energies from 50-60 kJ mol^{-1} for the low loading samples to 90-100 kJ mol^{-1} for the high loading samples can be understood from a decrease in the heat of adsorption by 40 kJ mol^{-1} in this range. Thus, as particle size increases equilibrium ethanol adsorption becomes less exothermic and adsorbate coverages decrease. As will be explained subsequently, this offsets increases in the rate constant with particle size so that overall rates do not change appreciably with loading. This is the origin of the compensation.

2.4.4. Controlling factor for reactivity

An important conclusion to be derived from the present work is that electronic factors are important in alcohol oxidation. The relevant results are the following. First, the loading of molyb0denum oxide does not have a major effect on the rate of oxidation. Instead, the identity of the support has a great influence on the rate, the order being TiO_2

> Al_2O_3 > SiO_2. However, interestingly, the activation energy for the reaction at similar loadings does not vary significantly with support. Isotopic studies[37] indicate that the same mechanism is operating in all cases, namely, equilibrated formation of an ethoxide intermediate followed by rate-determining decomposition of the intermediate. The rate is given by a power-rate law expression that is consistent with those steps. The expression contains the total number of sites, (L), a rate parameter, k', and a function of concentration, f(C).

Exactly, the same general observations have been made by others[3-22] for the methanol oxidation reaction. In recent work on methanol oxidation on V_2O_5[49] and MoO_3,[42] the 1-3 order of magnitude difference in rate with support was attributed to different numbers of active sites participating in the reaction. It is hard to believe that this would be the case on 1% loading samples used in those studies, which Raman spectroscopy showed to be molecularly dispersed. In the present study, the number of surface molybdenum atoms in the sample were carefully titrated by oxygen chemisorption,[1,2] and cannot account for the difference in rates. At most the error may be a factor of 2.

If the number of sites, (L), is not responsible for the difference, then the cause must lie elsewhere. Assuming that the equilibrium constants associated with adsorption shift in the same direction for the different supports, this points to the rate constant for the rate-determining step, k, as the cause for the difference. Moreover, since the activation

energies, E, are close, the quantity responsible must be the pre-exponential factor, A, of the rate constant.

$$k = A \exp(-\frac{E}{RT}) \qquad A_{TiO2} > A_{Al2O3} > A_{SiO2}$$

According to transition state theory the pre-exponential factor can be expressed as a product of the universal frequency, kT/h, and the ratio of partition functions of the activation complex, Q', and the reactant, Q.

$$A = \frac{kT}{h} \exp(\frac{\Delta S'}{R}) = \frac{kT}{h} \frac{Q'}{Q} \qquad Q'_{TiO2} > Q'_{Al2O3} > Q'_{SiO2}$$

The overall partition function can be factored into translational, vibrational, rotational, and electronic partition functions. The first three contributions are generally small, and should not differ very much for the same intermediate. The last, however, has no upper limit.

$$Q' = q^t q^v q^r q^e \qquad q^e_{TiO2} > q^e_{Al2O3} > q^e_{SiO2}$$

The conclusion is that the origin of the difference in rates resides in the electronic partition function of the activated complex. This is precisely the conclusion of Weber[39] based on his molecular orbital calculation of methanol oxidation on molybdenum oxide

that indicates that hydride transfer to a metal center is rate-determining. The way that this relates to the mechanism is as follows.

The rate-determining step remains the breaking of the C-H bond. Thus, the activation energy is constant for different supports. However, the probability that the system gets to the top of the barrier depends on the number of states available in the transition state to accept the electrons in the hydride transfer. The rate determining step is taken to include both proton and electron transfer. Here, the surface oxide-support complex is involved, with the larger density of empty states, the higher the rate. This is depicted in Fig. 2.10, which shows a number of equal-energy states for the activated complex, representing the electronic partition function. The density of empty states should track with the reducibility (electron accepting character) of the species, as has been observed.[38] The involvement of the density of empty states is also related to earlier suggestions that the conduction band of oxides acts as an electron sink.[50,51] It is also consistent with the observed increase in rate as the molybdenum species forms dimers[24,27-29] or larger ensembles, which are expected to have a larger number of empty electronic states. Of course, as discussed earlier, the increase in the pre-exponential factor is offset by the decrease in the heat of adsorption of ethanol in the equilibrated first step, so that a compensation in the rate is observed.

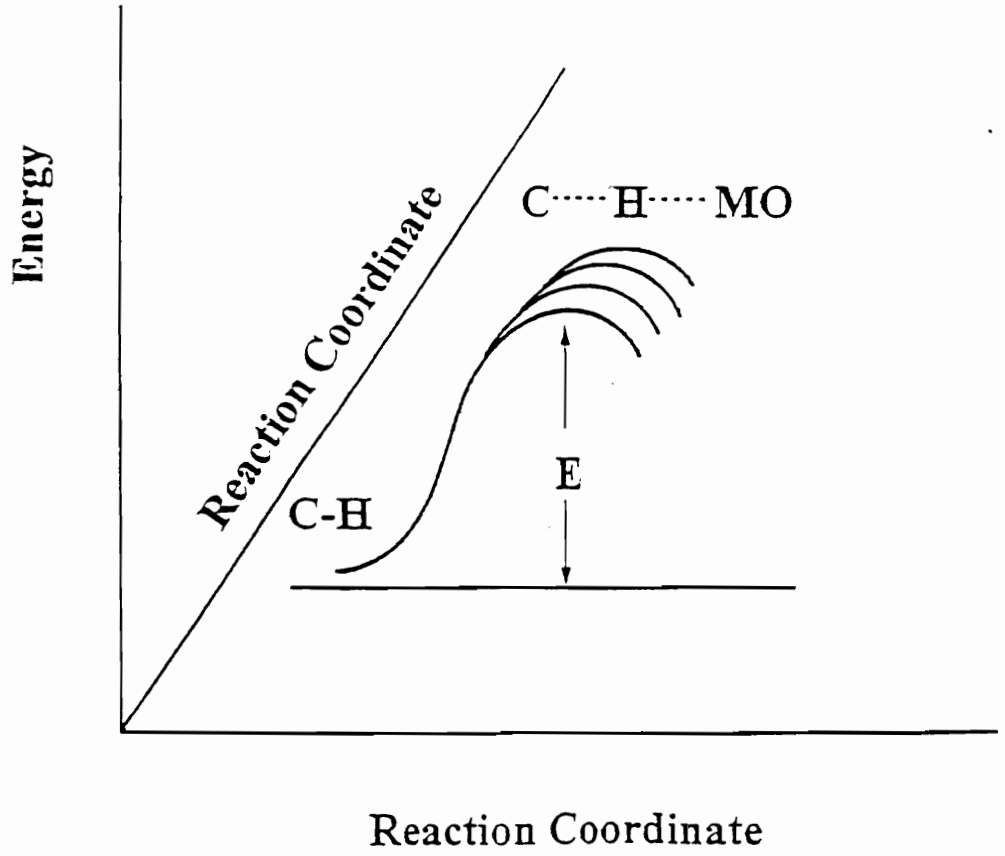

Figure 2.10. Energy diagram of transition state.

2.5. Conclusions

1. The reactivity of ethanol oxidation on supported molybdenum oxide at low and high loadings follows the order of $TiO_2 > Al_2O_3 > SiO_2$. Activation energy is independent of support.

2. The product distribution for ethanol oxidation over these supports is similar, acetaldehyde is the main product followed by diethyl ether and ethylene, and they are produced through ethoxide type intermediates adsorbed on different sites.

3. The reaction to form acetaldehyde proceeds in two stages, a quasi-equilibrated adsorption of ethanol to form adsorbed ethoxide and a second rate-determining decomposition of ethoxide through an α-hydrogen abstraction. Compensation between the two steps causes the overall rate not to vary with loading, although the reaction remains a structure-sensitive reaction.

4. The differences in rates with support can be associated with the availability of empty electronic energy states in the metal oxide-support complex.

2.6. References:

(1). Desikan, A. N.; Huang, L.; and Oyama, S. T. *J. Phys. Chem.* **1991**, 95, 10050.

(2). Desikan, A. N.; Huang, L.; and Oyama, S. T. *J. Chem. Soc., Faraday Trans. I*, **1992**, 88(22), 3357.

(3). Pernicone, N.; Altering, F.; Liberti, G.; and Lanzavecchia, G. *J. Catal.* **1969**, 14, 293.

(4). Edwards, J.; Nicollaidis, J.; Cutlip, M. B.; and Bennett, C. O. *J. Catal.* **1977**, 50, 24.

(5). Chung, J. S.; and Bennett, C. O. *J. Catal.* **1985**, 92,173.

(6). Chung, J. S.; Miranda, R.; and Bennett, C. O. *J. Chem. Soc. Faraday Trans. I*, **1985**, 81, 19.

(7). Chung, J. S. ; and Bennett, C. O. *J. Chem. Soc. Faraday Trans. I*, **1986**, 82, 2155.

(8). Chung, J. S.; Miranda, R.; and Bennett, C. O. *J. Catal.* **1988**, 114, 398.

(9). Farneth, W. E.; Ohuchi, F.; Staley, R. H.; Chowdhry, U.; and Sleight, A. W. *J. Phys. Chem.* **1985**, 89, 2493.

(10). Tatibouët, J. M.; and Germain, J. E. *J. Catal.* **1981**, 72, 375.

(11). Tatibouët, J. M.; Germain, J. E.; and Volta, J. C. *J. Catal.* **1983**, 82, 240.

(12). Ohuchi, F.; Firment, L. E.; Chowdhry, U.; and Ferretti, A. *J. Vac. Sci. Technol.* **1984**, A2, 1022.

(13). Chowdhry, U.; Ferretti, A.; Firment, L. E.; Machiels, C. J.; Ohuchi, F.; Sleight, A. W.; and Staley, R. H. *Appl. Surf. Sci.* **1984**, 19, 360.

(14). Machiels, C. J.; Cheng, W. H.; Chowdhry, U.; Farneth, W. E.; Hong, F.; Mc Carron, E. M.; and Sleight, A. W. *Appl. Catal.* **1986**, 25, 249.

(15). Machiels, C. J.; and Sleight, A. W. *J. Catal.* **1982**, 76, 238.

(16). Yang, T. J.; and Lunsford, J. H. *J. Catal.* **1987**, 103, 55.

(17). Nováková, J.; Jíru, P.; and Zavadil, V. *J. Catal.* **1970**, 17, 93.

(18). Cheng, W. H.; Chowdhry, U.; Ferretti, A.; Firment, L.; Groff, R. P.; Machiels, C. J.; McCarron, E. M.; Ohuchi, F.; Staley, R. H.; and Sleight, A. W. in "*Heterogenous Catalysis*" (B. L. Shapiro, Ed.), pp. 165-81, Texas A&M Univ. Press, College Station., Texas, **1984**.

(19). Allison, J. N.; and Goddard III, W. A. *J. Catal.* **1985**, 92, 127.

(20). Niwa, M.; Mizutani, M.; Takahashi, M.; and Murakami, Y. *J. Catal.* **1981**, 70, 14.

(21). Niwa, M.; Yamada, H.; and Murakami, Y. *J. Catal.* **1992**, 134, 331.

(22). Matsuoka, Y.; Niwa, M.; and Murakami, Y. *J. Chem. Phys.* **1990**, 94, 1477.

(23). Tatibouët, J. M.; and Germain, J. E. *J. Chem. Res.* **1981**, (S) 268; **1981**, (M), 3070.

(24). Iwasawa, Y.; Nakano, Y.; and Ogasawara, S. *J. Chem.Soc. Faraday Trans. I*, **1978**, 74, 2986.

(25). Ono, T.; Kamisuki, H.; Hisashi, H.; and Miyata, H. *J. Catal.* **1989**, 116, 303.

(26). Ono, T.; Nakagawa, Y.; Miyata, H.; and Kubokawa, Y. *Bull. Chem. Soc. Jpn.*, **1984**, 57, 1205.

(27). Iwasawa, Y.; and Tanaka, H. *Proc. Int. Congr. Catal.*, 8th Berlin , IV-381, **1984**.

(28). Iwasawa, Y.; Asakura, K.; Ishii, H.; and Kuroda, H. *Z. Phys. Chem.* **1985**, 144, 105.

(29). Alyea, E. C.; Brown, K. F.; Durham, L.; and Svazic, T. in"*Progress in Catalysis*" (K. J. Smith and E. C. Sanford Ed.), Elsevier Sci. Pub. B. V., pp. 309-314, **1992**.

(30). Farneth, W. E.; Staley, R. H.; and Sleigh, A. W. *J. Am. Chem. Soc.* **1986**, 108, 2327.

(31). Coward, H. F.; Jones, G. W. Bulletin 503 U.S. Bureau of Mines; *Limits of Flammability of Gases and Vapors*, U.S. Government Printing Office: Washington, DC, **1952**.

(32). Went, G. T.; Oyama, S. T.; and Bell, A. T. *J. Phys. Chem.* **1990**, 94, 4240.

(33). Williams, C. C.; Ekerdt, J. G.; Jehng, J.; Hardcastle, F. D.; Turek, A. M.; and Wachs, I. E. *J. Phys. Chem.* **1991**, 95, 8781.

(34). Bielanski, A.; and Haber, J. "*Oxygen in Catalysis*", Marcel Dekker, Inc., New York, **1991**.

(35). Freeman, S. K. "*Applications of Laser Raman Spectroscopy*", John Wiley & Sons, New York, **1974**.

(36). Little, L. H. "*Infrared Spectra of Adsorbed Species*", Academic Press, New York, **1966**.

(37). Zhang, W.; and Oyama, S. T. Manuscript in preparation.

(38). Desikan, A. N.; Zhang, W.; and Oyama, S. T. Submitted to J. Catal.

(39). Weber, R. S. *J. Phys. Chem.* **1994**, 98, 2999.

(40). Oyama, S. T.; Desikan, A. N.; and Zhang, W. in"*Catalytic Selective Oxidation*" (S. T. Oyama and J. W. Hightower Ed.), ACS Series 523, pp. 16-19, **1992**.

(41). Oyama, S. T. *J. Catal.* **1991**, 128, 210.

(42). Kim, D. S.; Wachs, I. E.; and Segawa, K. *J. Catal.* **1994**, 146, 268-277.

(43). Greener, R. G. *J. Phys. Chem.* **1962**, 37 (9), 2094.

(44). Blyholder, G.; and Neff, L. D. *J. Phys. Chem.* **1966**, 70 (3), 893.

(45). Uvdal, P.; MacKerell Jr, A. D.; and Wiegand, B. C. *J. Elect. Spectr. Rel. Phenom.* **1993**, 64/65, 193.

(46). Mikawa, Y.; Brasch, J. W.; and Jakobsen, R. J. *Spectrochim. Acta*, **1971**, 27A, 529.

(47). Lim-Vien, D; Colthup, N. B.; Fateley, W. G.; Gasselli, J. G. *"The Handbook of Infrared and Raman Characteristic Frequencies of Organic Molecules"*, Academic Press, Boston, 1991.

(48). Boudart, M.; and Djega-Mariadassou, G. "*Kinetics of Heterogeneous Catalytic Reactions*", Princeton Univ. Press, NJ, **1984**.

(49). Deo, G.; and Wachs, I. E. *J. Catal.* **1994**, 146, 335-345.

(50). Lim, W. J.; and Sleight, A. W. *Am. N. Y. Acad. Sci.* **1976**, 272, 22.

(51). Sleight, A. W. in "*Advanced Materials in Catalysis*" (J. J. Burton, and R. L. Garten Eds.), Academic Press, New York, pp. 181, **1977**.

Chapter 3

In Situ Laser Raman Studies of Intermediates in the Catalytic Oxidation of Ethanol over Supported Molybdenum Oxide

3.1. Introduction

Alcohol oxidation on MoO_3-containing catalysts has been extensively studied since the 1960's.[1-22] Most of the attention has focused on methanol oxidation to formaldehyde. In methanol oxidation, considerable work has been devoted to understanding the nature of the adsorbed intermediates,[1-7] the identity of the active sites (e.g. Mo=O, Mo-O-Mo),[1-12,15-19] the determination of the rate-determining step, [13-14] the nuclearity of active centers (e.g. monomer, or dimer),[1,15,16,19] and the kinetics of the reaction.[20-22] There is general agreement that a methoxide type intermediate produces formaldehyde,[1-7] and that the rate-determining step for this reaction is C-H bond cleavage from the adsorbed methoxy groups.[13-14] However, the identity of the active sites and the effect of supports are still under debate.

Kinetic studies of methanol oxidation to formaldehyde have been conducted on iron molybdate catalysts.[20-22] The first two studies neglected the effect of water contribution and assumed that the rate occurred uniformly over the entire surface leading

to very complicated expressions. Holstein and Machiels[22] showed that neglecting water inhibition led to lower activation energy and lower kinetic orders of reaction.

Less attention has been paid to ethanol oxidation than methanol oxidation over MoO_3-containing catalysts.[23-29] Tatibouët, *et al.*,[23] used oriented MoO_3 crystallites to study the structure-sensitivity of the reaction, and Iwasawa, *et al.*,[24,27,28] Ono, *et al.*,[25,26] Alyea, *et al.*,[29] and Zhang, *et al.*[30] used supported samples to study molybdate-support interactions. Based on studies of structure,[23] reactivity, infrared spectroscopy (IR), extended x-ray adsorption fine structure spectroscopy (EXAFS) and Raman spectroscopy (LRS),[24,25-28] various authors have concluded that Mo=O bonds are the active sites for acetaldehyde formation. Mo dimers were suggested to be present by Iwasawa, *et al.*,[24,27,28] on MoO_3/SiO_2 prepared from organometallic precursors, and by Alyea, *et al.*,[29] on MoO_3/Al_2O_3 and MoO_3/TiO_2 prepared by the metal oxide vapor synthesis (MOVS) method. The catalysts with Mo dimer structure on the surface showed very high activity and selectivity to acetaldehyde.[24,27-29]

Chapter 2 established that the effects of support on ethanol oxidation over supported molybdenum oxide can be related to the electronic partition function associated with the density of electron-accepting levels in the molybdate-support complex. Ethoxide type intermediates were found to be responsible for the formation of selective oxidation products. This chapter employs *in situ* laser Raman spectroscopy,[30] isotopic substitution and kinetic measurements to elucidate the mechanism of ethanol oxidation over supported molybdenum oxide catalysts. It will be shown that the kinetics results can be simply

described by power rate law expressions, and that the rate of acetaldehyde formation can be well modeled using Temkin's theory of non-uniform surfaces. Two types of ethoxide intermediates are observed on the SiO_2-supported catalysts. One with a $\nu_s(CH_2)$ vibrational frequency at 2872 cm^{-1} is associated with the Mo=O bonds and is a true reactive intermediate. The other with $\nu_s(CH_2)$ at 2892 cm^{-1} is associated with Mo-O-Mo bonds and, despite being the majority species on the surface, is an unreactive spectator.

3.2. Experimental

3.2.1. Sample preparation and characterization

The samples were prepared by the incipient wetness method as described elsewhere.[30-32] Briefly, the process consisted of impregnating silica (Cabosil L90, S_g = 89 $m^2\ g^{-1}$) with a solution of ammonium molybdate (Aldrich 98%), drying the resulting powder, and then calcining it at 773 K for 6 hours. The conventional flow reactor system, gas chromatographic analysis of reactant and gases, and characterization of the samples using BET specific surface area (S_g) determination, oxygen chemisorption, x-ray diffraction (XRD), and laser Raman spectroscopy (LRS) have also been described.[30-32]

3.2.2. *In situ* laser Raman spectroscopy

Raman spectra were obtained using the 514 nm line of an Ar ion laser (Lexel, Model 95) with a power of 100 mW at the sample. The scattered light was filtered with a holographic super notch-plus filter (Kaiser Optical) and directed into a single monochromator (Spex, Model 500M) equipped with a liquid nitrogen cooled CCD detector. A slit width of 50 μm was used to achieve a resolution better than 5 cm^{-1}. The samples (~ 0.3 g of powder) were pressed into thin wafers. The wafers were spun at a rate of 600 - 1000 rpm to avoid local laser heating.[30]

Laser Raman measurements of adsorbed species were carried out in a continuous flow reactor with a reaction mixture of ethanol and oxygen at a total flow rate of 270 μmol s^{-1} (400 cm^3 min^{-1}). The ethanol partial pressure was varied from 0.1 kPa to 0.55 kPa while maintaining the total space velocity constant by adjusting the flow of oxygen. A gas chromatograph (SRI Model 8610) equipped with a flame ionization detector (FID) and a thermal conductivity detector (TCD) was coupled with the Raman apparatus, thus allowing the simultaneous measurement of adsorbed species spectra and the rate of the reaction.

A 1% MoO_3/SiO_2 sample was chosen for the Raman studies because with the 9% MoO_3/SiO_2 sample most of the features from adsorbed ethanol species were covered by the intense Raman bands of crystalline molybdenum oxide.[30] If it is not specified, the

reaction mixture for *in situ* Raman studies was ethanol or water with pure oxygen. High oxygen partial pressure was chosen so as to keep a bright sample color and a low fluorescence level. Before reaction, samples were pretreated in pure O_2 at 723 K for 3 h.

3.2.3. Isotopic substitution

Isotopic substitution measurements were carried out on the 9% MoO_3/SiO_2 , 15% MoO_3/Al_2O_3 and 9% MoO_3/TiO_2 samples (1 g) under continuous flow conditions at steady-state. Three deuterated ethyl alcohols (Aldrich, C_2H_5OD, 99.5%D; CH_3CD_2OH, 98%D; and CD_3CH_2OH, 99%D) were used. The composition of the reaction mixture was the same as for the reactivity studies described in Chapter 2, which was P_{C2H5OH} (or $P_{deuterated\ ethanol}$) = 8 kPa, P_{O2} = 8 kPa, P_{H2O} = 4 kPa, and P_{He} = 81 kPa. The total flow rate was 160 $cm^3\ min^{-1}$ or 110 $\mu mol\ s^{-1}$. The temperatures at which these isotopic substitution experiments were performed were carefully chosen so as to keep the conversion below 15%.

3.2.4. Kinetics of ethanol oxidation

Reactivity was measured with a gas chromatographic system described in Chapter 2. Rates were expressed as turnover rates based on oxygen titration measurements.[31,32] Briefly, oxygen uptakes were measured by a pulse method on samples prereduced in

hydrogen at moderate temperatures (600 - 640 K). The reduction was carried out at a temperature just below that at which bulk reduction occurred, and the method was independently calibrated by laser Raman spectroscopy at low loadings and by x-ray diffraction at high loadings.

Care was paid to ensure the achievement of steady-state conditions and the stability of the sample. Each point took 2 hours for establishment of steady-state, and a beginning point was always checked after each set of runs to verify sample stability. During the experiments, carbon and oxygen balances were always better than 100 ± 8%. Occasionally after long runs some molybdenum oxide was observed to sublime, however, all the data were taken at conditions that were not affected by deactivation.

The 9% MoO_3/SiO_2 catalyst (1 g) was used for kinetics studies because it had a long life. The powder was pretreated before every set of experiments in an O_2, H_2O and He mixture (same as the reaction mixture except C_2H_5OH was absent) at a temperature of 623 K for 1 h. The temperature was then lowered to 523 K, where the kinetics measurements were performed. The measurements were carried out by varying the partial pressures of the reaction mixture components C_2H_5OH, O_2, H_2O, and He. During each set of experiments, the partial pressure of only one component in the reaction mixture was varied, while, simultaneously, keeping the total space velocity constant by adjusting the partial pressure of He.

3.3. Results

3.3.1. *In situ* laser Raman spectroscopy

Figures 3.1 and 3.2 show the Raman spectra of ethanol adsorption on 1% MoO_3/SiO_2 at room temperature (RT). The standard spectra of SiO_2 and 1% MoO_3/SiO_2 are plotted for comparison. The Raman bands at 604, 804, 974 and 1044 cm^{-1} are due to amorphous silica.[33] The bands at 819 and 984 cm^{-1} are respectively due to the asymmetric stretching mode of the Mo-O-Mo bond associated with small crystallites of MoO_3, and the stretching mode of the Mo=O bond associated with isolated and surface molybdate species ($O=MoO_4$).[30,31,34] The band at 1550 cm^{-1} is due to gas phase oxygen.[30] After the introduction of ethanol, three processes occur: the intensities of the 818 and 984 cm^{-1} bands dramatically decrease with increasing partial pressure of ethanol; the color of the sample changes from white to blue, indicating sample reduction; and new features at 1030 (ν(CCO)), 1086 ($\rho(CH_3)$), 1274 and 1292 ($tw(CH_2)$), 1446 and 1452 ($w(CH_2)$ + $\delta_{as}(CH_3)$), 1476 and 1480 ($\delta_s(CH_2)$), 2872 and 2892 ($\nu(CH_2)$), 2928 ($\nu_s(CH_3)$), and 2972 cm^{-1} ($\nu_{as}(CH_3)$)[35,36] develop. The terminology here is ν - stretch, ρ - rocking, *tw* - twist, *w* - wag, δ - deformation, s - symmetric, as - asymmetric. In Chapter 2, these Raman bands were assigned to two types of adsorbed ethoxide species: one associated with the Mo=O sites is characterized by a $\nu_s(CH_2)$ band at 2872 cm^{-1} and the other associated with the

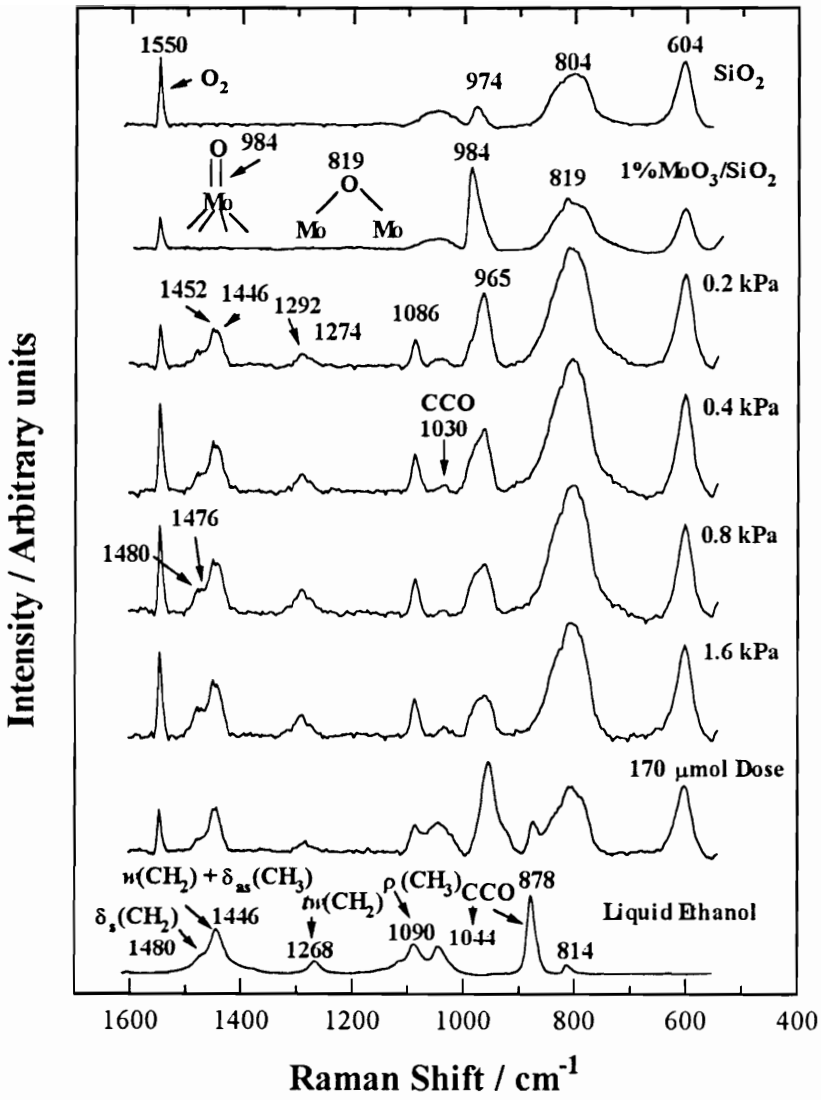

Figure 3.1. Raman study of ethanol adsorption on 1% MoO_3/SiO_2 at RT in the low frequency region.

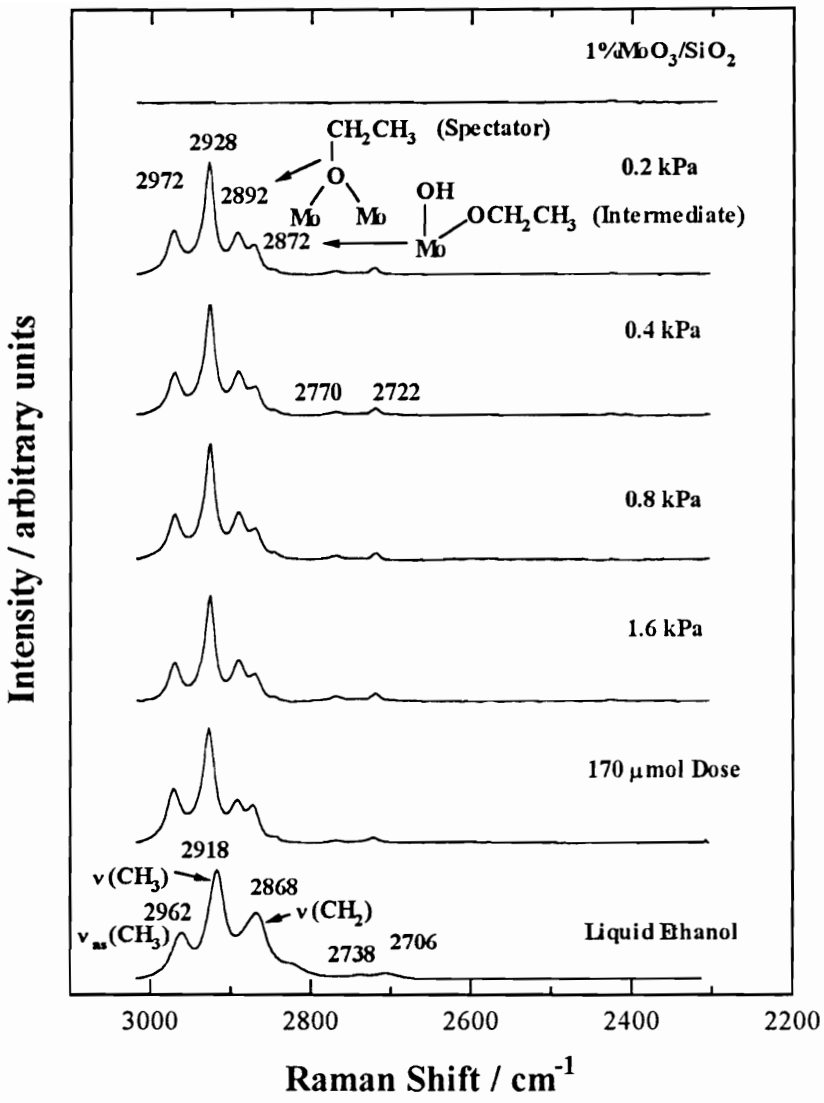

Figure 3.2. Raman study of ethanol adsorption on 1% MoO_3/SiO_2 at RT in the high frequency region.

Mo-O-Mo sites is characterized by a $\nu_s(CH_2)$ band at 2892 cm^{-1}. As will be shown later the former is a reactive intermediate and the latter a spectator on the surface. The spectrum obtained using a 170 μmol dose of liquid ethanol (P_{max} ~ 10 kPa) with O_2 flowing has two bands at 878 and 1044 cm^{-1} corresponding to the symmetric and asymmetric stretching modes of the CCO skeleton of liquid ethanol. Ethanol adsorbs only in molecular form on SiO_2, and the concentration of adsorbed species is about two orders of magnitude lower than that on 1% MoO_3/SiO_2.

Figure 3.3 and 3.4 show Raman spectra of adsorbed ethanol on 9% MoO_3/SiO_2 at 298 K. In the reference spectrum of the 9% MoO_3/SiO_2 sample, the Raman band at 997 cm^{-1} is due to the symmetric stretching mode of the Mo=O bond, while the phonon bands at 823 and 673 cm^{-1} can be roughly associated with modes involving Mo-O-Mo bond in crystalline MoO_3.[31] With increasing ethanol partial pressure, a sample color change from white to blue followed by shifts of the 997 and 823 cm^{-1} bands towards low frequency are observed. After ethanol is introduced at RT, only the C-H vibrational modes at 2872, 2892, 2929 and 2972 cm^{-1} are observed, the other features from adsorbed ethanol are covered by the intense Raman bands at 997, 823, and 673 cm^{-1} from the Mo=O and Mo-O-Mo vibrational modes.

Figure 3.5 shows standard Raman spectra of 1% MoO_3/SiO_2, 5% MoO_3/Al_2O_3, and 1% MoO_3/TiO_2. The Raman bands from 1% MoO_3/SiO_2 have been assigned in the previous section. The Raman band at 1008 cm^{-1} on 5% MoO_3/Al_2O_3 can be assigned to the terminal Mo=O stretching mode associated with isolated surface molybdate species,[37]

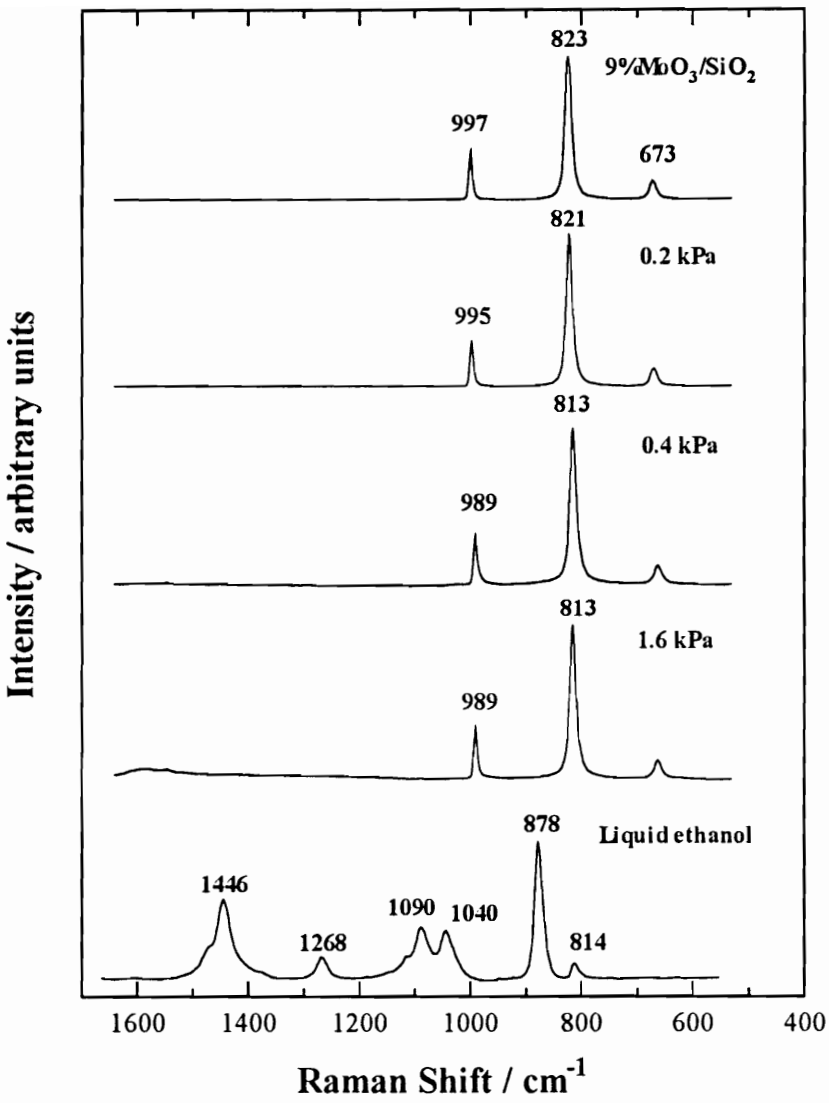

Figure 3.3. Raman study of ethanol adsorption on 9% MoO_3/SiO_2 at RT in the low frequency region.

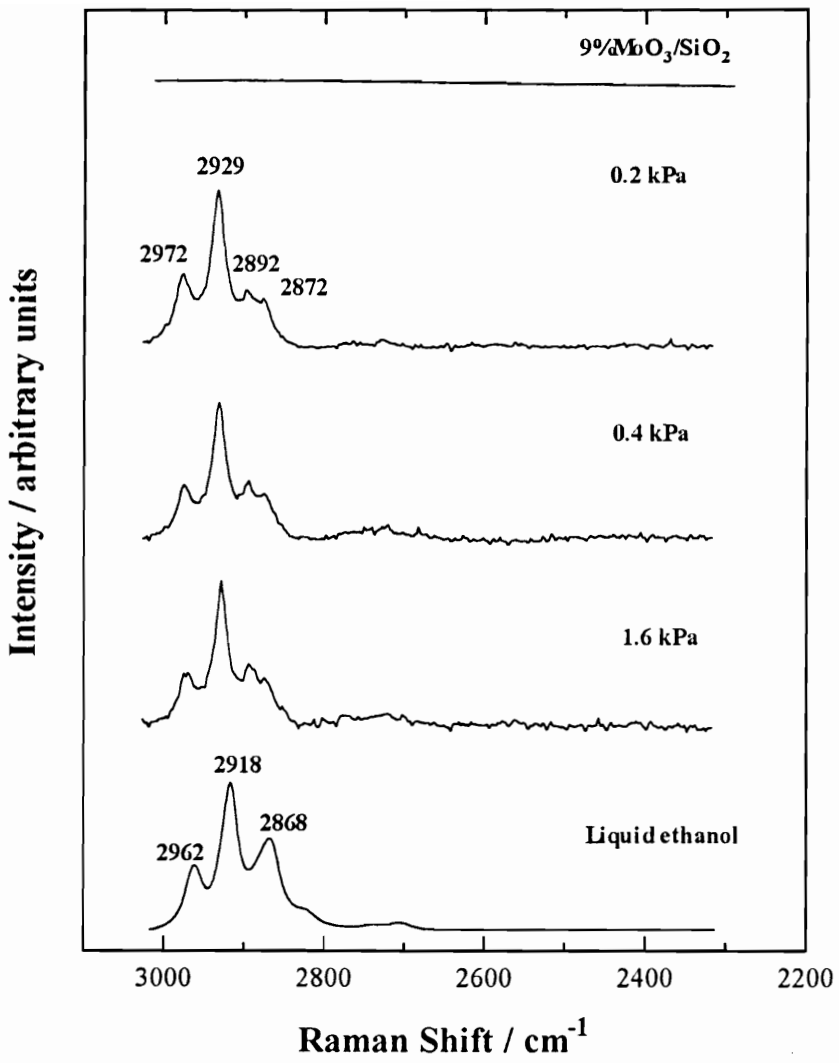

Figure 3.4. Raman study of ethanol adsorption on 9% MoO_3/SiO_2 at RT in the high frequency region.

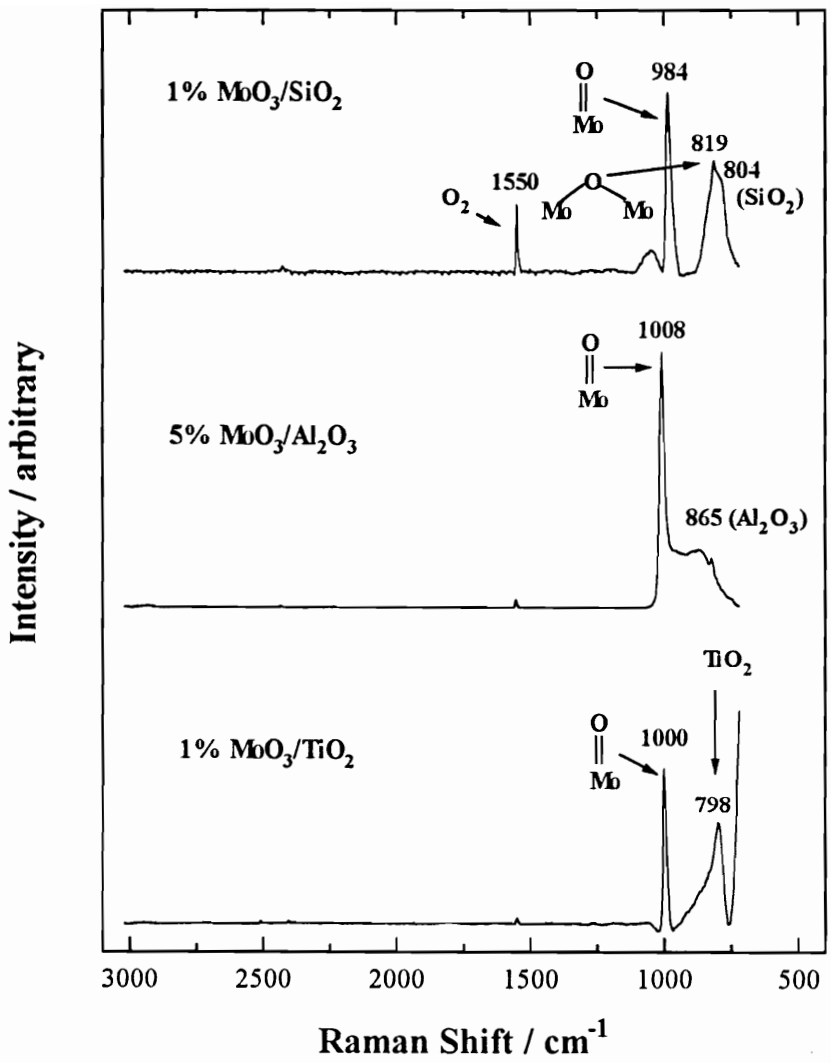

Figure 3.5. Raman spectra of 1% MoO_3/SiO_2, 5% MoO_3/Al_2O_3, and 1% MoO_3/TiO_2 after pretreatment in O_2 at 723 K for 3 h.

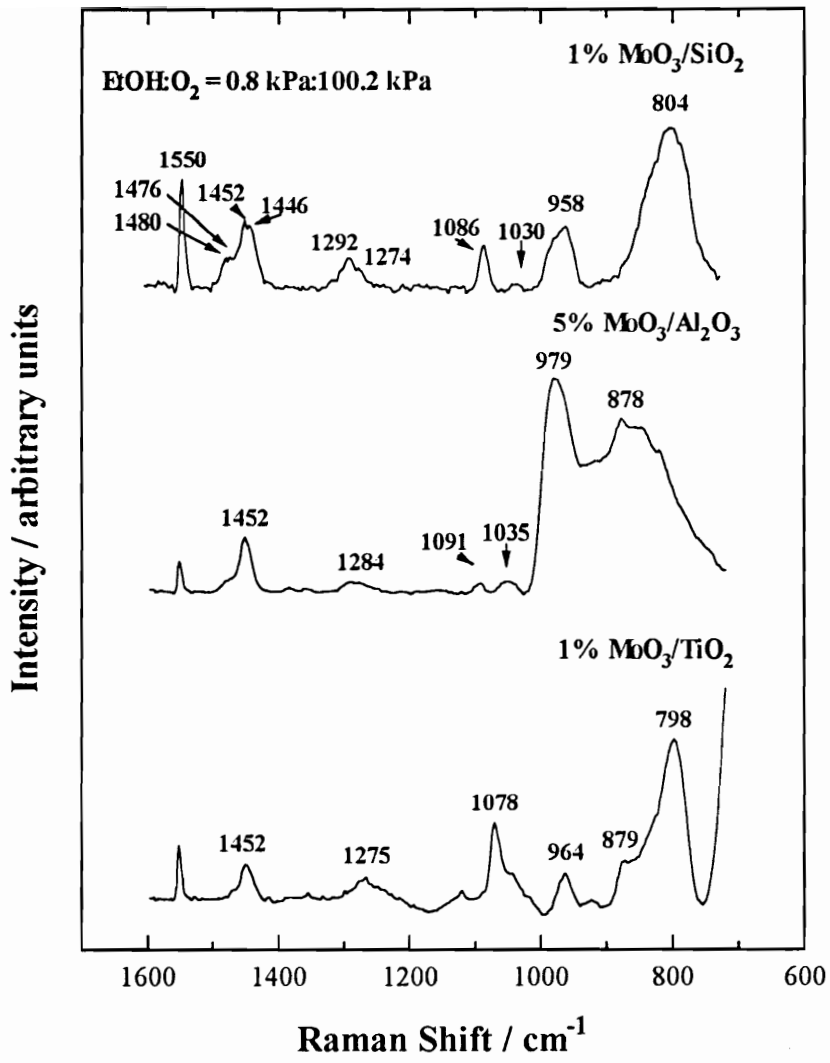

Figure 3.6. Raman study of ethanol adsorption on supported MoO_3 catalysts at RT in the low frequency region.

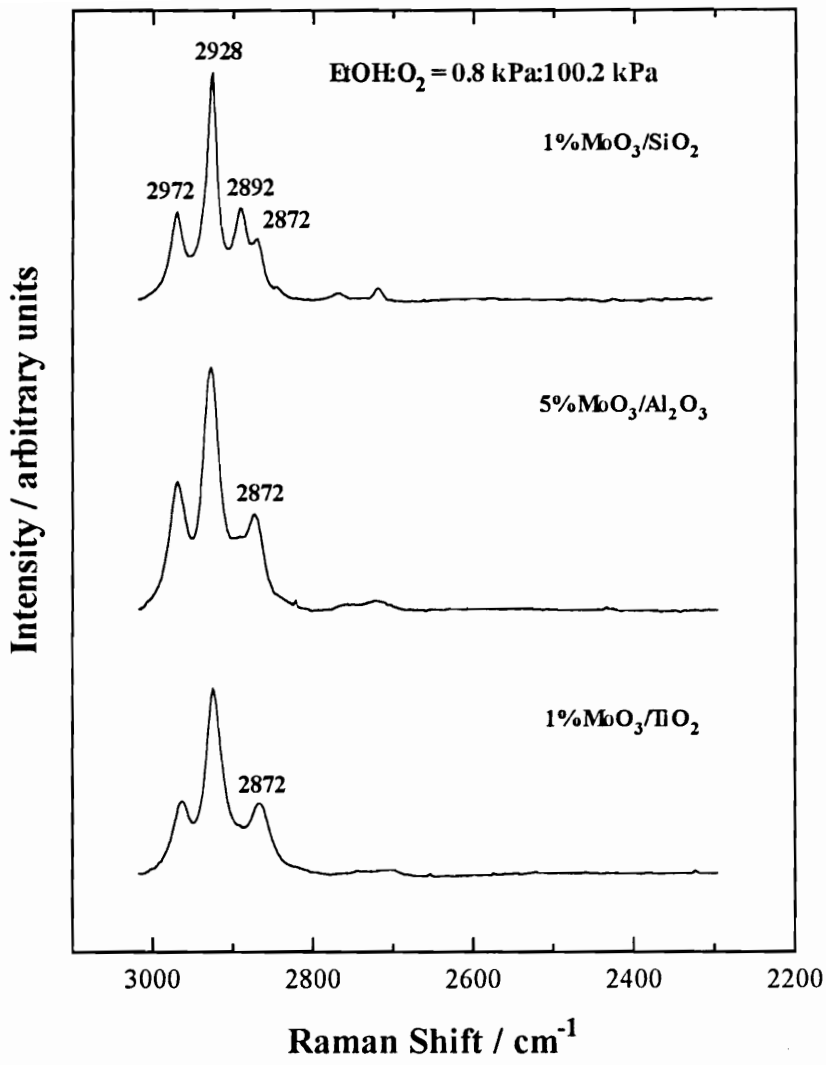

Figure 3.7. Raman study of ethanol adsorption on supported MoO_3 catalysts at RT in the high frequency region.

whereas the band at 865 cm^{-1} is due to the alumina support as verified with a blank experiment in the present study. The Raman band at 1000 cm^{-1} on 1% MoO_3/TiO_2 can be assigned to the terminal Mo=O stretching mode associated with the isolated surface molybdate species,[37] whereas the band at 798 cm^{-1} is due to a second-order feature of TiO_2.[38]

Figures 3.6 and 3.7 compare the Raman spectra of ethanol adsorbed at 298 K on these catalysts. Ethanol adsorption induces a peak shift of the Mo=O stretching mode towards low frequency to different degrees on different samples. The shift is from 984 to 958 cm^{-1} on 1% MoO_3/SiO_2, from 1008 to 979 cm^{-1} on 5% MoO_3/Al_2O_3, and from 1000 to 964 cm^{-1} on 1% MoO_3/TiO_2. The sample color for all three catalysts changes from white to blue indicating reduction. New Raman bands developed from ethanol adsorption on the samples are similar in peak position to those obtained on 1% MoO_3/SiO_2. They can be assigned to ν(CCO)(878-879 and 1030-1035 cm^{-1}), $\rho(CH_3)$ (1078 - 1091 cm^{-1}), $tw(CH_2)$ (1274 - 1292 cm^{-1}), $w(CH_2) + \delta_{as}(CH_3)$ (1446 - 1452 cm^{-1}), $\delta_s(CH_2)$ (1476 - 1480 cm^{-1}), $\nu_s(CH_2)$ (2872 - 2892 cm^{-1}), $\nu_s(CH_3)$ (2928 cm^{-1}), and $\nu_{as}(CH_3)$ (2972 cm^{-1}).[35,36] It is notable that the band at 2892 cm^{-1} present on 1% MoO_3/SiO_2 does not appear on 5% MoO_3/Al_2O_3 and 1% MoO_3/TiO_2, and that the bands at 1480 and 1452 cm^{-1} are not split in the latter samples. The weak bands at 878 cm^{-1} on 5% MoO_3/Al_2O_3 and 879 cm^{-1} on 1% MoO_3/TiO_2 indicate the presence of trace amounts of molecular ethanol. All the features associated with the CH_2 groups on 1% MoO_3/SiO_2 are split, as will be discussed

later, this is due to the presence of two different ethoxy groups, one characterized with $\nu_s(CH_2)$ = 2872 cm^{-1} and the other with $\nu_s(CH_2)$ = 2892 cm^{-1}.

Figure 3.8 presents the results of water adsorption on 1% MoO_3/SiO_2 at 298 K. The intense and broad Raman band centered at about 400 cm^{-1} is due to amorphous silica.[33] Introduction of water at different partial pressures causes a dramatic decrease in the intensity of the Raman bands from the Mo=O and Mo-O-Mo structures and silica, and a peak shift for the Raman band of the Mo=O asymmetric stretching mode from 984 to 974 cm^{-1}. The sample color changes slightly from white to light blue. No new Raman bands are observed in the hydroxyl region, probably because of the known small Raman scattering cross section of OH.

Figure 3.9 presents plots of the signal in the C-H stretching region versus ethanol partial pressure at 448, 473 and 498 K using the reaction mixture. The intensity of the bands increases with ethanol partial pressure and decreases with temperature, and is proportional to the surface ethoxide concentration (coverage). Figure 3.10 presents a plot of the intensity of the Mo=O asymmetric stretching mode at 984 cm^{-1} versus ethanol partial pressure at 448 K. The intensity of the 984 cm^{-1} band is seen to decrease with increasing ethanol partial pressure. The shoulder band at 986 cm^{-1} is due to a surface carbonate structure produced by the decomposition of ethoxy groups.[39] The increase in coverage and decrease in the relative intensity of the 984 cm^{-1} band can be clearly seen in Figure 3.11.

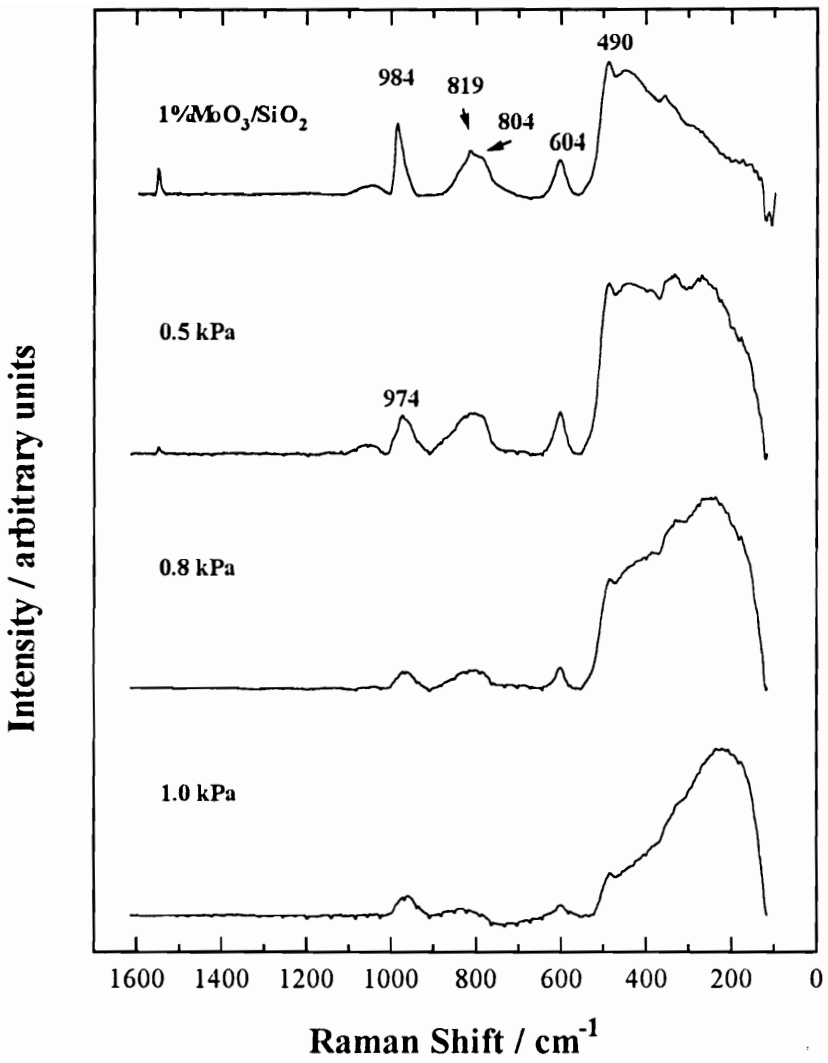

Figure 3.8. Raman study of water adsorption on 1% MoO_3/SiO_2 at RT.

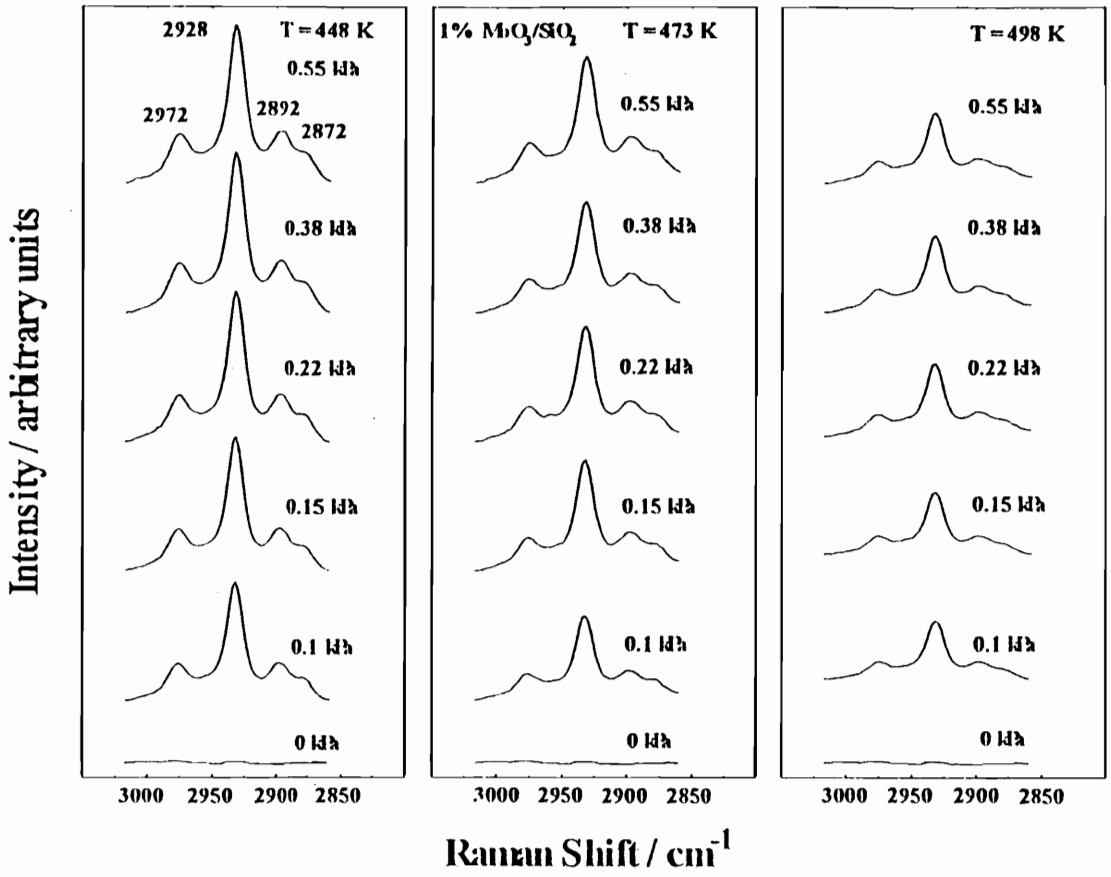

Figure 3.9. Dependence of the intensity of C-H stretching bands on ethanol partial pressure at different reaction temperature on 1% MoO_3/SiO_2.

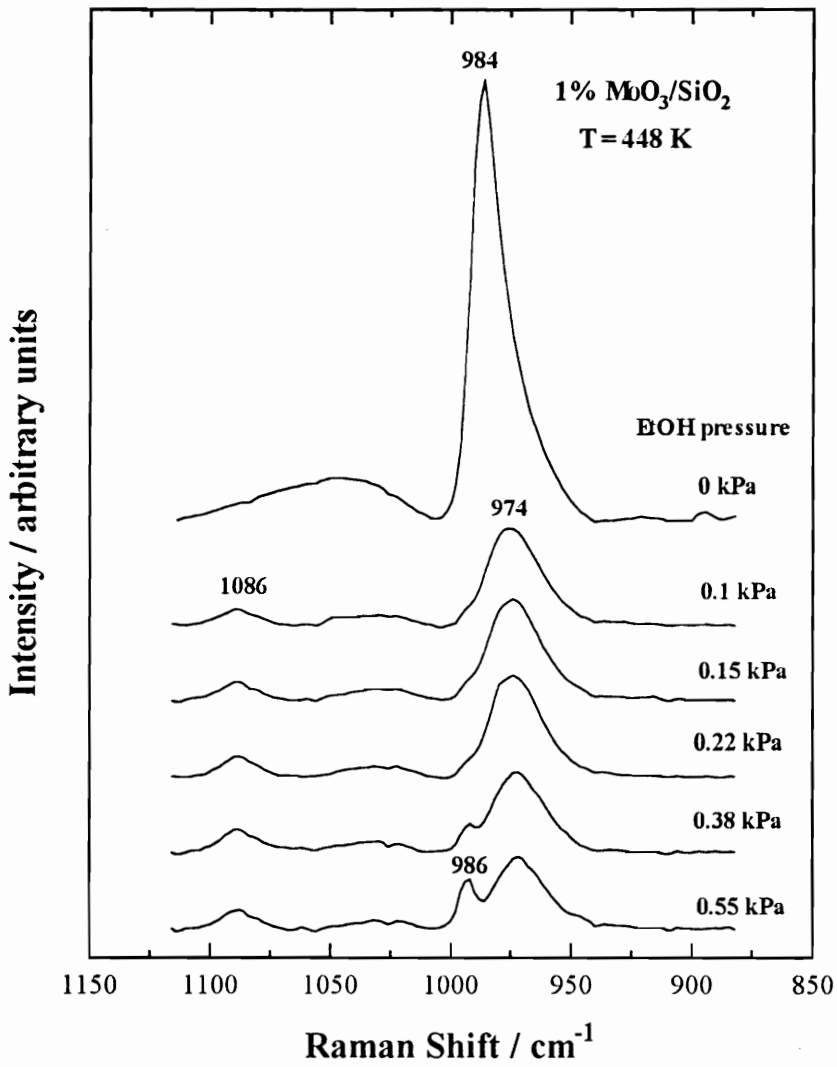

Figure 3.10. Waterfall plot of the Mo=O stretching band with ethanol partial pressure at 448 K on 1% MoO_3/SiO_2.

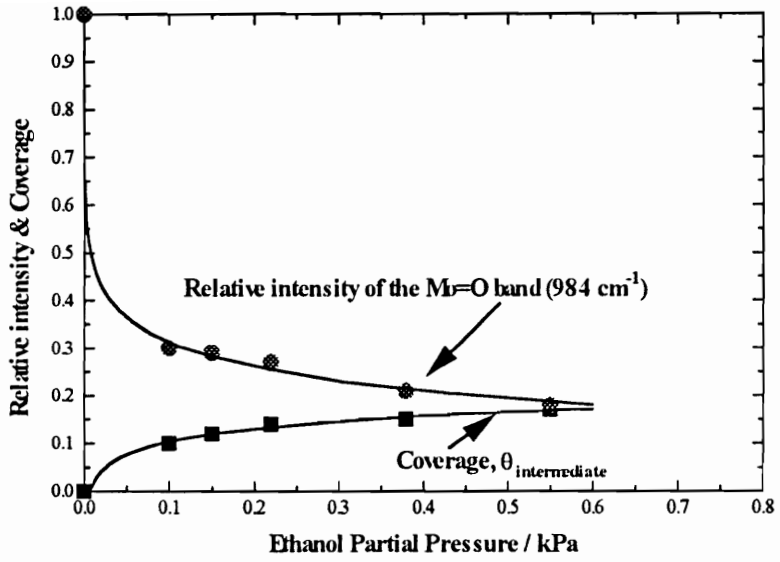

Figure 3.11. Coverage and relative intensity of the Mo=O band dependence on ethanol partial pressure at 448 K.

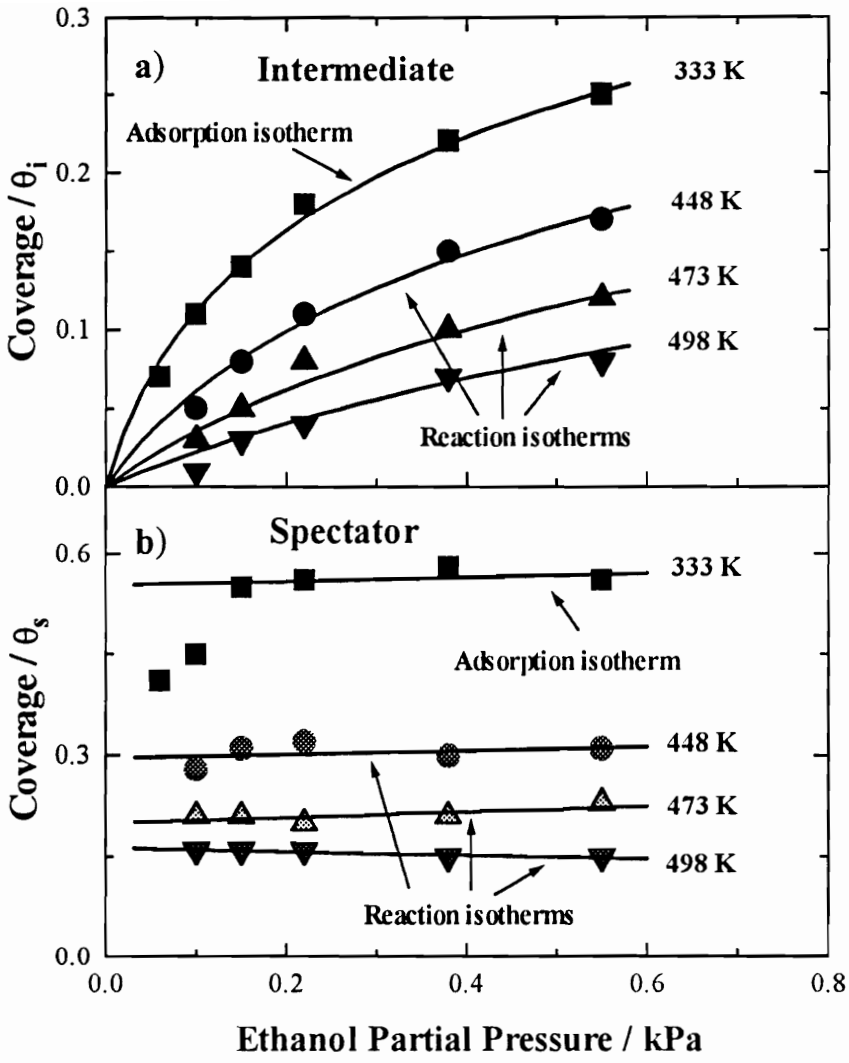

Figure 3.12. Reaction and adsorption isotherms on 1% MoO_3/SiO_2. a) The coverage with the ethoxide species with $\nu(CH_2) = 2872\ cm^{-1}$ b) the coverage with the species with $\nu(CH_2) = 2892\ cm^{-1}$.

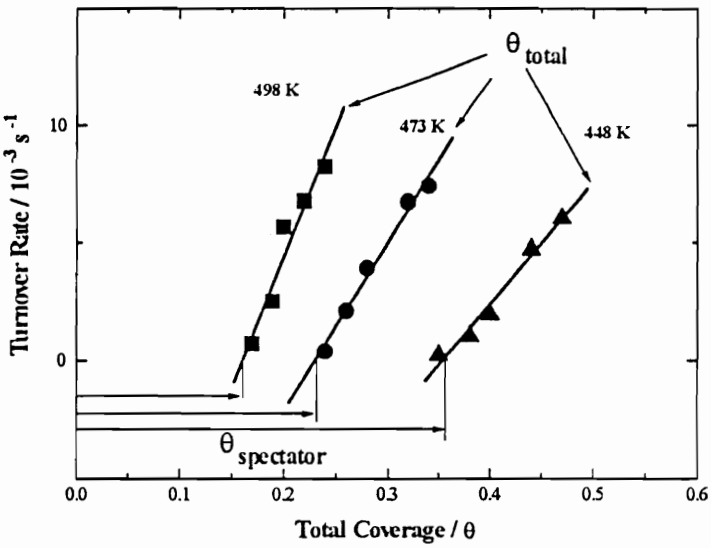

Figure 3.13. Turnover rate dependence on coverage on 1% MoO_3/SiO_2.

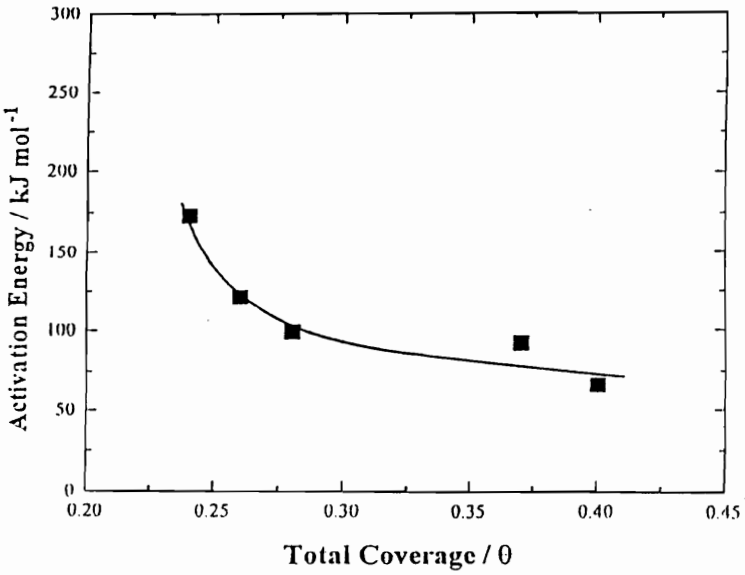

Figure 3.14. Activation energy dependence on coverage on 1% MoO_3/SiO_2.

The strong signals in the $\nu(CH_2)$ stretching region (deconvoluted) are used to define a coverage scale. This is based on a careful study of the change of surface concentration of the two types of adsorbed ethoxy groups with ethanol partial pressure and temperature. In this case, saturation is observed with an ethanol and helium mixture at 298 K. The saturation concentration can be regarded to be the full surface coverage with both species ($\theta = 1$). Other coverages can then be obtained by deconvoluting the $\nu(CH_2)$ peaks and normalizing the peak areas of the adsorbed ethoxy groups to the saturation peak area, where the calculations are made taking the defect mode of amorphous silica[33] at 604 cm^{-1} as an internal standard.

Figure 3.12 shows coverage versus partial pressure versus coverage in the form of isotherms for the two ethoxy species ($\nu(CH_2)$ = 2872 and 2892 cm^{-1}). In the top panel the coverage with the ethoxide group with $\nu(CH_2)$ = 2872 cm^{-1} decreases with increasing temperature, but at a fixed temperature increases rapidly to saturate at high ethanol partial pressures. In the bottom panel of Fig. 12 are shown the coverages with the ethoxide group with $\nu(CH_2)$ = 2892 cm^{-1}. As can be seen the curves are essentially flat indicating that the coverage with this species does not change with reaction conditions.

Figure 3.13 presents the turnover rate dependence on coverage. The rates increase linearly with increasing coverage for all three reaction temperatures. Selectivity to acetaldehyde is about 99% under the reaction conditions. Isosteric activation energies can be obtained by plotting the natural logarithm of the rates versus 1/T at fixed coverages.

Table 3.1. Isotopic substitution results

Catalysts	Temp. (K)	v_H / v_D [a]		
		C_2H_5OD	CD_3CH_2OH	CH_3CD_2OH
9% MoO_3/SiO_2	488	1.04	-	-
	508	1.06	1.33	2.20
15% MoO_3/Al_2O_3	423	1.19	1.25	2.08
9% MoO_3/TiO_2	413	1.04	1.08	1.70

[a] v is turnover rate.

The results are displayed in Figure 3.14. Clearly, the activation energy decreases monotonically with coverage.

3.3.2. Isotopic substitution studies

The results of isotopic substitution are summarized in Table 3.1. The turnover rate ratio (v_H/v_D) for C_2H_5OH oxidation versus C_2H_5OD was just slightly higher than unity. In contrast, the value of v_H/v_D for the CD_3CH_2OH substitution was moderately higher than unity (v_H/v_D = 1.2), while that for the CH_3CD_2OH substitution was even higher (v_H/v_D = 2). Selectivities of the various products change significantly for the CD_3CH_2OH and CH_3CD_2OH substitutions. In the case of CH_3CD_2OH substitution, the selectivity to diethyl ether increases by a factor of 2-3, while the selectivity of acetaldehyde drops dramatically. In the case of CD_3CH_2OH substitution, the selectivity to ethylene drops significantly on 9% MoO_3/SiO_2 and 15% MoO_3/Al_2O_3. At the chosen temperature, no ethylene is produced on 9% MoO_3/TiO_2.

3.3.3. Kinetics studies

Detailed kinetic studies of the effect of C_2H_5OH, O_2, and H_2O partial pressures are reported in another publication.[40] The observed rate expression was of a power-rate-law form $v_{CH3CHO} = k\, P_{C2H5OH}^{0.86}\, P_{H2O}^{-0.26}\, P_{O2}^{0.24}$.

Ethanol oxidation on 9% MoO_3/SiO_2 produced about 80 % acetaldehyde, 15% diethyl ether and less than 5% ethylene. Other than the three main products, small amounts of acetic acid and ethyl acetate at selectivities < 2% are also observed. No CO_x formation is detected at the chosen conditions.

3.4. Discussion

3.4.1. *In situ* laser Raman spectroscopy

In situ laser Raman studies of reaction kinetics have been a challenging area in catalytic science for the past twenty years.[41] In the literature, no reports conventional Raman studies of actual adsorbed reaction intermediates are found. The results here are obtained with a state-of-the-art Raman spectrometer incorporating a 0.5 m single monochromator equipped with a liquid nitrogen cooled CCD detector. A recently

developed holographic super-notch-plus filter is used to remove the Rayleigh line from the signal and allows the use of the short, high-light-throughput monochromator.

Chapter 2 presented preliminary laser Raman spectroscopy evidence for the existence of two types of adsorbed ethoxy groups associated with the Mo=O and Mo-O-Mo structures for ethanol oxidation on 1% MoO_3/SiO_2 under reaction conditions. In addition, the laser Raman and MoO_3 loading studies suggested that acetaldehyde, diethyl ether, and ethylene were produced on different sites. In order to elucidate the mechanism of the reaction, a combined *in situ* laser Raman and kinetic investigation was carried out in this chapter.

Figures 3.1 and 3.2 show the Raman results of ethanol adsorption on 1% MoO_3/SiO_2 at 298 K. The decrease in the intensity of the 984 and 818 cm^{-1} bands with ethanol partial pressure, together with the peak shift of the 984 cm^{-1} band to 965 cm^{-1} and the sample color change from white to blue, suggests a sample reduction.[30] The new features developed from ethanol adsorption at 1030 (ν(CCO)), 1274 and 1294 ($tw(CH_2)$), 1446 and 1452 ($w(CH_2) + \delta_{as}(CH_3)$), 1476 and 1480 ($\delta_s(CH_2)$), 2872 and 2892 ($\nu_s(CH_2)$), 2928 ($\nu_s(CH_3)$), 2972 cm^{-1} ($\nu_{as}(CH_3)$) are derived from the two types of ethoxy groups associated with the Mo=O and Mo-O-Mo sites (see Chapter 2). Because of the similarity in structure between the two species, their Raman spectra are very similar and are substantially overlaped, thus resulting in broadened spectra. However, the two can be distinguished from their $\delta s(CH_2)$, and $w(CH_2)$ doublets, and even more, from their resolved $\nu_s(CH_2)$ stretch vibrational modes, which appear separated at 2872 and 2892 cm^{-}

[1]. Schematic representations of their structure are included in Fig. 3.2. It is possible that ethanol adsorbs across a Mo=O bond to form an ethoxide species and a hydroxyl group. As will be seen, these two ethoxide adsorption modes behave differently under reaction conditions, indicating substantial differences in reactivity between the two species.

The presence of adsorbed ethoxy groups derived from dissociated ethanol was infered from the conversion of the strong CCO skeletal vibration at 878 cm^{-1} to a weak band at 1030 cm^{-1} as predicted by the *ab initio* calculations of Uvdal *et al.*[35] In order to differentiate molecularly adsorbed ethanol from adsorbed ethoxy groups, a transient experiment was performed by dosing 170 μmol liquid ethanol (P_{max} = 10 kPa) into the Raman cell with O_2 flowing. This dosage presumably generated a condensed layer of molecularly adsorbed ethanol. In fact, two more Raman bands at 878 and 1044 cm^{-1} corresponding to the CCO stretching modes of liquid ethanol were observed after dosing ethanol. This finding confirms the assignment of dissociative adsorption of ethanol into ethoxy groups on 1% MoO_3/SiO_2.

As is mentioned in the experimental section, the 9% MoO_3/SiO_2 sample was chosen for the kinetics study because of its long life. However, all the *in situ* Raman studies were carried out on the 1% MoO_3/SiO_2 since this well dispersed sample could be used to clarify the role of the different surface sites (Mo=O, Mo-O-Mo) and the structure of the adsorbed intermediates (see Chapter 2). In order to verify that the Raman results from the 1% MoO_3/SiO_2 could also be applied to the 9% MoO_3/SiO_2 sample, a study of ethanol adsorption at different partial pressures on 9% MoO_3/SiO_2 at RT was also

performed. The results are plotted in Figures 3.3 and 3.4. Similar to ethanol adsorption on 1% MoO_3/SiO_2, the sample color change from white to blue with ethanol partial pressure is followed by a peak shift of the Raman bands associated with the Mo=O and Mo-O-Mo bonds from 997 and 823 cm^{-1} to 989 and 813 cm^{-1}, respectively, indicating sample reduction. In analogy to ethanol oxidation on 1% MoO_3/SiO_2, the Raman bands at 2872 and 2893, 2929, and 2972 cm^{-1} can be assigned to $\nu_s(CH_2)$, $\nu_s(CH_3)$, and $\nu_{as}(CH_3)$ associated with the two types of ethoxy groups adsorbed on the Mo=O and Mo-O-Mo sites. The other weak features from these ethoxy groups are covered by the intense Raman bands of crystalline MoO_3 at 997, 823, and 673 cm^{-1}.

Figure 3.5 presents the standard Raman spectra of 1% MoO_3/SiO_2, 5% MoO_3/Al_2O_3, and 1% MoO_3/TiO_2. The Raman bands at 984 cm^{-1} on 1% MoO_3/SiO_2, 1008 cm^{-1} on 5% MoO_3/Al_2O_3 and 1000 cm^{-1} on 1% MoO_3/TiO_2 can be assigned to the terminal Mo=O stretching mode associated with isolated surface molybdate species.[30,37] The band at 819 cm^{-1} characteristic of small crystallites of MoO_3 is not observed on 5% MoO_3/Al_2O_3 and 1% MoO_3/TiO_2, suggesting that MoO_3 is better dispersed on Al_2O_3 and TiO_2 at the present loadings. Raman spectra of adsorbed ethanol are shown in Figures 3.6 and 3.7. Ethanol adsorption induces a peak shift of the Mo=O stretching band to low frequency and a reduction in its intensity to different degrees on all three catalysts, suggesting that the Mo=O bond reacts with ethanol. A sample color change from white to blue indicates sample reduction. The new Raman bands from ethanol adsorption on 1% MoO_3/SiO_2 have been assigned to two types of ethoxide intermediates associated with the

Mo=O and Mo-O-Mo bonds. The new bands from ethanol adsorption on 5% MoO_3/Al_2O_3 and 1% MoO_3/TiO_2 are very close to those on 1% MoO_3/SiO_2 in peak position. Importantly, only the species with $\nu_s(CH_2)$ at 2872 cm^{-1}, assigned to the reactive ethoxide structure found on 1% MoO_3/SiO_2, is present on 5% MoO_3/Al_2O_3 and 1% MoO_3/TiO_2. In addition, all the Raman bands associated with CH_2 vibration modes are not split on the Al_2O_3- and TiO_2-supported samples. Together with the absence of the Mo-O-Mo vibration modes on the catalysts, these results strongly suggest that only one type of ethoxide intermediate exists on 5% MoO_3/Al_2O_3 and 1% MoO_3/TiO_2, and can be associated with the Mo=O bond. The similarity in the adsorbed ethoxy intermediates for the SiO_2-, Al_2O_3-, and TiO_2-supported samples is consistent with the earlier findings of the same activation energy for reaction, and, as will be seen, the isotope effects.

Another interesting aspect of the system is the adsorption behavior of water, an important byproduct from ethanol oxidation. Since the introduction of water at reaction temperature induced a high level of fluorescence covering all Raman signals of interest, the Raman study of water adsorption was performed at RT. The results are shown in Figure 3.8. Water adsorption at different partial pressure causes a decrease in the intensity of the Raman bands at 984 and 819 cm^{-1} and a sample color change from white to blue. This strongly suggests that water also adsorbs on molybdenum oxide, and is consistent with the negative order obtained in the kinetic studies. Water adsorption induces fluorescence at high water partial pressures and high temperatures, and makes the discussion about its precise role in the reaction very difficult.

Figure 3.9 presents the dependence of the surface ethoxide signal (represented by the C-H stretching region) on ethanol partial pressure at a reaction temperature of 448, 473, and 498 K. Integration of the areas under the peaks gives the total surface ethoxide concentration. The areas under the 2872 and 2892 cm^{-1} peaks give, respectively, the amounts of the two ethoxide species. Our previous results in Chapter 2 over a larger temperature range showed that the peak at 2872 cm^{-1} decreased with temperature, while that at 2892 cm^{-1} was relatively insensitive to temperature. From this it was suggested that the peak at 2872 cm^{-1} corresponded to an actual reaction intermediate, while that at 2892 cm^{-1} was associated with a relatively unreactive surface spectator. The results of Fig. 3.9 show a similar behavior towards pressure. Integration of the areas under the peaks shows that the 2872 cm^{-1} peak responds sensitively, but the peak at 2892 cm^{-1} is more sluggish (This is confirmed in Fig. 12). Figure 3.10 presents the dependence of the intensity of the Mo=O asymmetric stretching mode at 984 cm^{-1} on ethanol partial pressure at 448 K. Like the 2872 cm^{-1} peak, it also shows considerable sensitivity to ethanol partial pressure. At higher pressures of ethanol, a new peak at 986 cm^{-1} is observed due to a surface carbonate. The carbonate is only seen in a limited temperature range; it is not present at low or high temperatures (See Chapter 2). It can also be considered to be an unreactive spectator, leading to the formation of CO_2. Figure 3.11 summarizes the results from Figures 3.9 and 3.10 at 448 K, and shows that the coverage with the ethoxide intermediate (2872 cm^{-1}) increases with ethanol partial pressure, whereas the intensity of

the 984 cm^{-1} band decreases with ethanol partial pressure indicating the reaction of the terminal bonded oxygen site. Similar results were obtained at 473 and 498 K.

Figure 3.12 reports coverages as a function of ethanol partial pressure for the two ethoxide species. The top panel for the species with $\nu(CH_2)$ = 2872 cm^{-1} shows that the civerages increase with ethanol pressure, but decrease with temperature. The three bottom isotherms of the panel were obtained at temperatures where ethanol was oxidized, and are reaction isotherms. The top isotherm, however, was obtained at low temperature and represents an equilibrium adsorption isotherm. All four data sets could be fit (curves) to a single logarithmic isotherm, the Frumkin-Temkin isotherm. The significance of this will become clear shortly. The bottom panel of Fig. 12 shows that the coverage with the ethoxide species, characterized by $\nu(CH_2)$ = 2892 cm^{-1}, does not change with pressure. Clearly it does not respond to reaction conditions, and can be considered an inactive spectator on the surface.

Figure 3.13 presents the turnover rate dependence on coverage. At these reaction temperatures, the selective oxidation product is predominantly acetaldehyde at a selectivity of 99%. This is probably the most important result of this paper. It shows some expected behavior: the rate increases with coverage and temperature, but coverage decreases with temperature; this is the behavior precisely expected for a reactive intermediate. However, peculiarly, the rates do not extrapolate to zero coverage. The reason for this is the presence of the unreactive spectator with $\nu_s(CH_2)$ at 2892 cm^{-1}. The true intermediate responds sensitively to pressure and temperature, where the spectator is

inert. The response of the intermediate to pressure follows that of the Mo=O bond (Fig. 3.11) indicating that the two are somehow associated as an adsorption complex.

Isosteric activation energies are plotted vs coverage in Figure 3.14. These activation energies were obtained by plotting the natural logarithm of the rates vs 1/T at fixed coverages. The activation energy decreases with coverage, strongly suggesting a non-uniform surface.[42]

3.4.2. Isotopic substitution studies

The deuterated ethanol substitution results are summarized in Table 3.1. The ratio of C_2H_5OH oxidation rate to C_2H_5OD oxidation rate is just slightly larger than unity, suggesting the formation of an ethoxide species in an equilibrated step before the rate-determining step. The ratio of C_2H_5OH to C_2H_5OD oxidation rates for 15% MoO_3/Al_2O_3 is slightly off from unity. This is due to a slight temperature variation during the experiment. Aside from this sample, the deviation from unity is small and consistent with an equilibrium isotope effect. The ratios of C_2H_5OH oxidation rate to CH_3CD_2OH oxidation rate are much greater than unity and suggest that α-hydrogen abstraction from the methylene groups is rate-determining for acetaldehyde formation on 9% MoO_3/SiO_2, 15% MoO_3/Al_2O_3, and 9% MoO_3/TiO_2. C_2H_5OH and C_2H_5OD give almost identical product distributions, but in the case of CH_3CD_2OH, the rate of acetaldehyde production decreases significantly giving rise to an increase in the selectivity to diethyl ether by a

factor of 2-3. The explanation for this is straightforward: no carbon-hydrogen bond needs to be broken for diethyl ether formation. The isotope effect on CH_3CD_2OH oxidation is different from sample to sample. The v_H/v_D values are 2.20 for 9% MoO_3/SiO_2, 2.08 for 15% MoO_3/Al_2O_3, and 1.70 for 9% MoO_3/TiO_2. This is due to the different selectivities to acetaldehyde on the different samples (The diethyl ether formation rate does not chnage). Under the chosen conditions, the selectivity to acetaldehyde is about 80% on 9% MoO_3/SiO_2, 77% on 15% MoO_3/Al_2O_3, and 60% on 9% MoO_3/TiO_2. Again, the ratio of C_2H_5OH to CD_3CH_2OH oxidation rate is greater than unity, suggesting that β-hydrogen abstraction is rate-determining for ethylene formation. In the case of CD_3CH_2OH oxidation on 9% MoO_3/SiO_2 and 15% MoO_3/Al_2O_3, a dramatic decrease in the rate of ethylene formation is observed. Overall, the results are consistent with the following sequence of steps:

$$CH_3CH_2OH + M^* + O^* \overset{K_1}{\rightleftharpoons} CH_3CH_2OM^* + HO^*$$

$$CH_3CH_2OM^* \overset{k_2}{\longrightarrow} CH_3CHO + HM^*$$

The symbol $\rightleftharpoons$ represents equilibrium adsorption, the symbol $\longrightarrow$ represent a rate-determining step, and while M* and O* represent metal and oxygen surface sites, respectively. Where K_1 is the equilibrium constant of the adsorption step, and k_2 is the rate constant of the rate-determining step. Other steps involving water formation and oxygen chemisorption are taken to be in equilibrium, and are omitted for clarity.

The results of Fig. 12a) can now be understood. Irrespective of whether reaction (high T) or simple adsorption (low T) occurs, the coverage with the reactive ethoxide species is governed by an equilibrium. The equilibrium expression is the logarithmic equation of Frumkin-Temkin,[42] characteristic of a non-uniform surface:

$\theta = \frac{1}{f}\ln(1 + K_1^0 P_{C2H5OH})$. The fitted parameters are f = 11 and

$K_1^0 = 0.058 \exp(-17 \text{ kJ mol}^{-1} / RT)$. The latter gives an adsorption entropy change of $\Delta S^0 = -24 \text{ J mol}^{-1} \text{ K}^{-1}$, which is reasonable for the adsorption of ethanol.

3.4.3. The kinetics

In the study of ethanol oxidation on MoO_3/SiO_2 prepared from organometallic precursors, Iwasawa *et. al.*,[43] showed that the partial pressure effects of ethanol and oxygen on rate can be described by a power rate law expression ($r = k P_{C2H5OH}^{0.2} P_{O2}^{0.5}$). A rate expression ($P_{C2H5OH} / r = 1 / k_1 + P_{C2H5OH} / 2k_2 \sqrt{P_{C2H5OH}}$) derived from a two-step redox mechanism was found to be consistent with the experiment results. However, this rate expression does not give a good description for the rates in the present case, because this mechanism omitted the effect of water inhibition, and because only one type of surface site (terminal Mo=O bond) was involved.

In a detailed study of the kinetics of the reaction (Chapter 4), it was found that the experimentally-found rate expression was $v_{CH3CHO} = k P_{C2H5OH}^{0.86} P_{H2O}^{-0.26} P_{O2}^{0.24}$. This was

approximated by a theoretical expression $v_{CH3CHO} = k\, P_{C2H5OH}^{1-m}\, P_{H2O}^{-1/2(1-m)}\, P_{O2}^{1/4(1-m)}$ derived using Temkin's theory of rates on non-uniform surfaces, which gave with m = 0.14, $v_{CH3CHO} = k\, P_{C2H5OH}^{0.86}\, P_{H2O}^{-0.43}\, P_{O2}^{0.21}$. The sequence of steps was the same as that deduced from the isotopic exchange experiments. The finding of a non-uniform surface on 1% MoO_3/SiO_2 by laser Raman spectroscopy is consistent with the Temkin expression found theoretically and the previously reported Frumkin-Temkin isotherms. The theory also predicts that the rate was given by $v_{CH3CHO} = k_2^0\theta$. This expression states that rate depends linearly on coverage, which is exactly what is obtained (Fig. 13). The slopes give the rate constant k_2^0. In this case the values are $k_2^0 = 0.10\ s^{-1}$ at 498 K, $k_2^0 = 0.080\ s^{-1}$ at 473 K, and $k_2^0 = 0.049\ s^{-1}$ at 448 K. The corresponding activation energy is $E_2^0 = 24$ kJ mol^{-1}, which is low compared to the values reported in Fig. 14. The reason is that k_2^0 is referred to full coverage,[42] whereas the isosteric values are obtained at lower coverages.

The kinetic results here give strong support to our preliminary findings using *in situ* laser Raman spectroscopy and reactivity measurements in Chapter 2, that the Mo=O sites are responsible for acetaldehyde formation. The study showed that the Mo=O bonds are initially reduced when ethanol adsorbs at 298 K and can be easily reoxidized at an intermediate reaction temperature (373 - 523 K) with a reaction mixture flowing. In contrast, the Mo-O-Mo bonds cannot be reoxidized even at 523 K after reduction at RT. The two ethoxide species associated with the Mo=O and Mo-O-Mo sites, thus have different reactivities. The ethoxide associated with the Mo=O double bond reacts readily to form acetaldehyde, while the ethoxide attached to the Mo-O-Mo site is relatively stable

and remains on the surface as a spectator. The study of the loading effects in Chapter 2 suggests that it is likely to be involved in the production of diethyl ether and ethylene, which are obtained at low rates at these conditions. This is the reason that the reactivity curves in Fig. 3.13 do not extrapolate to zero coverage. They extrapolate to the coverage of the spectator at a given temperature. Interestingly, although for MoO_3/SiO_2 two distinct CH_2 bands at 2872 and 2892 cm^{-1} are observed corresponding to two types of adsorbed ethoxide species. On the Al_2O_3- and TiO_2-supported samples only one bond at 2872 cm^{-1} for the reactive intermediate is observed (Fig. 3.8). The spectator appears to be absent in these samples.

Our results are consistent with the findings by Chung *et al.*[4,6] Based on an extensive IR study of methanol and water chemisorbed on unsupported molybdenum oxide, Chung *et al.* proposed that there were three types of methoxy groups present on MoO_3: a methoxy on the vacancy of a terminal bonded oxygen Mo=O (form A), a methoxy on the vacancy of a bridging oxygen Mo-O-Mo (form B), and a methanol molecule dissociated into methoxy and hydrogen across a Mo=O bond (form C). They also proposed that form B was responsible for the formation of byproducts such as dimethyl ether, dimethoxymethane and ethyl formate. The investigation here cannot distinguish between form A and C, but the data are consistent with either form.

In summary this study presents a detailed mechanistic investigation of ethanol oxidation on supported molybdenum oxide. As far as is known this is the first study in which two types of adsorbed intermediates were observed, one a true reactive

intermediate and the other a surface spectator, which was the most abundant species on the surafce.

3.5. Conclusions

1. Selective oxidation products from ethanol oxidation on molybdenum oxide are produced through ethoxide type intermediates adsorbed on different sites.

2. Deuterium isotope effect measurements on 9% MoO_3/SiO_2, 15% MoO_3/Al_2O_3, and 9% MoO_3/TiO_2 indicate that the same mechanism controls ethanol oxidation over the different supported catalysts: ethanol adsorbs through an equilibrated step to form ethoxide intermediates, α-hydrogen abstraction from ethoxy groups is rate-determining for acetaldehyde formation and β-hydrogen abstraction is rate-determining for ethylene formation.

3. The kinetics for ethanol oxidation over 9% MoO_3/SiO_2 can be modeled using the Temkin's theory of rates on non-uniform surface.

4. *In situ* laser Raman measurements show that there are two types of adsorbed ethoxy groups. One is associated with Mo=O bonds and is a true reactive intermediate, the other is associated with Mo-O-Mo bonds and is an unreactive spectator on the surface.

3.6. References:

(1). Pernicone, N.; Altering, G.; and Lanzavecchia, G. *J. Catal.* **1969**, 14. 293.

(2). Edwards, J.; Nicollaidis, J.; Cutlip, M. B.; and Bennett, C. O. *J. Catal.* **1977**, 50, 24.

(3). Chung, J. S.; and Bennett, C. O. *J. Catal.* **1985**, 92, 173.

(4). Chung, J. S.; Miranda, R.; and Bennett, C. O. *J. Chem. Soc. Faraday Trans. I*, **1985**, 81, 19.

(5). Chung, J. S.; and Bennett, C. O. *J. Chem. Soc. Faraday Trans. I*, **1986**, 82, 2155.

(6). Chung, J. S.; Miranda, R.; and Bennett, C. O. *J. Catal.* **1988**, 114, 398.

(7). Farneth, W. E.; Ohuchi, F.; Staley, R. H.; Chowdhry, U.; and Sleigh, A. W. *J. Phys. Chem.* **1985**, 89, 2493.

(8). Tatibouët, J. M.; and Germain, J. E. *J. Catal.* **1981**, 72, 375.

(9). Tatibouët, J. M.; Germain, J. E.; and Volta, J. C. *J. Catal.* **1983**, 82, 240.

(10). Ohuchi, F.; Firment, L. E.; Chowdhry, U.; and Ferretti, A. *J. Vac. Sci. Technol.* **1985**, A2, 1022.

(11). Chowdhry, U.; Ferretti, A.; Firment, L. E.; Machiels, C. J.; Ohuchi, F,; Sleight, A. W.; and Staley, R. H. *Appl. Surf. Sci.* **1984**, 19. 360.

(12). Machiels, C. J.; Cheng, W. H.; Choedhry, U.; Farneth, W. E.; Hong, F.; Mc Carron, E. M.; and Sleight, A. W. *Appl. Catal.* **1986**, 25, 249.

(13). Machiels, C. J.; and Sleight, A. W. *J. Catal.* **1982**, 76, 238.

(14). Yang, T. J.; and Lunsford, J. H. *J. Catal.* **1987**, 103, 55.

(15). Cheng, W. H.; Chowdhry, U.; Ferretti, A.; Firment, L.; Groff, R. P.; Machiels, C. J.; McCarron, E. M.; Ohuchi, F.; Staley, R. H.; and Sleight, A. W. in"*Heterogeneous Catalysis*" (Shapiro, B. L. Eds.), pp. 165-81, Texas A&M Univ. Press, College Station, Texas, **1984**.

(16). Niwa, M.; Yamada, H.; and Murakami, Y. *J. Catal.* **1992**, 134,331.

(17). Kim, D. S.; and Wachs, I. E. *J. Catal.* In press.

(18). Weber, R. S. *J. Phys. Chem.* **1994**, 98, 2999.

(19). Allison, J. N.; and Goddard III, W. A. *J. Catal.* **1985**, 92, 127.

(20). Evmenenko, N. P.; and Gorrohkovatskii, Y. B. *Kinet. Katal.* **1969**, 10, 1071.

(21). Jiru, P.; Witchterlova, B.; Tichy, J. *Proc. Int. Cong. Catal. 3rd*, North Holland Pub. Co., Amsterdam, I, pp. 199 , **1964**.

(22). Holstein, W. L.; and Machiels, C. J. Unpublished work.

(23). Tatibouët, J. M.; and Germain, J. E. *J. Chem. Res.* **1981**, (S) 268; **1981**, (M) 3070.

(24). Iwasawa, Y.; Nakano, Y.; and Ogasawara, S. *J. Chem. Soc. Faraday Trans. I*, **1978**, 74, 2986.

(25). Ono, T.; Kamisuki, H.; Hisashi, H.; and Miyata, H. *J. Catal.* **1989**, 116, 303.

(26). Ono, T.; Nakagawa, Y.; Miyata, H.; and Kubokawa, Y. *Bull. Chem. Soc. Jpn.*, **1984**, 57, 1205.

(27). Iwasawa, Y.; and Tanaka, H. *Proc. Int. Congr. Catal., 8th*, Berlin, IV-381, **1984**.

(28). Iwasawa, Y.; Asakura, K.; Ishii, H.; and Kuroda, H. *Z. Phys. Chem.* **1985**, 144, 105.

(29). Alyea, E. C.; Brown, K. F.; Durham, L.; and Svazic, T. in"*Progress in Catalysis*", (Smith, K.J., and Sanford, E. C. Ed.), Elsevier Sci. Pub. B. V., pp. 309-14, **1992**.

(30). Zhang, W.; Desikan, A. N.; and Oyama, S. T. *J. Phys. Chem.* In press.

(31). Desikan, A. N.; Huang, L.; and Oyama, S. T. *J. Phys. Chem.* **1991**, 95 10050.

(32). Desikan, A. N.; Huang,, L.; and Oyama, S. T. *J. Chem. Soc., Faraday Trans. I*, **1992**, 88, 22.

(33). Chen, D. G.; Potter, B. G.; and Simmons, J. H. *J. Non-Crystall. Solids*, **1994**, 178, 135.

(34). Kim, D. S.; Wachs, I. E.; and Segawa, K. *J. Catal.* **1994**, 146, 268-277.

(35). Uvdal, P.; MacKerell Jr, A. D.; and Wiegand, B. C. *J. Elect. Spectr. Rel. Phenom.* **1993**, 64/65, 193.

(36). Mikawa, Y.; Brasch, J. W.; and Jakobsen, R. J. *Spectrochim. Acta* **1971**, 27A, 529.

(37). Hu, H.; and Wachs, I. E. *J. Phys. Chem.* **1995**, 99, 10897.

(38). Vuurman, M. A.; Stufken, D. J.; Oskam, A. *J. Mol. Catal.* **1992**, 76, 263.

(39). Little, L. H. "*Infrared Spectra of Adsorbed Species*", Academic Press, New York, **1966**.

(40). Zhang, W.; and Oyama, S. T. Submitted.

(41). Cooney, R. P.; Gurthoys, G.; and Tam, N. T. *Adv. Catal.* **1975**, 24, 293.

(42). Boudart, M.; and Djéga-Mariadassou, G. "*Kinetics of Heterogeneous Catalytic Reactions*", Princeton Univ. Press, **1984**.

(43). Iwasawa, Y.; Nakano, Y.; and Ogasawara, S. *J. Chem. Soc. Faraday Trans. I*, **1978**, 74, 2968.

Chapter 4

Non-Uniform Surface Kinetics with Two Types of Sites: The Case of Ethanol Oxidation on Molybdenum Oxide

4.1. Introduction

The Temkin theory of non-uniform surfaces was introduced in 1957[1] to explain the kinetics of ammonia synthesis on iron[2] and was generalized in 1965.[3] Since then the theory has been applied to a limited number of cases which include ammonia decomposition on polycrystalline tungsten[4] and molybdenum,[5] and ethene hydrogenation on supported palladium-gold clusters.[6]

The Temkin formalism is based on a two-step catalytic sequence:

Scheme I

$$M_1 + A_1 \rightleftharpoons B_1 + M_2$$

$$M_2 + A_2 \rightleftharpoons B_2 + M_1$$

where A_1 and A_2 are reactants, B_1 and B_2 are products, and M_1 and M_2 are active centers in the sense of Taylor.[7] An implicit assumption in Temkin's derivation is that M_1 and M_2 consist of one type of site, usually considered to be empty or occupied. A modification of

the above sequence, with the second step irreversible, has been used to explain the observed kinetics of ethanol oxidation to acetaldehyde.[8]

Scheme II

$$M_1 + A_1 \rightleftharpoons B_1 + M_2$$

$$M_2 + A_2 \xrightarrow{} B_2 + M_1$$

The symbol $\rightleftharpoons$ represents equilibrium and the symbol $\xrightarrow{}$ represents a rate-determining step. Reactivity measurements coupled with *in situ* laser Raman determination of the concentration of adsorbed ethoxide intermediates duly confirm that there is a distribution of sites of different activation energy, and that a non-uniform analysis is applicable.[9] However, the simple sequence employed cannot account for the full kinetics, which include water vapor, oxygen, as well as ethanol partial pressures. This chapter presents a rigorous extension of the Temkin analysis to allow handling of more complicated sequences. The key assumption is that there are two types of sites, one of which is a Temkin site and the other a uniform Langmuir site. An example of such a situation has been presented for the case of the hydroisomerization of pentane over supported platinum, but was not solved rigorously.[10] Although the results here are specific to the particular sequence of steps adopted, the method is general, and should be applicable to other sequences. The analysis shown here follows closely that presented by Boudart for two steps.[11] The paper concludes with the fitting of the kinetic model to

actual ethanol oxidation rate data.

4.2. Kinetic rate expression

The oxidation reaction of ethanol is assumed to involve two types of sites, metal sites and oxygen sites. The metal sites are considered to include vacant sites, M*, and sites with adsorbed ethoxide species, $CH_3CH_2OM^*$, or hydrogen atoms, H-M*. The oxygen sites are assumed to include vacant sites, *, and sites with adsorbed hydroxyl species, H-O*, or oxygen atoms, O*. The symbol * denotes active sites, and is used to more easily ascertain conservation of sites. As will be seen, two independent site balances are taken to give the total concentration of metal-type sites (M) and oxygen-type sites (L), respectively. The parenthesis are used to indicate surface concentrations.

The independence of the sites may seem contradictory, but is easily understood from the surface chemistry of oxides. A hydrocarbon like an alcohol can adsorb on a fully oxidized surface by simple addition across an M=O or M-O-M bond to form $CH_3CH_2OM^*$ and H-O* species.

The sequence of steps considered is shown below. The first two steps are essentially the two steps in the Temkin sequence and, as will be seen, are analyzed in the same manner. The third step represents the transfer of a hydrogen atom from a metal site to an oxygen site. It is assumed to occur very fast and not to be kinetically significant.[12] It is included because theoretical work indicates that hydride elimination reactions involve

the metal center, not a nearby oxygen atom or ligand.[12,13] The last steps are standard equilibrated steps. In the sequence k_i is the rate constant of step (i) and K_i is the equilibrium constant of step (i).

The fundamental assumption employed in the analysis is that the species involved with the oxygen sites behave kinetically like the other chemical species in the system. As will be seen, this permits their concentration to be factored out of the integral rate expression.

Scheme III

$$CH_3CH_2OH + M^* + O^* \underset{k_{-1}}{\overset{k_1}{\rightleftharpoons}} CH_3CH_2OM^* + H\text{-}O^* \quad (1)$$

$$CH_3CH_2OM^* \xrightarrow{k_2} CH_3CHO + H\text{-}M^* \quad (2)$$

$$H\text{-}M^* + O^* \xrightarrow{\text{fast}} M^* + H\text{-}O^* \quad (3)$$

$$2H\text{-}O^* \underset{}{\overset{K_4}{\rightleftharpoons}} H_2O + O^* + * \quad (4)$$

$$2^* + O_2 \underset{}{\overset{K_5}{\rightleftharpoons}} 2O^* \quad (5)$$

The equilibrium step (1), yields:

$$\frac{(M^*)}{(CH_3CH_2OM^*)} = \frac{k_{-1}}{k_1}\frac{(H-O^*)}{(CH_3CH_2OH)(O^*)} \quad (6)$$

A non-uniform surface may be considered to be formed from a number of domains or ensembles, not necessarily adjacent, differing in the heat of formation of adsorption complexes.[11] In the ensemble E_j, the site balance can be written as:

$$(M^*) + (CH_3CH_2OM^*) = (M)_j \quad \text{(Assuming (H-M*) is small)} \tag{7}$$

Where $(M)_j$ is the concentration of metal atom sites in ensemble i, and (H-M*) , the surface concentration of the H-M* species is assumed to be small because of its conversion to H-O* species. Combining equations (6) and (7) gives:

$$(CH_3CH_2OM^*) = (M)_j \frac{k_1(CH_3CH_2OH)(O^*)}{k_1(CH_3CH_2OH)(O^*) + k_{-1}(H-O^*)} \tag{8}$$

The turnover rate, v_t, in the ensemble E_j can be then expressed as:

$$v_t^j = \frac{k_2}{(M)_j}(CH_3CH_2OM^*) = \frac{k_2 k_1(CH_3CH_2OH)(O^*)}{k_1(CH_3CH_2OH)(O^*) + k_{-1}(H-O^*)} \tag{9}$$

Each ensemble contains dS' sites per cm^2. Assuming a continuous site distribution, the total rate, v, can be obtained by integrating the partial rates on each ensemble over the entire surface.

$$v = \int v_t^j dS_j' \tag{10}$$

The definitions of the rate constants and the Temkin site distribution function on non-uniform surfaces follows Boudart,[11]

$$k_1 = k_1^0 \exp\alpha(t - t_0) \tag{11}$$

$$k_{-1} = k_{-1}^0 \exp[(\alpha - 1)(t - t_0)] \tag{12}$$

$$k_2 = k_2^0 \exp[(\alpha - 1)(t - t_0)] \tag{13}$$

$$dS' = \frac{(M)\gamma \exp(\gamma t_0)}{[\exp(\gamma f)] - 1} \exp(-\gamma t) dt \tag{14}$$

Where k_i^0 is the rate constants referenced to zero coverage, α is the Brønsted transfer coefficient, t is a dimentionless affinity, f is defined as $f = t_0 - t_1$, and is the difference between the maximum and the minimum values of t, (M) is the total number of metal atom sites, and γ is a parameter characterizing the site distribution.

Substituting equations (9), (11), (12), (13), and (14) into equation (10) and simplifying the resulting equation, results in:

$$v = \frac{(M)\gamma}{[\exp(\gamma f)]-1}\int_{t_1}^{t_0}\frac{k_2{}^0 k_1{}^0(CH_3CH_2OH)(O^*)\exp[(\alpha-\gamma)(t-t_0)]}{k_1{}^0\exp(t-t_0)(CH_3CH_2OH)(O^*)+k_{-1}{}^0(H-O^*)}dt \quad (15)$$

An auxiliary variable is introduced[11] to integrate equation (15):

$$u = \frac{(M^*)}{(CH_3CH_2OM^*)} = \frac{k_{-1}}{k_1}\frac{(H-O^*)}{(CH_3CH_2OH)(O^*)} = u_0\exp(t_0-t) \quad (16)$$

Where: $u_0 = \frac{k_{-1}{}^0}{k_1{}^0}\frac{(H-O^*)}{(CH_3CH_2OH)(O^*)}$ (17)

Manipulating equation (16) gives:

$$\frac{u_0}{u} = \exp(t-t_0) \quad (18)$$

$$dt = -\frac{du}{u} \quad (19)$$

Replacing $\alpha - \gamma = m$, and substituting equations (16) - (19) into equation (15), then simplifying it, the total rate becomes:

$$v = -\frac{(M)\gamma}{[\exp(\gamma f)]-1}\frac{k_2{}^0 k_1{}^{0^{1-m}}(CH_3CH_2OH)^{1-m}(O^*)^{1-m}}{k_{-1}{}^{0^{1-m}}(H-O^*)^{1-m}}\int_{u_1}^{u_0}\frac{u^{-m}}{1+u}du \qquad (20)$$

The further hypothesis in the non-uniform surface analysis[11] concerning the limits u_0 and u_1 is that for the upper bound value of t, all sites are occupied, and for the lower bound value of t, all sites are empty. This means:

$$u_0 \rightarrow 0, \text{ and } u_1 \rightarrow \infty$$

and leads to:

$$\int_0^{\infty}\frac{u^{-m}}{1+u}du \equiv \frac{\pi}{\sin(\pi m)} \qquad (21)$$

Let us consider the site balance associated with the oxygen atom sites. Assuming adsorbed oxygen (O*) is the mari, site conservation yields:

$$(L) = (*) + (O^*) \qquad (22)$$

Where (L) is the total number of oxygen atom sites.

From the equilibrium step (5) in the reaction sequence, one can get:

$$(*) = \frac{(O^*)}{K_5^{1/2}(O_2)^{1/2}} \tag{23}$$

Where (O_2) is the oxygen concentration in the feed stream. Solving equations (22) and (23) together for (*) and (O*), gives:

$$(*) = \frac{(L)}{K_5^{1/2}(O_2)^{1/2} + 1} \tag{24}$$

$$(O^*) = \frac{(L)K_5^{1/2}(O_2)^{1/2}}{K_5^{1/2}(O_2)^{1/2} + 1} \tag{25}$$

$$(*)(O^*) = \frac{(L)^2 K_5^{1/2}(O_2)^{1/2}}{[K_5^{1/2}(O_2)^{1/2} + 1]^2} \tag{26}$$

Equilibrium step (4) yields:

$$(H - O^*)^2 = \frac{(H_2O)(O^*)(*)}{K_4} \tag{27}$$

Where (H_2O) is the water concentration in the feed stream. Substituting equation (26) into (27), and taking the square root of the right side of the resulting equation gives:

$$(H-O^*) = \frac{(L)K_5^{1/4}}{K_4^{1/2}} \frac{(O_2)^{1/4}(H_2O)^{1/2}}{K_5^{1/2}(O_2)^{1/2}+1} \tag{28}$$

With the further assumption that (O*) is the most surface abundant species:

$$(O^*) \cong (L) \text{ and } K_5^{1/2}(O_2) >> 1 \text{ (see equation (25))} \tag{29}$$

Equation (28) can be then simplified into:

$$(H-O^*) \cong \frac{(L)}{K_4^{1/2}K_5^{1/2}} \frac{(H_2O)^{1/2}}{(O_2)^{1/4}} \tag{30}$$

Substituting equations (21), (29) and (30) into equation (20), and using the definition of the turnover rate, $v_t = \frac{v}{(M)}$:

$$v_t = k(CH_3CH_2OH)^{1-m}(O_2)^{\frac{1}{4}(1-m)}(H_2O)^{-\frac{1}{2}(1-m)} \tag{31}$$

Where $k = \frac{\pi\gamma}{\sin(\pi m)[\exp(\gamma f)-1]} \frac{k_2{}^0 k_1{}^{0\,1-m}}{k_{-1}{}^{0\,1-m}} (K_4K_5)^{\frac{1}{2}(1-m)}$ (32)

Following Boudart and Djéga-Mariadassou [10] it can also be shown that the coverage,

$\theta = \frac{(CH_3CH_2OM^*)}{(CH_3CH_2OM^*)+(M^*)} = \frac{1}{1+u_0}$, is given by:

$$\theta = k_\theta\,(CH_3CH_2OH)^{1-m}(O_2)^{\frac{1}{4}(1-m)}(H_2O)^{-\frac{1}{2}(1-m)} \qquad (33)$$

$$\text{where } k_\theta = \frac{\pi\gamma}{\sin(\pi m)[\exp(\gamma f)-1]}\frac{{k_1}^{0\,1-m}}{{k_{-1}}^{0\,1-m}}(K_4K_5)^{\frac{1}{2}(1-m)} \qquad (34)$$

Thus, the rate is given by $v_t = {k_2}^0\theta$, as expected from the kinetic sequence (Scheme III).

The above expressions give the full dependence of the rate on the partial pressures of ethanol, oxygen and water. Interestingly, if only the two step sequence (Scheme II) at the beginning is used the results are very similar[8]:

$$v_t = k\,(CH_3CH_2OH)^{1\text{-}m} \qquad (35)$$

$$\text{Where } k = \frac{\pi\gamma}{\sin(\pi m)[\exp(\gamma f)-1]}\frac{{k_2}^0{k_1}^{0\,1-m}}{{k_{-1}}^{0\,1-m}} \qquad (36)$$

$$\text{and } \theta = \frac{\pi\gamma}{\sin(\pi m)[\exp(\gamma f)-1]}\frac{{k_1}^{0\,1-m}}{{k_{-1}}^{0\,1-m}}(CH_3CH_2OH)^{1\text{-}m} \qquad (37)$$

4.3. Kinetic results

A sample of 9% MoO_3/SiO_2 was used for the kinetic studies. Details of the catalyst preparation[14] and reactivity[8] studies have been reported earlier. To summarize, 1 g of powder was pretreated in a mixture of O_2 (8 kPa), H_2O (4 kPa) and He (89 kPa) for 1 h at 623 K. The kinetic measurements were then taken at 523 K by varying the partial pressures of the reaction mixture components: C_2H_5OH, O_2, H_2O and He. During each set of experiments, the partial pressure of only one component in the reaction mixture was varied while maintaining the total pressure constant by adjusting the partial pressure of He. The partial pressures of the components were varied from 0.1 kPa to 45 kPa for ethanol, from 2 kPa to 38 kPa for oxygen, and from 0.3 to 65 kPa for water. The total pressure was 1 bar, and the flow rate was maintained at 110 μmol s^{-1} (160 cm^3 min^{-1}). Analysis was done by gas chromatography.

Rates are expressed as turnover rates based on oxygen titration measurements.[14] Briefly, oxygen uptakes were measured by a pulse method on samples prereduced in hydrogen at moderate temperatures (600-640 K), below that at which bulk reduction occured. The method was independently calibrated by laser Raman spectroscopy at low loadings and by x-ray diffraction at high loadings.

Ethanol oxidation on 9% MoO_3/SiO_2 produced about 80% acetaldehyde, 15% diethyl ether, and less than 5% ethylene. Other than the three main products, small amounts of acetic acid and ethyl acetate at selectivities < 2% were also produced. No

CO_x formation was detected at the chosen conditions. The partial pressure effect for ethanol is positive for the three main products and slightly less than one, while the partial pressure effect of water is negative for all. The partial pressure effect of oxygen is slightly positive for acetaldehyde formation, but slightly negative for diethyl ether and ethylene production. With P_{C2H5OH}, P_{O2}, and P_{H2O} the partial pressures of ethanol, oxygen and water in the feed stream, the overall the results can be summarized as:

$$v_{CH3CHO} = k\ P_{C2H5OH}^{0.86}\ P_{H2O}^{-0.26}\ P_{O2}^{0.24}$$

$$v_{C2H4} = k'\ P_{C2H5OH}^{0.91}\ P_{H2O}^{-0.43}\ P_{O2}^{-0.15}$$

$$v_{(C2H5)2O} = k''\ P_{C2H5OH}^{1.4}\ P_{H2O}^{-0.31}\ P_{O2}^{-0.37}$$

The kinetics results for acetaldehyde production can be well described with m = 0.14 in the non-uniform surface expression (31):

$$v_t = k' P_{C2H5OH}^{0.86} P_{H2O}^{-0.43} P_{O2}^{0.21} \qquad (35)$$

The kinetics results presented here are in good agreement with previous findings in Chapters 2 and 3 using *in situ* laser Raman spectroscopy, isotopic substitution, and reactivity measurements that show that ethanol adsorbs through an equilibrated step into ethoxide intermediates, C-H bond cleavage is rate-determining for acetaldehyde formation,

and water adsorbs competitively with ethanol on the same sites. Analysis of reaction isotherms and coverages during reaction showed that the isosteric activation energy decreased with increasing coverage, supporting the use of a non-uniform surface analysis for the kinetics.

4.4. Conclusions

1. Temkin's theory of rates on non-uniform surfaces can be extended to the case of two independent sites on a surface.

2. The rate of ethanol oxidation on MoO_3/SiO_2 follows a power-rate law and can be modeled using a non-uniform surface consisting of metal and oxygen sites.

4.5. References

(1). Temkin, M. I. *Zhur. Fiz. Khim.* **1957**, 31, 1.

(2). Temkin, M. I.; and Pyzhev, V. *Acta Physicochim USSR* **1940**, 12, 217.

(3). Temkin, M. I. *Dokl. Akad. Nauk SSSR* **1965**, 161, 160.

(4). Shindo, H.; Egawa, C.; Onishi, T.; and Tamaru, K. *J. Chem. Soc. Faraday I* **1980**, 76, 280.

(5). Boudart, M.; Egawa, S.; Oyama, S. T.; and Tamaru, K. *J. Chim. Phys.* **1981**, 78, 987.

(6). Davis, R. J.; and Boudart, M. in "*Catalytic Science and Technology*", (Yoshida, S.; Takezawa, N.; and Ono, T. Eds.), Vol. 1, p. 129, Kodansha, Tokyo, **1990**.

(7). Taylor, H. S. *Proc. Roy. Soc. London A* **1925**, 108, 105.

(8). Zhang, W.; Desikan, A.; and Oyama, S. T. *J. Phys. Chem.*, In press.

(9). Zhang, W.; and Oyama, S. T. *J. Phys. Chem.*, Submitted.

(10). Boudart, M. and Djéga-Mariadassou, G. "*Kinetics of Heterogeneous Catalytic Reactions*", Princeton University Press, Princeton, New Jersey, **1984**, p. 115.

(11). Boudart, M. "*Kinetics of Chemical Processes*", Butterworth-Heinemann, Boston, **1991**.

(12). Weber, R. S. *J.Phys. Chem.* **1994**, 98, 2999.

(13). Koga, N.; Obara, S.; Kitaura, K.; and Morokuma, K. *J. Am. Chem. Soc.* **1985**, 107, 7109.

(14). Desikan, A. N.; Huang, L.; and Oyama, S. T. *J. Phys. Chem.* **1991**, 95, 10050.

Chapter 5

The Effect of Acid-Base Properties of Supported Molybdenum Oxide in Propylene Oxidation

5.1. Introduction

Molybdenum oxide is a principal component in catalysts for the selective oxidation and ammoxidation of propylene as well as many other catalysts of industrial importance.[1-5] Characterization and reactivity studies of these catalysts have been the topic of numerous investigations.[6-13] To understand the role of molybdenum oxide in these multicomponent catalysts, a number of studies on propylene oxidation over unsupported and supported molybdenum oxide have been performed.[14-19] The main body of literature on propylene oxidation over molybdenum oxide, however lacks a thorough study of the effect of catalyst support. It is known that the surface properties of molybdenum oxide are strongly influenced by the type of oxide support and result in different catalytic activity.[6-10, 20] The lack of systematic studies with well-characterized samples (surface area, acidity, basicity) has made it difficult to compare activity on different supports. In this investigation we employ the results of a recently developed method for counting surface sites on unsupported and supported molybdenum oxide to obtain turnover rates for

propylene oxidation and to study the effect of support on the activity. We show that acid/base interactions of the molybdenum oxide with the support affects not only the structure and properties of the surface species, but also their catalytic reactivity and selectivity.

The importance of molybdenum oxide catalysts in catalytic applications has prompted a large number of studies concerning the surface structures and the effect of the oxide support on the surface properties using various spectroscopic techniques such as ultraviolet-visible spectroscopy (UV-Vis),[21-24] infrared spectroscopy (IR),[22, 25-27] electron spin resonance spectroscopy (ESR),[28-30] ion scattering spectroscopy (ISS),[31,32] x-ray photoelectron spectroscopy (XPS),[31,32] and laser Raman spectroscopy,[32-39] There is increasing evidence that the acid base properties of the support influence the surface structures and the level of interaction of the support with molybdenum oxide.[9,10,40,41]

Surface acidity and basicity measurements on oxide catalysts have received considerable attention in recent years since they play and important role in the selective oxidation of hydrocarbons.[42-44] Catalytic activity has been closely related to the acidity and basicity of binary oxides.[45,46] The acidic properties of multicomponent metal oxides are generally determined by means of appropriate probe molecules acting as titrants or adsorbents.[44,47] In this paper we utilized the temperature programmed surface reaction (TPSR) of ethanol as a method for determining the acid-base properties of MoO_3 supported on SiO_2, Al_2O_3 and TiO_2. The effect of the acid-base properties of these

supported molybdenum oxides samples on the propylene oxidation reaction will be presented.

5.2. Experimental

Gases used in these studies were helium (Linde Ultra High Purity Grade 99.999%), hydrogen (Linde Ultra High Purity Grade 99.999%), oxygen (Linde Ultra High Purity Extra Dry Grade 99.6%), nitrogen (Linde Ultra High Purity Grade 99.999%), carbon monoxide (Linde Research Grade 99.97%) and propylene (Linde 99.0%). The liquids used were research grade dehydrated ethanol (Pharmco 99%), acetaldehyde (Aldrich 99%) and diethyl ether (Mallinckrodt).

Supported MoO_3 catalysts were prepared by impregnating SiO_2 (Cabosil L90, SA 90 m^2g^{-1}), Al_2O_3 (Degussa Aluminumoxid C, SA 100 m^2g^{-1}) and TiO_2 (Degussa P25, SA 50 m^2g^{-1}) with solutions of ammonium molybdate (Aldrich 98%) in distilled water to the point of incipient wetness. These materials were then dried at 393 K for 6 h and calcined at 773 K for 6 h.

Oxygen chemisorption, surface area, reactivity, temperature programmed desorption (TPD), temperature programmed reduction (TPR), and temperature programmed surface reaction (TPSR) experiments were measured in a flow apparatus equipped with a computer-interfaced mass spectrometer (Dycor/Ametek Model MA 100). For the oxygen uptake measurements, 0.5 g samples were oxidized in air at 773 K and

then reduced in flowing 50 mol% H_2/He mixtures for 2 h at various temperatures. Uptakes were determined at the same temperature by injecting 10 μmol pulses of oxygen from a calibrated on-line sampling valve onto a He stream passing over the reduced samples. Surface areas were determined by the conventional single-point BET method. The measurements were made by flowing a 30 mol% N_2/He mixture over samples held at liquid N_2 temperatures and subsequently flashing off the adsorbed amount.

Catalytic activity was obtained in a 15 mm OD/ 13 mm ID quartz packed-bed flow reactor at a total flow rate of 70-71 μmol s^{-1} and a total pressure of 101 kPa. (Flow rates in μmol s^{-1} may be converted to cm^3 (NTP) min^{-1} by multiplying by 1.5) In the reactivity experiments the partial pressure of the reactants were $P_{C_3H_6}$ = 10 kPa, P_{O_2} = 10 kPa, P_{H_2O} = 5 kPa and P_{He} = 75.1 kPa. In all the experiments amounts of catalyst corresponding to 21 μmol of O_2 uptake were loaded in the reactor. Particular care was used to ensure that the catalysts were stable at the reaction conditions employed. Before every run the catalysts were pretreated in the O_2-He-H_2O mixture (without C_3H_6) for 1 h at the maximum temperature of reaction. During the reactivity measurements, after the highest temperature was attained, a lower temperature measurement was always repeated to verify catalyst stability and lack of deactivation. To further check for any changes in the properties of the catalyst during reaction, oxygen chemisorption and surface area measurements were performed on the catalysts after reactivity measurements. For analysis of the reactants and products a multiple linear least square regression technique was used to account for the fragmentation of the different components. Mass fragmentation

patterns and the relative abundance of the relevant compounds were determined by performing independent calibration experiments. Carbon balances closed to 100 ± 10%. Rates are reported as turnover rates based on the surface molybdenum atoms counted by chemisorbed oxygen atoms.

$$v_t = \frac{Qyx}{Vw2S}$$

In the equation above v_t is the total propylene turnover rate, Q is the total volumetric flow rate, y is the mole fraction of propylene, V is the molar volume at the condition of flow measurement, w is the weight of the catalyst and S is the molecular oxygen uptake value.

TPR experiments employed a 5% H_2/He mixture (33.3 μmol s^{-1}), a linear heating rate of 0.17 K s^{-1}, a standard pretreatment in air at 773 K for 3600 s, followed by a He purge, and a final isothermal heating period of 1800 s. A desiccant bed ($CaSO_4$- Drierite) removed water produced during reduction and hydrogen consumption was recorded in the form of negative peaks. For the ethanol TPSR studies, ethanol was adsorbed at 298 K for 3600 s, by passing a continuous mixture of 10 % ethanol/He over the catalyst calcined at 773 K for 3600 s. After the system was purged with He at 298 K for 3600 s, a flow of 33 μmol s^{-1} of He was established and the product distribution was followed by mass spectrometry as the temperature was ramped at 0.10 K s^{-1}. Again, independent calibrations were performed to determine the fragmentation patterns and relative abundance's of the different components formed during the surface reaction. The raw data

was then analyzed by multiple linear least square regression to yield the amounts of the various compounds desorbed during the experiment.

5.3. Results

5.3.1. Oxygen chemisorption

Figure 5.1 shows the oxygen uptake values for SiO_2-, Al_2O_3-, and TiO_2-supported samples plotted versus the amount of molybdenum in the samples. The values in units of μmol m^{-2} account for the sample surface area. In all cases the uptakes increase with MoO_3 loading and at low loadings (1wt% for SiO_2, 1 - 9 wt% for Al_2O_3, and 1 - 5 wt% for TiO_2) the uptake curves approach the dashed lines corresponding to complete dispersion, defined as a stoichiometry of one oxygen atom per molybdenum atom (O: Mo = 1). At high loadings (5 - 9 wt% for SiO_2, 12 - 20 wt% for Al_2O_3 and 5 -9 wt% for TiO_2) the uptakes deviate from the dashed lines indicating lower dispersions.

5.3.2. Temperature programmed reduction of supported molybdenum oxide

Figure 5.2 presents the TPR patterns of three low-loading supported samples and compares them with that of unsupported MoO_3. The appearance of the first reduction

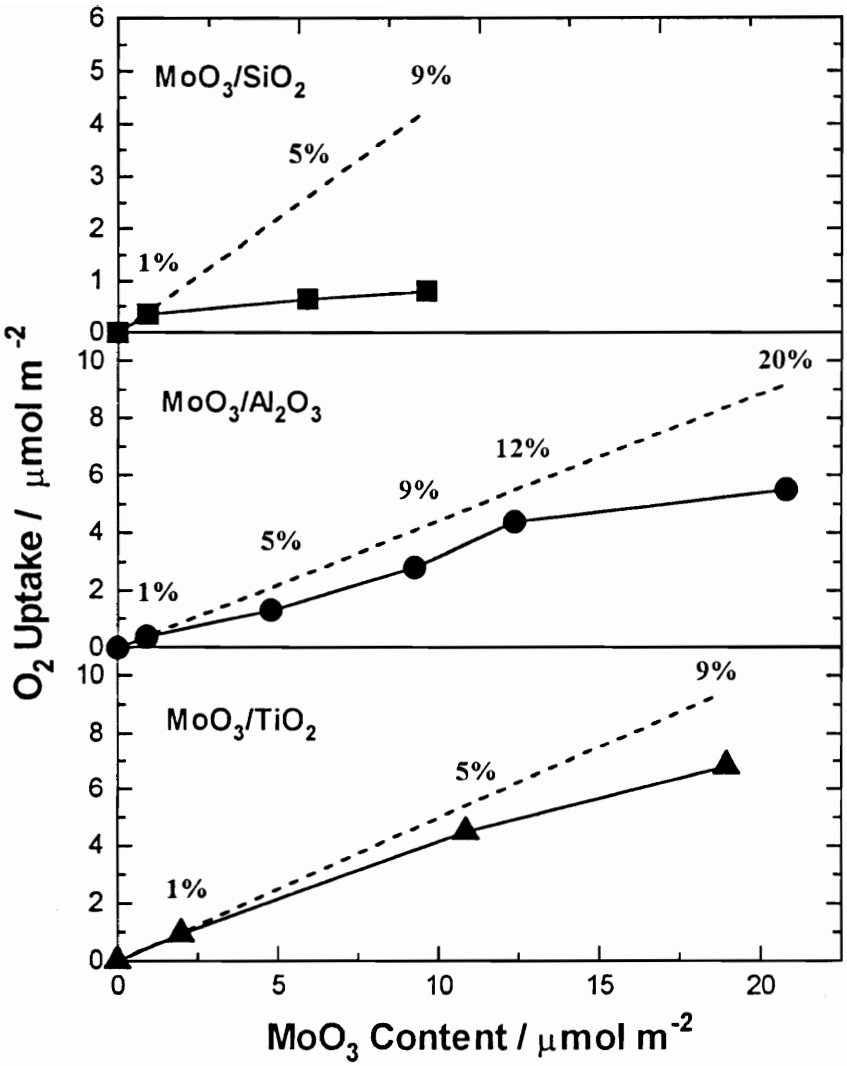

Figure 5.1. Comparison of oxygen uptakes on supported MoO_3 catalysts.

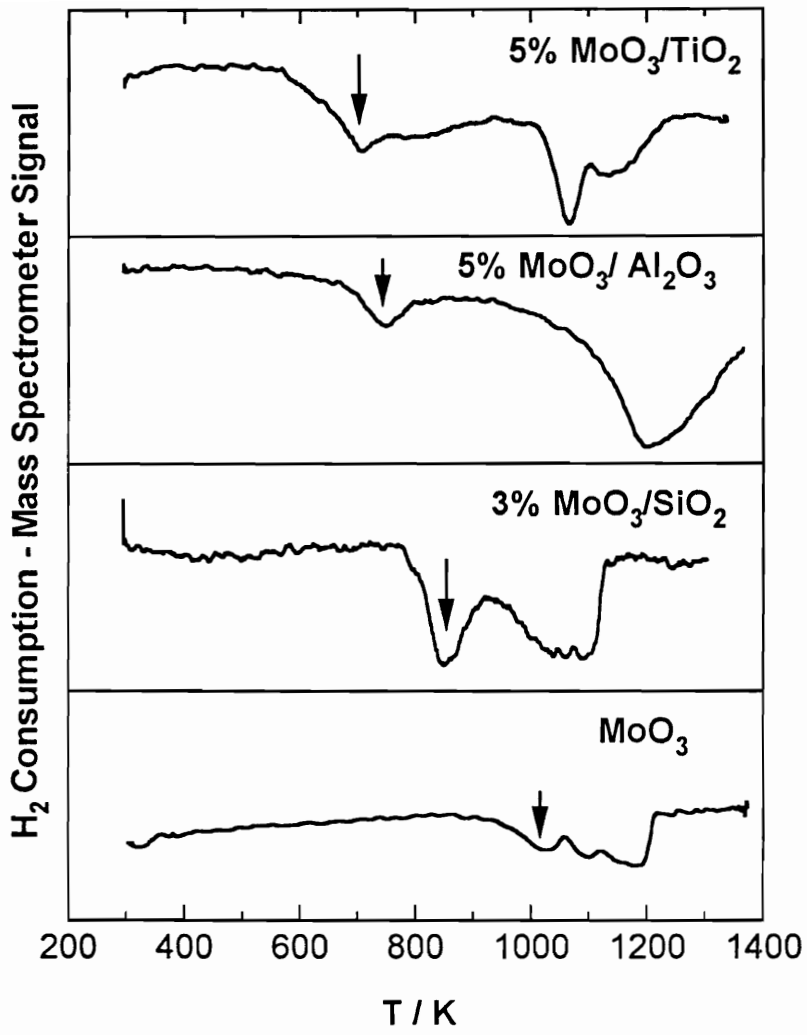

Figure 5.2. Temperature programmed reduction traces of low loading supported MoO_3 and unsupported MoO_3. Samples were reduced in 5 mol % H_2/He (33 μmol s^{-1}) as the temperature was ramped at 0.17 Ks^{-1}. Prior to the TPR catalysts were calcined in O_2 at 773 K for 3600 s.

peak (T_{red}) indicated by arrows depends on the support material used with T_{red} - TiO_2 < T_{red} - Al_2O_3 < T_{red}-SiO_2 . The other reduction peaks at higher temperature appear close to those of unsupported MoO_3 and correspond to reduction of Mo to a low oxidation state.

5.3.3. Temperature programmed surface reaction of adsorbed ethanol

Figure 5.3 displays the ethanol TPSR traces on the pure supports. There is considerable desorption of ethanol (> 40%) on all supports (SiO_2-356 K, Al_2O_3-378 K and TiO_2-361 K). All percentages reported in this paper are in mol % based on ethanol (CO and CO_2 ÷ 2, diethylether x 2). On Al_2O_3 and TiO_2 ethylene desorbs at around 524 K and 598 K and diethylether desorbs at around 462 K and 555 K, respectively. On SiO_2 traces of the ethylene desorb at around 830 K. On TiO_2 traces of carbon oxides are produced at around 740 K.

Figure 5.4 compares the ethanol TPSR traces on the low loading samples on the three different supports. Again on all the samples, there is considerable amount of ethanol desorption (> 45%) with the T_{max} of desorption varying slightly with the support (MoO_3/SiO_2 - 354 K, MoO_3/Al_2O_3 - 371 K, and MoO_3/TiO_2 - 363 K). The desorption characteristics of the other products differ considerably on the three samples. On the SiO_2-supported sample diethylether is not produced and ethylene desorbs at around 770 K. On the Al_2O_3- supported sample, diethylether and ethylene desorb at around 455 K.

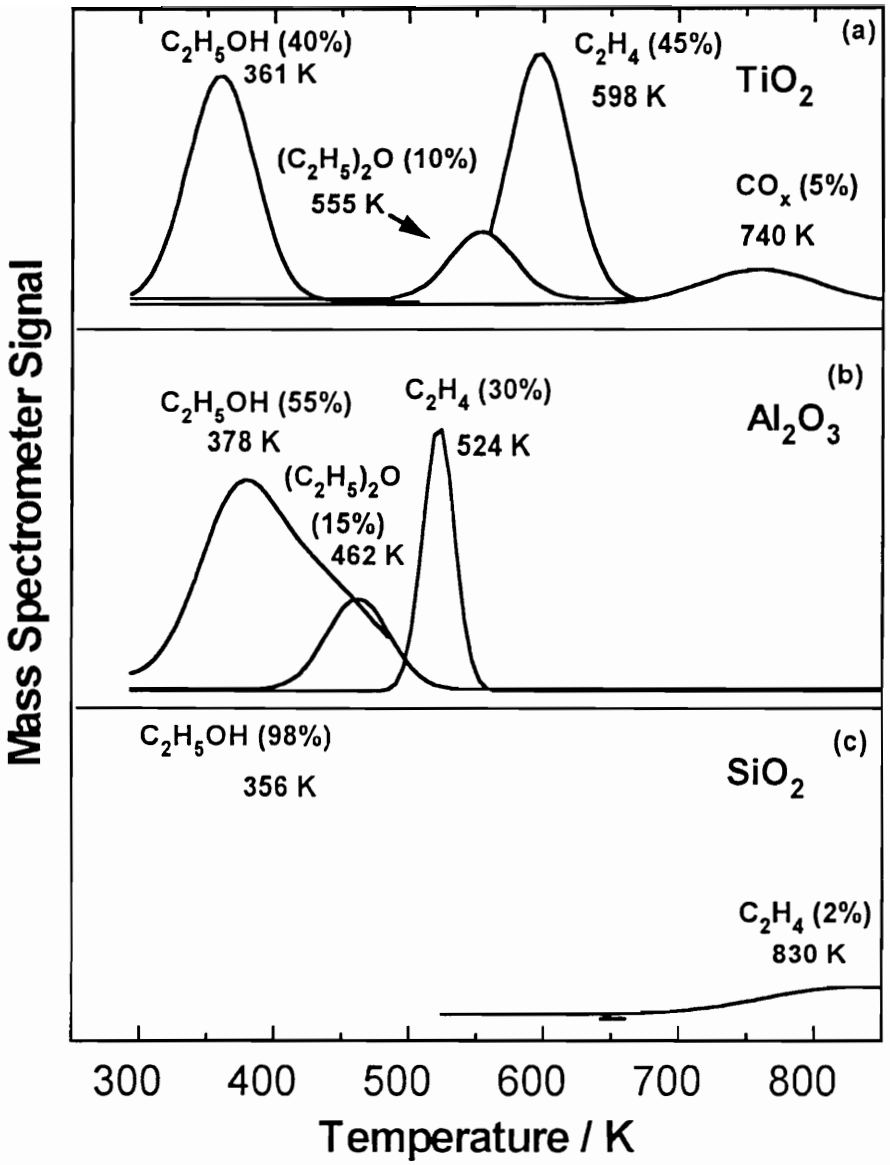

Figure 5.3. Temperature programmed surface reaction of adsorbed ethanol on catalyst supports.

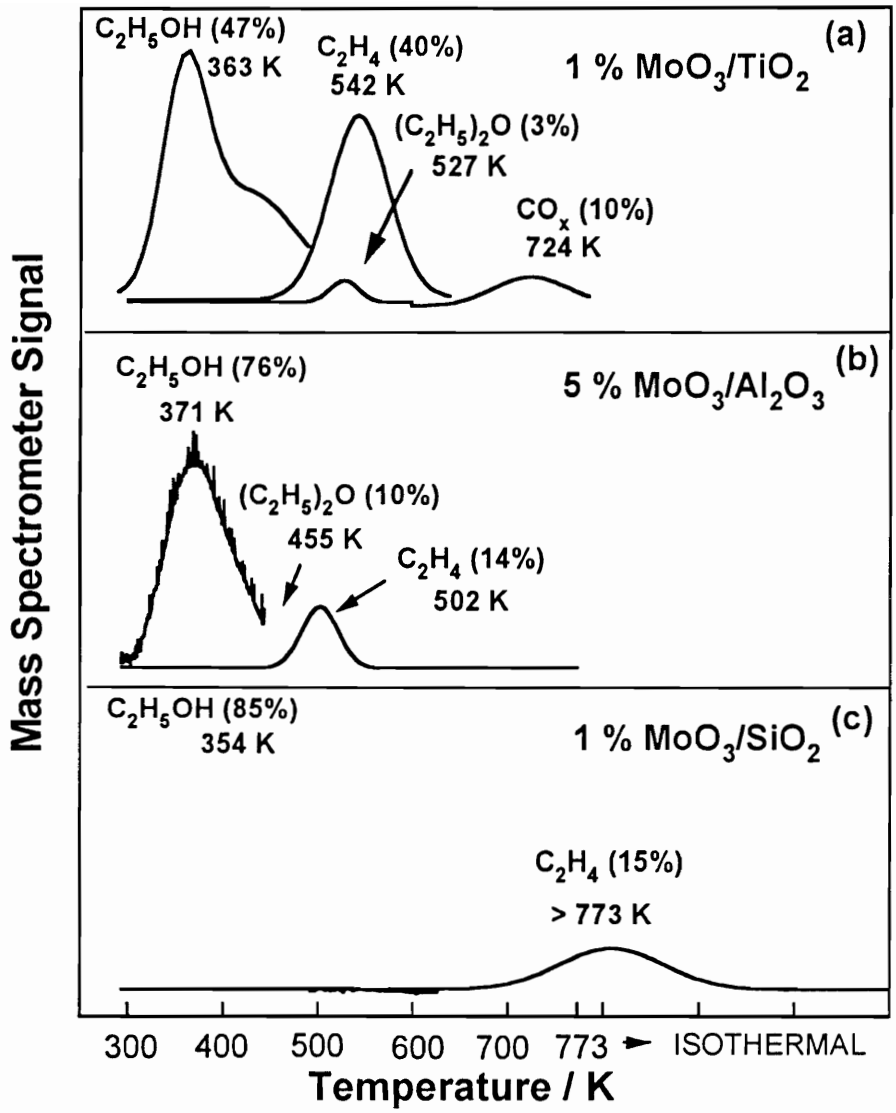

Figure 5.4. Temperature programmed surface reaction of adsorbed ethanol on the low loading samples.

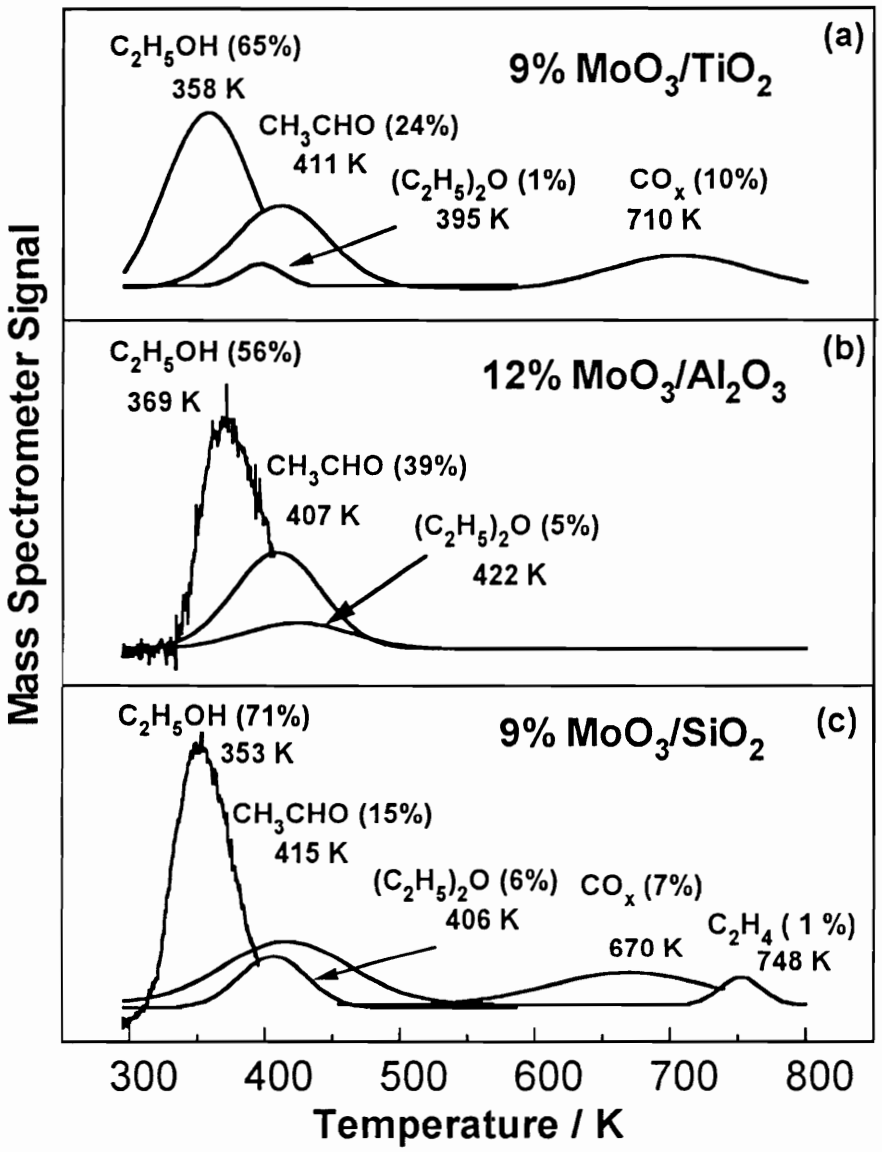

Figure 5.5. Temperature programmed surface reaction of adsorbed ethanol on the high loading samples.

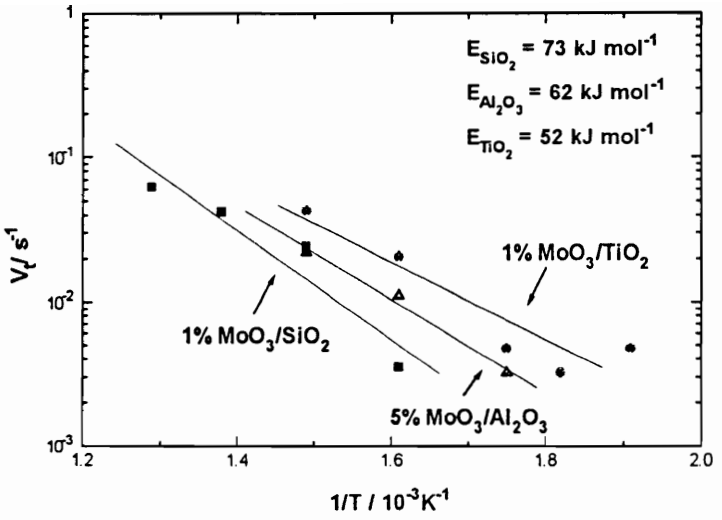

Figure 5.6. Arrhenius plots for propylene oxidation on the low loading samples.

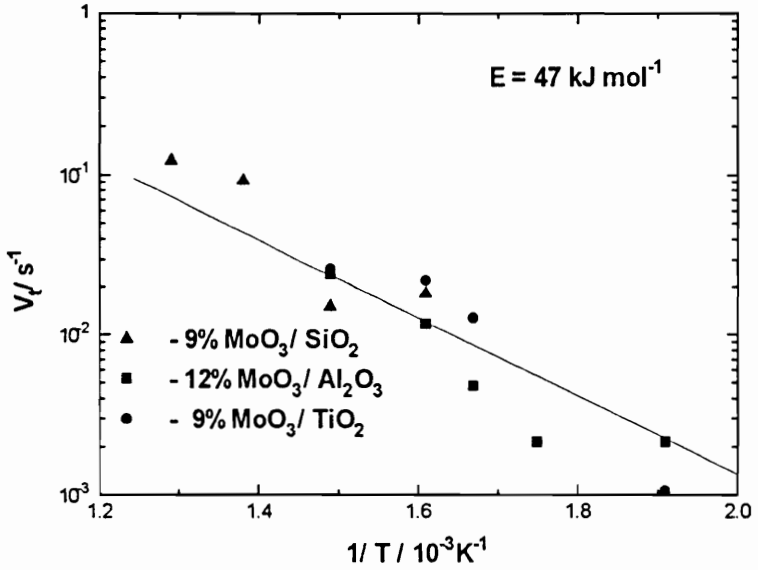

Figure 5.7. Arrhenius plots for propylene oxidation on the high loading samples.

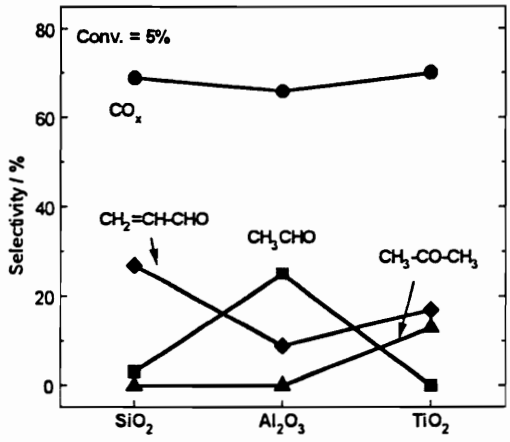

Figure 5.8. Effect of catalyst support for the low loading samples on product selectivity in propylene oxidation.

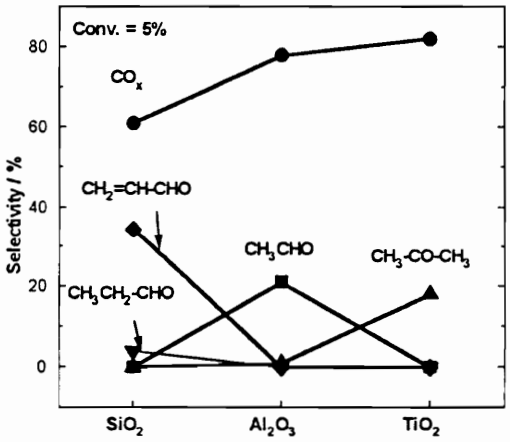

Figure 5.9. Effect of catalyst support for the high loading samples on product selectivity in propylene oxidation.

and 500 K, respectively. On the TiO_2-supported sample diethylether, ethylene and carbon oxides desorb at around 530 K, 540 K and 720 K, respectively.

Figure 5.5 presents the ethanol TPSR traces of the high loading supported samples. As in the case of the low loading samples, there is considerable ethanol desorption (> 55%) with a slight variation of T_{max} of desorption (MoO_3/SiO_2-353 K, MoO_3/Al_2O_3-369 K, and MoO_3/TiO_2-358 K). Acetaldehyde is produced in considerable amounts on all the samples (MoO_3/SiO_2-15%, MoO_3/Al_2O_3-39% and MoO_3/TiO_2-24%) and desorbs at around 410 K. Diethylether is also produced on all the samples (< 10%) and desorbs at around 410 K (MoO_3/SiO_2), 420 K (MoO_3/Al_2O_3) and 400 K (MoO_3/TiO_2), respectively. In addition, carbon oxides are produced on the SiO_2 (670 K) and TiO_2 (710 K) supported samples and ethylene (748 K) is produced on the SiO_2 supported sample. Ethanol TPSR from medium-loading samples (5% MoO_3/TiO_2, and 9% MoO_3/Al_2O_3) were also measured, but these showed results very similar to those of high 'loading samples and the data for these are not presented here.

5.3.4. Reactivity study of propylene oxidation

Figure 5.6 compares Arrhenius plots for propylene oxidation on the low loading samples for the three different supports. The plots show that the turnover rates increase in the order $SiO_2 < Al_2O_3 < TiO_2$ while the activation energies decrease in the same order, 73, 67, 52 kJ mol^{-1}. The blank activity of the pure supports were completely negligible

even at the highest temperature reached in this study. Figure 5.7 displays the Arrhenius plots for propylene oxidation on the high loading samples. On these samples the activity differences are largely leveled and the points fall on one line with activation energy 47 kJ mol^{-1}. The magnitudes of the rates are close to the low loading samples.

Figure 5.8 compares the effect of support in the low loading samples on the selectivity to different products for propylene oxidation made at similar conversions (< 5%). There are considerable differences between the supports. On the SiO_2-supported sample, acrolein along with traces of propionaldehyde are the selective oxidation products. On the Al_2O_3- supported sample, acetaldehyde is the only selective oxidation product and selectivity in propylene oxidation. On the TiO_2-supported sample, acetone is the only selective oxidation product. The selectivity to partial oxidation is ~ 30-40 % on all the supported samples

Figure 5.9 shows the effect of support in the high loading samples on the selectivity to different oxidation products for propylene oxidation again, at similar conversions (< 5%). As with the activity, differences in selectivity are also leveled, and acrolein is produced on all samples. There is some residual effect of support and, similarly to the low loading samples, some acetaldehyde is produced on the Al_2O_3 -supported sample, and acetone is produced on the TiO_2-supported sample. Selectivity to total oxidation products is ~ 30 % on all the supported samples. Table 5.1 summarizes the values of conversion, turnover rates and selectivities for all the supported samples.

Table 4.1. Propylene oxidation on supported MoO_3 catalysts.

Samples	T/K	Selectivity / %					Conversion / %	v_t / s^{-1}
		CH_3CHO	C_3H_6CHO	C_3H_4O	CH_3COCH_3	CO_x		
1.0 % MoO_3/SiO_2	623	-	5	35	-	60	4	0.0070
	673	2	3	31	-	64	3	0.0050
	723	4	3	17	-	76	50	0.084
9.0 % MoO_3/SiO_2	623	3	-	28	-	69	11	0.018
	673	-	8	28	-	64	9	0.015
	723	5	3	16	-	76	55	0.092
1.0 % MoO_3/Al_2O_3	573	20	-	-	2	78	1.9	0.0030
	623	6	-	1	7	85	6.6	0.011
12.0 % MoO_3/Al_2O_3	573	25	-	6	-	66	1.2	0.0020
	623	6	-	1	8	85	7.2	0.012
1.0 % MoO_3/TiO_2	573	-	-	-	18	82	2.8	0.0048
	623	-	-	-	19	81	12.4	0.021
	673	-	-	-	6	94	25.7	0.043
9.0% MoO_3/TiO_2	573	-	-	17	13	70	0.95	0.0016
	623	8	-	9	8	77	14.3	0.023
	673	8	-	7	6	79	14.6	0.024

5.4. Discussion

5.4.1. Oxygen chemisorption and temperature programmed reduction

Complete studies of oxygen chemisorption on unsupported and supported MoO_3 have been reported elsewhere.[48,49] In these studies, reduction and chemisorption temperatures were varied systematically to give results consistent with Raman spectroscopy at low loadings and x-ray diffraction at high loadings. Oxygen uptakes are compared for the SiO_2 -, Al_2O_3 - and TiO_2 - supported samples as a function of MoO_3 loading in Figure 5.1. In the SiO_2 system, samples of 3 wt % loading and higher have oxygen uptakes that fell well beneath the dashed line corresponding to O/Mo =1, indicating low dispersion. For the Al_2O_3- and TiO_2- supported samples the drop off occurs at loadings of 5 wt % and 9 wt % respectively. Allowing for differences in surface area, these values indicate that the order of interaction is $SiO_2 < Al_2O_3 \leq TiO_2$. Raman spectroscopy further shows that at high loadings on all supports molybdenum oxide is in the form of small crystallites with structures identical to bulk MoO_3.[36,48-50] At low concentrations the supported molybdenum oxide consists of highly dispersed surface molybdate species containing a single molybdenum atom. The structure of the highly dispersed phase in the absence of water is probably an $O{=}MoO_4$ monomer with four bridging oxygen links to the surface. On silica this may hydrated to a dioxo form.[48]

Temperature programmed reduction (Fig. 5.2) confirms the order of interaction to be $SiO_2 < Al_2O_3 < TiO_2$ as seen in the progression of T_{red} in the low temperature reduction peak. The high temperature reduction peaks for the alumina-supported sample occur at the highest temperature probably because of strong interactions of MoO_2 with the support surface. All of these high-temperature reduction features are irrelevant to the work presented in this paper because they involve Mo in very low oxidation states. The first reduction peak alone occurs in the temperature range where reaction is observed.

5.4.2. Temperature programmed surface reaction

Figures 5.3 -5.5 summarize the temperature programmed desorption traces of ethanol on a series of supported samples and supports. On all samples, ethanol desorbs intact at relatively low temperatures (< 380 K), while at higher temperatures, reaction products start to appear. On the supports (Fig. 5.3) and the low loading TiO_2 - and Al_2O_3 - supported samples (Fig. 5.4), dehydration of ethanol to form diethylether and ethylene are the major reaction pathways. On the low loading SiO_2 sample, a small amount of ethylene desorbs at very high temperatures. On the high loading samples (Fig. 5.5), dehydrogenation of ethanol to acetaldehyde and dehydration to diethylether are the major channels.

At low loadings, MoO_3 is highly dispersed on the support and the desorption pathways are controlled to a certain extent by the properties of the support. As the

loading increases the MoO_3 coverage increases and isolated crystallites of bulk MoO_3 appear. The desorption products on these samples are increasingly controlled by the properties of bulk MoO_3.

There are very few studies in the literature on the temperature programmed desorption of ethanol from molybdenum oxide catalysts. Sleight and coworkers studied the structural effects of alcohol chemisorption and temperature programmed desorption on unsupported MoO_3 catalysts.[51] They found that at low temperatures (~ 373 K) ethanol desorbs intact, and at higher temperatures as acetaldehyde. Dehydration occurred to a very minor extent. This agrees with our results for the high loading samples which are more representative of the properties of unsupported MoO_3.

There has been considerable work in the area of methanol dehydration over oxide and zeolite catalysts.[52-55] Various mechanisms have been proposed for the dehydration of methanol to dimethylether involving interactions with both surface acid and base sites. Padamanabhan *et al.* have shown kinetic evidence for the dual site mechanism for ether formation from methanol involving acid/base pairs on an alumina catalyst.[52] Selectivity in the decomposition reaction of isopropanol has long been regarded as one of the typical reactions for investigating the acid-base properties of catalytic sites on metal oxides.[56-59] The catalysts can be classified according to their propensity toward dehydration to propene or dehydrogenation to acetone. As in the case of methanol decomposition, the isopropanol decomposition involves an acid-base dual site mechanism.[60,61]

The group of Sleight also found on unsupported MoO_3 that the desorption characteristics of methanol, ethanol and isopropanol were essentially the same.[51] Thus the same acid-base mechanism found to apply for methanol desorption probably also applies to the ethanol reaction. Recently, Decanio *et al.* have studied the nature of acid-base sites on γ-alumina and fluorided alumina by using TPR of [^{18}O]ethanol.[62,63] They concluded that surface bound alkoxides are formed by (a) dissociative adsorption on Lewis acid sites and (b) nucleophilic attack by the surface oxide on the alcohol. They also state that alkenes may be formed by the dehydration of alkoxides adsorbed on basic sites rather than the dehydration of adsorbed alcohol as suggested by Knözinger *et al.*[64] Their results also suggest that when the surface alkoxide population decreases, alkenes can form from the dehydration of adsorbed alkoxides on either of the two sites. Studies on MgO catalysts have shown that alkenes are formed with high selectivities via a base-catalyzed dehydration of alcohols.[65] It has also been shown that on alumina, acid site strength distribution controls the selectivity to ether and olefin formation. Lower strength acid sites lead to the formation of ether while relatively strong acid sites promote olefin formation.[66] Thus, in Figures 5.3-5.5, ethanol is probing both the acid and base properties of the supported catalysts.

Although SiO_2 is almost inert for the production of diethylether and ethylene (Fig. 5.4(c)), on the low loading TiO_2- and Al_2O_3- supported samples considerable amounts of diethylether indicate the presence of a bifunctional surface supporting both acid and base sites (Fig. 5.4(a) and 5.4(b)). However, the acid/base site strength distribution is different

for the two supports, with TiO_2 supported samples having more basic sites of higher strength as seen from the larger production of ethylene on these samples (40% - TiO_2, 14% Al_2O_3). The T_{max} of ethylene desorption also varies considerably indicating the difference in the strength of the sites with TiO_2 (542 K) > Al_2O_3 (502 K). On the pure TiO_2 and Al_2O_3 supports (Fig. 5.3(a) and 5.3(b)) the acid/base site strength distribution is almost the same on both supports, sites on TiO_2 being slightly stronger. The same trend is followed in the T_{max} of ethylene desorption with TiO_2 (598 K) > Al_2O_3 (524 K). In contrast, the T_{max} for ethylene and diethylether desorption on the supports is higher than that for the low loading samples. This difference may be caused by a decrease in the number of acid/base sites with higher strength due to the presence of MoO_3 on the support. Decanio *el al.* have also reported that when the Al_2O_3 is poisoned with a base the T_{max} of ethylene and diethylether desorption increases.[62] Again, as in the case of the low loading samples, the SiO_2 support is inert (Fig. 5.3(c)), as is known from the literature.[67,68] As the MoO_3 loading increases ethylene desorption is completely suppressed and a very small amount of diethylether is produced, indicating that the number of acid-base sites is reduced and the catalyst surface behaves almost like bulk MoO_3. On the high loading SiO_2 sample, however, there is some formation of diethylether and ethylene along with acetaldehyde. This picture is completely consistent with our previous oxygen chemisorption, XRD and laser Raman results. The interaction between the surface molybdenum oxide and the supports may be viewed as generalized

acid-base reaction. Under dehydrated conditions MoO_3 is weakly acidic, SiO_2 is slightly acidic, while Al_2O_3 and TiO_2 are amphoteric. Both *acidity* and *basicity* increase in the order $SiO_2 < Al_2O_3 \leq TiO_2$. The interaction of MoO_3 with the supports thus increases in the order $SiO_2 < Al_2O_3 < TiO_2$, in agreement with earlier results.[49,68,69]

5.4.3. Reactivity of propylene oxidation

Reactivity results are shown in Figures 5.6 and 5.7. It should be stressed that our catalytic measurements are carried out in the presence of water vapor (10 kPa). Water is a side-product of oxidation which otherwise increases with conversion and could offset the kinetics of the reaction. The Arrhenius plots shown in Figure 5.6 and 5.7 summarize the effect of support on steady-state catalytic activity for the low and high loading MoO_3 catalysts. In both cases, activity increases in the order $SiO_2 < Al_2O_3 < TiO_2$. In recent studies of methanol oxidation on various supported molybdenum and vanadium oxides the activity was also found to increase in the order $SiO_2 < Al_2O_3 < TiO_2$.[20,70] Wachs *et al.* attributed the difference in activity to the surface oxide-support interaction. The onset temperature of reduction for the supported V_2O_5 catalysts seemed to correlate with this activity difference.[6] Similar trends in reactivity were found for ethanol oxidation on supported MoO_3 catalysts.[71] In this study, Ono *et al.* attributed the difference in activity

to the surface structures of the catalysts. We find that in propylene oxidation, the dependence of activity on support follows the same order as found in the alcohol oxidation reactions. As presented earlier, this order corresponds to the strength of metal oxide support interaction, as indicated by Raman spectroscopy[48,49] and the first reduction peak during temperature programmed reduction (Fig. 5.2).

However, there are also important differences. On the low loading samples (Fig. 5.8) the predominant selective oxidation products were not the same, acrolein on MoO_3/SiO_2, acetaldehyde on MoO_3/Al_2O_3, and acetone on MoO_3/TiO_2. This indicates that the nature of the support-oxide interaction has a strong influence on the catalytic chemistry of the active surface species. With an increase in loading, the degree of interaction is decreased and differences are reduced, so that acrolein is produced on all the samples. However acetaldehyde is still produced on the Al_2O_3-supported sample while acetone is formed on the TiO_2-supported sample. As will be amplified below, we suggest that the acid-base nature of the interaction is responsible for directing the reaction to such different products.

There are few studies on the oxidation of propylene on MoO_3 supported on SiO_2,[14-16] Al_2O_3,[17,18] and TiO_2.[19] Unfortunately it is difficult to compare our present work with that reported earlier due to the vast differences in conditions used. For example, some studies were done in the pulse mode[14,17,18] and some were done in the absence of water vapor.[16,19]

On the SiO_2 - supported samples where the acid-base interactions between MoO_3 and SiO_2 are weak, the oxidation of propylene to acrolein probably occurs through a homolytic pathway involving the initial formation of allyl radicals. Such intermediates are well documented on bismuth molybdate catalysts.[5]

On the Al_2O_3-supported samples with increasing acid-base interactions, the more polarizable portion of the molecule is activated, and it is likely that a π-complex, is formed. As in the case of butene oxidative cleavage[72] this is followed by carbenium ion formation and scission of the molecule.

On the TiO_2 -supported samples, again with strong acid-base interactions, activation of the double bond occurs, only this time to form isopropyl alcohol by hydration. This is then followed by dehydrogenation to acetone through an isopropoxy intermediate.[73,74] The mechanism is probably similar to that which occurs on Sn-Mo.[24,75] It has been shown in that system by using $H_2{}^{18}O$ tracer, that the oxygen atom in the ketone is incorporated from the water molecule and not from molecular oxygen.[76]

It is clear that acid-base properties influence the products formed. This may be related fundamentally to the manner in which intermediates are bonded to the surface.[77] Different intermediates are formed because on bonding to the surface the transition state derived from propylene is polarized in different manners depending on the acid-base environment it encounters.

In summary, oxygen chemisorption along with complementary evidence from XRD and laser Raman spectroscopy, provides information on the nature of the MoO_3-support

interaction. The interaction increases in the order $SiO_2 < Al_2O_3 < TiO_2$. The interaction of the MoO_3 with the support is of an acid-base nature. Temperature programmed desorption of ethanol from these samples indicate the presence of acid-base sites on the Al_2O_3 and TiO_2 supported samples. An increase in the MoO_3 loading tends to suppress these sites and characteristics of bulk MoO_3 start manifesting themselves in the samples. The low loading and high loading SiO_2 supported samples seem to be inert. The acidity and basicity of the supported samples increase in the same order as the MoO_3 support interaction. The activity for propylene oxidation increases in the order: $SiO_2 < Al_2O_3 < TiO_2$ and correlates with the interaction of MoO_3 with the supports, the acid-base properties of the samples and the initial temperature of reduction during temperature programmed reduction of these samples. Selectivity to partial oxidation products on the low loading samples show major differences and is influenced by the acid-base characteristics of the surface and the nature of the reaction intermediate.

5.5. Conclusions

1. The oxygen chemisorption technique indicates the order of affinity of the supports for molybdenum oxide is : $SiO_2 < Al_2O_3 < TiO_2$.

2. The interaction of the molybdenum oxide with the support is of an acid-base nature.

3. Ethanol temperature programmed desorption, is an effective technique to probe the acid-base and oxidizing sites on the surfaces of these catalysts. TPD patterns indicate that both acidity and basicity increase in the order: $SiO_2 < Al_2O_3 \leq TiO_2$.

4. The order for increase in activity for propylene oxidation is consistent with the MoO_3-support interaction, acid-base characteristics and the reducibility of the catalysts.

5.6. References

(1). Weissermel, K.; and Arpe, H.-J. "*Industrial Organic Chemistry*", VCH, New York, **1993**.

(2). Adams, C. R.; and Jennings, T. S. *J. Catal.* **1963**, 2, 63.

(3). Krenze, J. D.; and Keulks, G. W. *J. Catal.* **1980**, 61, 316.

(4). Burrington, J. D.; Kartisch, C. T.; and Grasseli, R. K. *J. Catal.* **1983**, 81, 489.

(5). Snyder, T. P.; and Hill. Jr, C. G. *Cat. Rev.-Sci. Eng.* **1983**, 31, 43.

(6). Bond, G. C.; Flamerz, S.; and Shukri, R. *Faraday Discuss., Chem. Soc.* **1989**, 87, 65.

(7). Zaki, M. I.; Vielhabor, B.; and Knozinger, H. J. *J. Phys. Chem.* **1986**, 90, 3176.

(8). Nag, N. K. *J. Phys. Chem.* **1987**, 91, 2324.

(9). Fransen, T.; Mars, P.; and Gellings, P. J. *J. Colloid Int. Sci.* **1979**, 70, 97.

(10). Cáceres, C. V.; Fierro, J. L. G.; Lázaro, J.; López Agudo, A.; and Soria, J. *J. Catal.* **1979**, 122, 113.

(11). Hattori, H.; Tanabe, K.; Tanaka, K.; and Okazaki, S. in "*Proceedings of 3rd International Conference on the Chemistry and Uses of Molybdenum.*" Climax Molybdenum Co., Ann Arbor, MI, **1979**.

(12). Muralidhar, G.; Massoth, F. E.; and Shabtai, J. *J. Catal.* **1979**, 85, 44.

(13). Yang, J-T.; and Lunsford, J. *J. Catal.* **1987**, 103, 55.

(14). Vaghi, A.; Castellan, A.; Bart, J. C. J.; Giordano, N.; and Ragaini, V. *J. Catal.* **1976**, 42, 381.

(15). Grabowski, R.; Machej, T.; Mazurkiewicz, A.; and Sloczynski, J. *Bul. Pol. Acad. Sci.* **1987**, 35.

(16). Liu, T.; Forissier, M.; Coudurier,G.; and Védrine, J. *J. Chem. Soc., Faraday, Trans. I.* **1989**, 85, 1607.

(17). Giordano, N.; Padovan, M.; Vaghi, A.; Bart, J. C. J.; and Castellan, A. *J. Catal.* **1975**, 38, 1.

(18). Giordano, N.; Vaghi, A.; Bart, J. C. J.; and Castellan, A. *J. Catal.* **1975**, 38, 11.

(19). Ono, T.; Nakagawa, Y.; Miyata, H.; and Kubokawa, Y. *Bull. Chem. Soc. Jpn.* **1984**, 57, 1205.

(20). Matsuoka, Y.; Niwa, M.; and Murakami, Y. *J. Phys. Chem.* **1990**, 94, 1477.

(21). Ashley, J. H.; and Mitchell, P. C. H. *J. Chem. Soc. (A)*, **1969**, 2730.

(22). Lipsch, J. M. J. G.; and Schuit, G. C. A. *J. Catal.* **1969**, 15, 174.

(23). Asmolov, G. N.; and Krylov, O. V. *Kinet. Catal.* **1970**, 11, 847.

(24). Giordano, N.; Bart, J. C. J.; Vaghi, A.; Castellan, A.; and Martinotti, G. *J. Catal.* **1970**, 36, 81.

(25). Sonnemans, J.; and Mars, P. *J. Catal.* **1973**, 31, 209.

(26). Fransen, T.; van der Meer, O.; and Mars, P. *J. Catal.* **1975**, 42, 79.

(27). Giordano, N.; Bart, J. C. J.; Castellan, A.; and Vaghi, A. *J. Less Common Met.* **1977**, 54, 387.

(28). Seshadri, K. S.; and Petrakis, L. *J. Phys. Chem.* **1977**, 74, 4102.

(29). Dufaux, M.; Che, M.; and Naccache, C. *J. Chim. Phys.* **1970**, 67, 527.

(30). Masson, J.; Delmon, B.; and Nachtschein, J. C. R. *Acad. Sci. Paris, Ser. C.* **1968**, 266, 1257.

(31). Kasztelan, S.; Payen, E.; Toulhoat, H.; Grimblot, J.; and Bonnelle, J. P. *Polyhedron* **1986**, 5, 157.

(32). Zingg, D. S.; Makovsky, L. E.; Tischer, R. E.; Brown, F. R.; and Hercules, D. M. *J. Phys. Chem.* **1980**, 84, 2898.

(33). Brown, F. R.; Makovsky, L. E.; and Rhee, H. K. *J. Catal.* **1977**, 50, 162.

(34). Knözinger, H.; and Jeziorowski, H. *J. Phys. Chem.* **1978**, 82, 2002.

(35). Jeziorowski, H.; and Knözinger, H. *J. Phys. Chem.* **1979**, 83, 1166.

(36). Williams, C. C.; Ekerdt, J. G.; Jehng, J. -M.; Hardcastle, F. D.; and Wachs, I. E. *J. Phys. Chem.* **1991**, 95, 8791.

(37). Chan, S. S.; Wachs, I. E.; Murrell, L. L.; Wang, L.; and Hall, W. K. *J. Phys. Chem.* **1984**, 88, 5831.

(38). Stencel, J. M.; Makovsky, L. E.; Sarkus, T. A.; de Vries, J.; Thomas, R.; and Moulijn, J. A. *J. Catal.* **1984**, 90, 314.

(39). Payen, E.; Kasztelan, S.; Grimblot, J.; and Bonnelle, J. P. *J. Raman Spectrosc.* **1986**, 30, 233.

(40). Kim, D. S.; Segawa, K.; Soeya, T.; and Wachs, I. E. *J. Catal.* **1992**, 136, 539.

(41). Datta, A. K.; Ha, J-W.; and Regalbuto, J. R. *J. Catal.* **1992**, 133, 55.

(42). Kung, H. H. *Ind. Eng. Chem. Prod. Dev.* **1992**, 25, 172.

(43). Tanabe, K. *Solids Acids and Bases*, Academic Press, New York, **1970**.

(44). Kijenski, J.; and Baiker, A. *Catal. Today* **1989**, 5, 1.

(45). Tanabe, K.; Shibata, T.; Kitagawa, J. *Bull. Chem. Soc. Jpn.* **1974**, 47, 1064.

(46). Jin, T.; Hattori, H.; and Tanabe, K. *Bull. Chem. Soc. Jpn.* **1982**, 55, 2279.

(47). Gervasini, A.; and Auroux, A. *J. Phys. Chem.* **1993**, 97, 2628.

(48). Desikan, A. N.; Huang, L.; and Oyama, S. T. *J. Phys. Chem.* **1991**, 95, 10050.

(49). Desikan, A. N.; Huang, L.; and Oyama, S. T. *J. Chem. Soc. Faraday Trans.* **1992**, 88, 3357.

(50). Williams, C. C.; Ekerdt, J. G.; Jehng, J. -M.; Hardcastle, F. D.; and Wachs, I. E. *J. Phys. Chem.* **1991**, 95, 8781.

(51). Farneth, W. R.; Staley, R. H.; and Sleight, A. W. *J. Phys. Chem.* **1986**, 108, 2327.

(52). Padmanabhan, V. R.; and Eastburn, F. J. *J. Catal.* **1972**, 24, 88.

(53). Swabb, E. A.; and Gates, B. C. *Ind. Eng. Chem. Fund.* 1972, 11.

(54). Bandiera, J.; and Naccache, C. *Appl. Catal.* **1991**, 69, 139.

(55). Spivey, J. J. *Chem. Eng. Comm.* **1991**, 110, 123.

(56). Tanabe, K.; Misono, M.; Ono,Y.; and Hattori, H. in *New Solid Acids and Bases*, (Delmon, B.; and Yates, J. T. Eds.), Vol. 51. Elsevier, Amsterdam, **1989**.

(57). Cunningham, J.; Hodnett, B. K.; Ilyas, M.; Leahy, E. L.; Fierro, J. L. G. *Faraday Disc., Chem. Soc.* **1981**, 72, 283.

(58). Ai, M. *Bull. Chem. Soc. Jpn.* **1981**, 50, 2579.

(59). Nollery, H.; and Ritter, G. J. *Chem. Soc. Faraday Trans. I.* **1984**, 80, 275.

(60). Ai, M. *J. Catal.* **1975**, 40, 318.

(61). Ai, M. *J. Catal.* **1975**, 40, 327.

(62). Decanio, E. C.; Nero, V. P.; and Bruno, J. W. *J. Catal.* **1992**, 135, 444.

(63). Decanio, E. C.; Bruno, J.W.; Nero, V. P.; and Edwards, J. C. *J. Catal.* **1993**, 140, 84.

(64). Knözinger, H.; Bühl, H.; and Kochloefl, K. *J. Catal.* **1972**, 24, 57.

(65). Peng, X. D.; and Barteau, M. *Langmuir* **1991**, 7, 1426.

(66). Figoli, N. S.; Hillor, S.A.; and Parera, J. M. *J. Catal.* **1971**, 20, 231.

(67). Tanabe, K. in *"Catalysis, Science and Technology"*, (Anderson, J. R.; and Boudart, M. Eds.), Springer-Verlag, Berlin, 231, **1981**.

(68). Auroux, A.; and Gervasini, A. *J. Phys. Chem.* **1990**, 94, 6371.

(69). Gervasini, A.; and Auroux, A. *J. Catal.* **1990**, 131, 190.

(70). Deo, G.; and Wachs, I. E. in "*Catalytic Selective Oxidation*", (Oyama, S. T.; and Hightower, J. Eds.), ACS Symposium Series 523, **1993**, 31.

(71). Ono, T.; Kamisuki, H.; Hisashi, H.; and Miyata, H. *J. Catal.* **1989**, 116, 303.

(72). Takita, Y., Nita, K., Machara, T., Yamazol, N., and Seiyama, T. J. Catal. **1977**, 50, 364.

(73). Buiten, J. *J. Catal.* **1969**, 13, 373.

(74). Buiten, J. *J. Catal.* **1972**, 27, 232.

(75). Takita, Y.; Ozaki, A.; and Moro-oka, Y. *J. Catal.* **1972**, 27, 185.

(76). Moro-oka, Y.; Takita, Y.; and Ozaki, A. *J. Catal.* **1972**, 27, 177.

(77). Oyama, S. T., Desikan, A. N., and Zhang, W. in "*Catalytic Selective Oxidation*", (Oyama, S. T.; and Hightower, J. W. Eds.), ACS Series 523, **1993**, 16.

Chapter 6

Ethanol Oxidation by Ozone over Supported Molybdenum Oxide

6.1. Introduction

In the literature, only few publications on oxidation of hydrocarbons using ozone can be found.[1-4] In a study of methane oxidation over magnesium oxide, lithium/magnesium oxide and alumina, Hutchings, *et al.*,[1,3] reported that ozone is a more active and more selective oxidant than oxygen at low temperatures (473 K - 573 K), while at high temperatures (> 773 K), no difference was found between the two oxidants. The kinetics of complete catalytic oxidation of benzene by ozone on MnO_2 was studied by Naydenov and Mehandjiev.[2] They found that the activation energy for benzene oxidation by ozone was much lower than that by oxygen (30 kJ/mol by ozone, 88 kJ/mol by oxygen), and the starting reaction temperature with ozone was significantly lowered than that with oxygen (283 K by ozone, 433 K by oxygen). Klimova, *et al.*,[4] investigated the oxidation of lower aliphatic alcohols by ozone over silica and γ-alumina. They found that ethanol oxidation produced acetaldehyde and carbon dioxide, n-propanol oxidation formed propionaldehyde, carbon dioxide and a trace amount of propinonic acid, and isopropanol oxidation yielded acetone. They demonstrated that aliphatic alcohol oxidation

by ozone proceeded mainly on the catalyst surface with experiments in which the reactor volume was changed while maintaining a constant surface area of catalysts.

In the chapter, we present a comparative study of ethanol oxidation in a mixture of ozone plus oxygen over MoO_3 supported on SiO_2, Al_2O_3, and TiO_2. This is the first reported study of alcohol oxidation over molybdenum catalysts.

6.2. Experimental

Catalyst preparation and characterization has been described in detail elsewhere.[5-7] The reactor system used for the steady-state reaction study was a conventional plug-flow reactor. Mass flow controllers (Brooks Model 5850E) were used to obtain the desired composition and flow rate of the feed stream. A liquid mixture of ethanol and water was injected through an injection port with a syringe pump (Sage Model 341B). The product analysis was performed by an on-line gas chromatograph (SRI Model 8610) equipped with FID and TCD detectors. All gases used in this study were of high purity and further purified before use. The standard partial pressures of reactants in this study were P_{C2H5OH} = 8 kPa, P_{O2} (or $P_{O3/O2}$) = 8 kPa, P_{H2O} = 4 kPa, and P_{He} = 81 kPa. The flow rate for all experiments was 110 μmol s^{-1} (160 cm^3 min^{-1}). Introduction of ozone was done by passing pure oxygen through an ozone generator (OREC Model V5-O) and then blending the O_3/O_2 stream with the reaction mixture. The ozone concentration was analyzed by an on-line ozone monitor (AFX, Model H1). The ozone concentration was ~ 1.5 mol% in the O_3/O_2 mixture and 0.12 mol% in the reaction feed stream. Rates were expressed as

turnover rates based on surface Mo atoms titrated by high temperature oxygen chemisorption.[5-7] Briefly, oxygen uptakes were measured by a pulse method on samples prereduced in hydrogen at moderate temperatures (600 - 640 K). The temperature of reduction was chosen to be just below the temperature at which bulk reaction occurred, and the method was independently calibrated by laser Raman spectroscopy at low loadings and x-ray diffraction at high loadings.

Study of ozone decomposition on 9% MoO_3/SiO_2, 15% MoO_3/Al_2O_3 and 9% MoO_3/TiO_2, and plain supports was carried out at 300 K with a flow rate of O_3/O_2 mixture at 670 $\mu mol\ s^{-1}$ (1000 $cm^3\ min^{-1}$). The ozone concentration in the mixture was ~ 1.5 mol%. The experiments were done by varying the weight of the catalysts and plain supports while keeping the loaded specific surface area (Sg) constant. Typically, 20-40 mg of the sample was used so as to achieve a reasonable zone conversion (0-52%).

6.3. Results and discussion

Table 6.1 and 6.2 summarize ethanol oxidation over supported molybdenum oxide by O_3/O_2 and O_2. The products resulting from ethanol oxidation by the two different oxidants are the same: acetaldehyde, diethyl ether, ethylene, trace amounts of acetic acid and acetic acetate, and CO_x at high temperatures. The data for oxidation with O_3/O_2 appear to split into two regions, a high temperature region which shows little difference from those for oxidation with O_2 and a low temperature region in which selectivity to

Table 6.1. Ethanol oxidation over supported MoO_3 using O_3/O_2.

Sample	Temp. / K	Selectivity / %						Conv. / %	v_t * / 10^{-1} s^{-1}
		C_2H_4	CH_3CHO	$(C_2H_5)_2O$	CH_3COOH	$CH_3COOC_2H_5$	CO_x		
	398	-	79	15	6	-	-	3.4	2.4
	423	-	82	13	5	-	-	4.0	2.9
	448	-	90	4	6	-	-	4.5	3.2
	473	-	84	9	5	2	-	4.9	3.6
9% MoO_3/SiO_2	498	-	85	10	4	1	-	6.2	4.4
	523	2	70	22	3	3	-	11.0	7.9
	548	6	68	21	3	2	-	21.0	15.0
	558	8	72	14	3	3	-	29.5	21.2
	573	9	74	11	3	3	-	40.0	28.7
	373	-	100	-	-	-	-	1.0	0.1
	398	-	97	3	-	-	-	2.2	0.2
	423	-	87	6	6	1	-	4.0	0.4
15% MoO_3/Al_2O_3	438	-	87	8	3	2	-	6.8	0.6
	448	-	83	13	3	1	-	10.0	0.9
	458	-	79	14	4	3	-	19.0	1.8
	473	1	84	11	2	2	-	31.4	2.9
	498	5	82	5	-	2	6	60.2	5.6
	398	-	62	29	9	-	-	3.2	0.5
	408	-	57	38	5	-	-	3.3	0.5
9% MoO_3/TiO_2	423	1	60	36	3	-	-	7.3	1.2
	438	1	61	36	2	-	-	14.0	2.4
	443	2	63	33	2	-	-	15.4	2.6
	448	8	56	9	2	-	25	70.0	11.8

* v_t is turnover rate.

Table 6.2. Etahnol oxidation over supported MoO_3 using O_2.

Sample	Temp. / K	Selectivity / %						Conv. / %	v_i / 10^{-3} s^{-1}
		C_2H_4	CH_3CHO	$(C_2H_5)_2O$	CH_3COOH	$CH_3COOC_2H_5$	CO_x		
	478	3	63	23	11	-	-	1.1	0.8
	490	2	69	7	27	-	-	4.7	3.4
9% MoO_3/SiO_2	506	1	72	11	8	-	-	7.5	5.5
	533	2	77	10	3	6	-	20.7	15.0
	563	4	72	7	4	10	13	42.7	31.0
	408	-	71	-	29	-	-	0.7	0.1
	423	2	77	7	14	-	-	3.1	0.3
15% MoO_3/Al_2O_3	438	2	90	6	2	-	-	9.9	1.0
	453	3	82	10	3	2	-	17.7	1.7
	473	1	84	10	1	2	2	43.0	4.1
	398	-	50	35	15	-	-	2.8	0.5
	413	-	63	32	5	-	-	10.9	1.8
9% MoO_3/TiO_2	433	3	60	28	3	-	6	35.8	6.2
	448	12	48	8	3	-	29	81.4	14.0

acetaldehyde is improved to different degrees on all samples compared to ethanol oxidation with O_2. The transition temperatures are 523 K on 9% MoO_3/SiO_2, 448 K on 15% MoO_3/Al_2O_3 and 443 K on 9% MoO_3/TiO_2. The improvement in selectivity to acetaldehyde is large on 9% MoO_3/SiO_2, and small on 15% MoO_3/Al_2O_3 and 9% MoO_3/TiO_2, although there is considerable scatter in the latter two data sets. The results are in general agreement with the findings by Hutchings, *et al.*,[1,3] in which ozone was found to be a more selective oxidant than oxygen for methane oxidation over magnesium oxide and alumina. As will be shown, the variation of selectivity to acetaldehyde on the present samples is probably due to the different ozone decomposition activity of the different catalysts.

Blank ozone decomposition experiments with the supported catalysts and the bare supports at 300 K were carried out by varying the weight of the supports while keeping the surface area constant. Among the supported catalysts, 9% MoO_3/SiO_2 is inactive for ozone decomposition, but 15% MoO_3/Al_2O_3 and 9% MoO_3/TiO_2 are equally active: ozone conversion is 0% on 9% MoO_3/SiO_2, 9% on 15% MoO_3/Al_2O_3, and 6% on 9% MoO_3/TiO_2. The order in reactivity for ozone decomposition follows the order 15% MoO_3/Al_2O_3 (9%) $\geq$ 9% MoO_3/TiO_2 (6%) > 9% MoO_3/SiO_2 (0%). On the plain supports, the order is found to be TiO_2 (52%) > Al_2O_3 (25%) > SiO_2 (0.2%). Preliminary work in our laboratory[8] showed that molybdenum oxide alone is relatively inert for ozone decomposition. Thus, the difference in ozone decomposition activity between the

supported catalysts and the plain supports can be attributed to generation of inactive surface compounds of molybdenum oxide.

Figure 6.1 presents Arrhenius plots of turnover rates for ethanol oxidation by O_3/O_2 and O_2 on 9% MoO_3/SiO_2. The data for oxidation with ozone (indicated by (□)) are seem to divide into two regions, a high temperature region with high activation energy and a low temperature region with low activation energy. In the low temperature region (<523 K), the activation energy for the reaction by O_3/O_2 is lower than that by O_2 (10 kJ/mol by O_3/O_2 and 92 kJ/mol by O_2). The rate of ethanol oxidation in this region is slightly smaller than the rate of ozone consumption indicated by the circle (O) and the dashed line, but has the same activation energy. The rate of the reaction with O_3/O_2 goes through a transition temperature (523 K) and then becomes equivalent, within experimental error, to the rate of the reaction with O_2 (Δ). No ozone can be detected above this temperature. It is well known in the literature that ozone is thermally decomposed above 523 K.[9] Thus, the change on the rates by O_3/O_2 above 523 K is due to the thermal decomposition of ozone. As is verified in the present study, 9% MoO_3/SiO_2 is inactive for ozone decomposition. These results, together with the findings that the activation energy of ethanol oxidation is close to that of ozone reacted (~ 10 kJ/mol) below 523 K, suggest that ethanol mainly reacts with ozone in this temperature range. The slight higher rate of ozone reacted than ethanol oxidation rate below 523 K probably suggests that a minor amount of ozone decomposition occurs on 9% MoO_3/SiO_2.

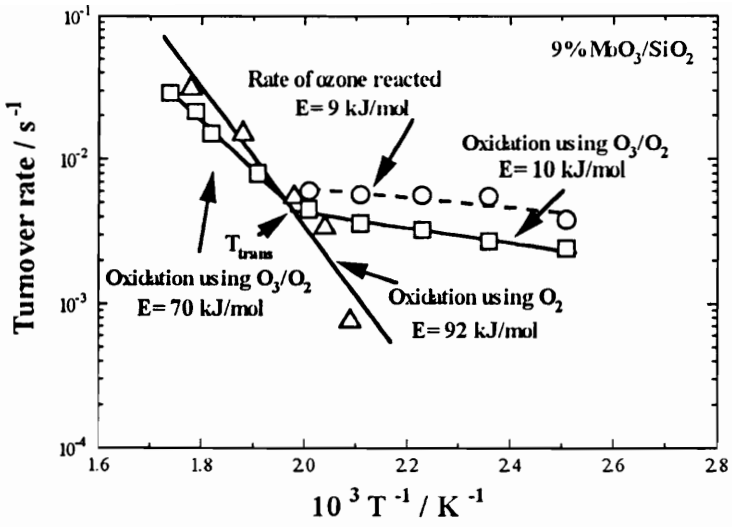

Figure 6.1. Arrhenius plots of ethanol oxidation by O_3/O_2 and O_2 over 9% MoO_3/SiO_2.

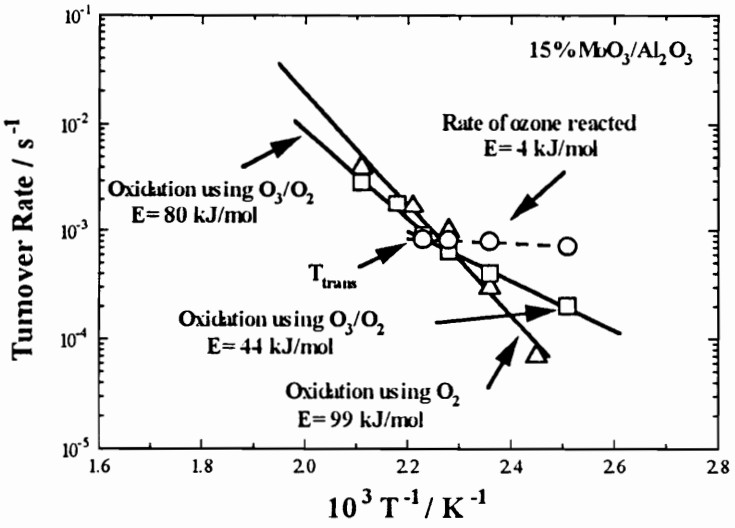

Figure 6.2. Arrhenius plots of ethanol oxidation by O_3/O_2 and O_2 over 15% MoO_3/Al_2O_3.

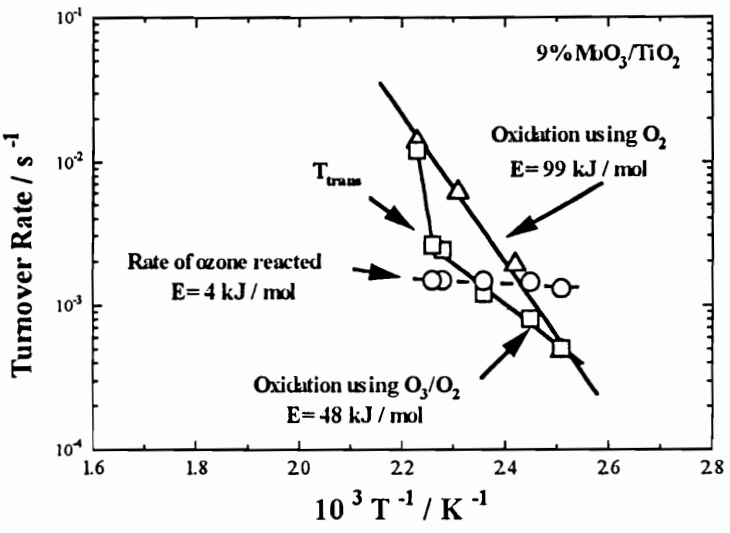

Figure 6.3. Arrhenius plots of ethanol oxidation by O_3/O_2 and O_2 over 9% MoO_3/TiO_2.

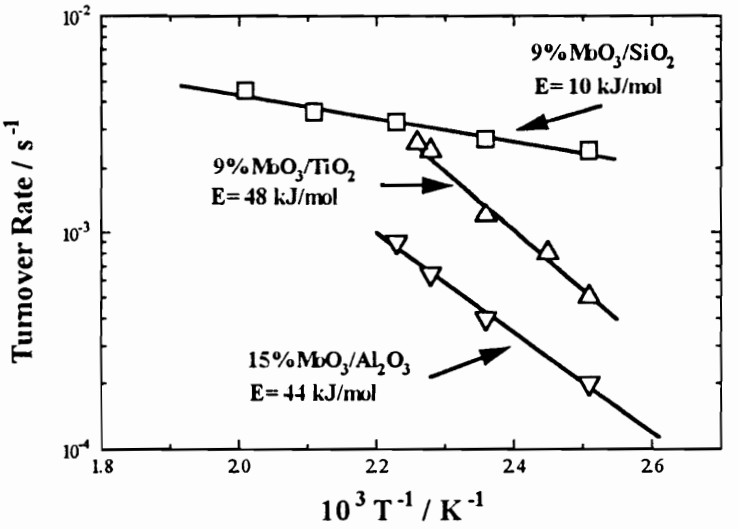

Figure 6.4. Arrhenius plots of ethanol oxidation by O_3/O_2 below the transition temperature.

Effects of reactor volume on reactivity for ethanol oxidation with O_3/O_2 on 9% MoO_3/SiO_2 was studied by varying the reactor volume while keeping the surface area of the catalyst constant at 423 and 448 K. The results shows that turnover rate and selectivities do not change with reactor volume. This strongly suggests that ethanol oxidation by ozone occurs on the catalyst surface. This finding is consistent with the work by Klimova, *et al.*,[4] in which aliphatic alcohol oxidation by ozone proceeded mainly on the surfaces of SiO_2 and Al_2O_3.

Figures 6.2 and 6.3 show similar Arrhenius plots of ethanol oxidation by O_3/O_2 and O_2 on 15% MoO_3/Al_2O_3 and 9% MoO_3/TiO_2. Similar to ethanol oxidation by O_3/O_2 on 9% MoO_3/SiO_2, a transition temperature is observed for ethanol oxidation by O_3/O_2 on the two catalysts. It is 448 K on 15% MoO_3/Al_2O_3 and 443 K on 9% MoO_3/TiO_2 corresponding total ozone decomposition. The activation energies of the reaction by O_3/O_2 below the transition point are lower than those by O_2 (44 kJ/mol by O_3/O_2 and 99 kJ/mol by O_2 on 15% MoO_3/Al_2O_3, 48 kJ/mol by O_3/O_2 and 99 kJ/mol by O_2 on 9% MoO_3/TiO_2), but the effect appears to be small in comparison to that on 9% MoO_3/SiO_2. After temperature is increased above the transition point, the rates of ethanol oxidation by O_3/O_2 tend to come back to the rates of the reaction by O_2, and ozone concentration is undetectable. These findings, together with the high ozone decomposition activity of 15% MoO_3/Al_2O_3 and 9% MoO_3/TiO_2, suggest that ozone decomposition compete with ethanol oxidation with O_2 and O_3 on the two catalysts. Thus, the difference in the effect

of ozone on ethanol oxidation below the transition temperature on the three catalysts can be attributed to the different ozone decomposition activity of the supports.

Figure 6.4 presents Arrhenius plots of ethanol oxidation by O_3/O_2 below the transition temperature on 9% MoO_3/SiO_2, 15% MoO_3/Al_2O_3 and 9% MoO_3/TiO_2. The reactivity follows the order $SiO_2 > TiO_2 > Al_2O_3$. This is the reverse of the order obtained for ozone decomposition and suggests that decomposition competes with selective oxidation.

6.4. References:

(1). Hutchings, G. J.; Scurrell, M. S.; and Woodhouse, J. R. *Appl. Catal. A*, **1988**, 38, 157.

(2). Naydenov, A; and Mehandjiev, D. *Appl. Catal. A*, **1993**, 97, 17.

(3). Hutchings, G. J.; Scurrell, M. S.; and Woodhouse, J. R. in"*Methane Conversion*" (D. M. Bibby, C. D. Chang, R. F. Howe and S. Yurchak eds.), pp. 415, **1988**.

(4). Klimova, M. N.; Tarunin, B. L.; and Aleksandrov, Y. A. *Kinet. Katal.*, **1988**, 26, 1143.

(5). Desikan, A. N.; Huang, L.; and Oyama, S. T. *J. Phys. Chem.*, **1991**, 95, 10050.

(6). Desikan, A. N.; Huang, L.; and Oyama, S. T. *J. Chem. Soc., Faraday Trans. I*, **1992**, 88, 3357.

(7). Zhang, W.; Desikan, A. N.; and Oyama, S. T. accepted by *J. Phys. Chem.*

(8). Dhandapani, B.; and Oyama, S. T. accepted by *Chem. Letters*.

(9). Cotton, F. A.; and Wilkinson, G. "*Advanced Inorganic Chemistry*", Wiley, New York, **1988**.

Chapter 7

Concluding remarks

This dissertation presents an in-depth study of the mechanism of ethanol oxidation over supported molybdenum oxide using *in situ* Raman spectroscopy. The findings that ethoxide species are the reactive intermediates, and that they are associated with certain functional groups of molybdenum oxide is unique. Furthermore, the observation of true intermediates and relatively inert surface spectators is unprecedented.

Study of true reaction intermediates by means of spectroscopies under *in situ* reaction conditions is one of the most challenging fields in catalytic science. A major problem is that adsorbed species observed during reactions, even if they can be detected, are not guaranteed to be real reactive intermediates. In many cases, the observed adsorbed species are only unreactive spectators, for example, formate ions in the decomposition of formic acid on alumina,[1] or long-chain alkyl groups on the surface of Ru[2,3] or Ni[4] in the course of CO hydrogenation.

To identify true reactive intermediates, dynamic measurements using spectroscopies under reaction conditions are necessary.[5] In the literature, in only a few cases have the adsorbed species been identified to be true reactive intermediates, for example, N atoms formed in the course of low-pressure decomposition of NH_3 on

tungsten[6] and molybdenum[7] as studied by Auger electron spectroscopy, NH_4^+ species in the NH_3 and NO reaction on vanadia-titania catalysts as measured by Fourier transform infrared spectroscopy,[8,9] N atoms in the CO and NO reaction on rhodium as detected by surface-enhanced Raman spectroscopy (SERS),[10] and CO in CO oxidation on platinum as observed by photoemission electron microscopy.[11,12] This dissertation is the first study in which both a spectator and an actual reaction intermediate are simultaneously observed.

Effects of support on reactivity of ethanol oxidation over molybdenum oxide was attributed to the Mo=O bond strength as measured by infrared and laser Raman spectroscopy.[13] However, the studies in this dissertation and by others[14] on methanol oxidation show that the reactivity dependence on support cannot be simply related to the Mo=O bond strength. In Chapter 2, based on reactivity, isotopic substitution, kinetics, and *in situ* laser Raman measurements, the density of the empty electronic states in an activated molybdate-support complex is suggested to be responsible for the dependency. This hypothesis is subject to confirmation in future studies by both theoretical calculations and spectroscopic measurements.

Only one study[15] dealing with the kinetics of ethanol oxidation over SiO_2-supported molybdenum oxide was found in the literature. Iwasawa, *et al.*, showed in this paper that a rate-expression derived from a two-step redox mechanism was consistent with the experimental results (see Chapter 3). However, this rate expression does not give a good description for the rates in the present case, because this mechanism omitted the effect of water inhibition, and because only one type of surface site (terminal Mo=O bond)

was involved. The sequence of steps for ethanol oxidation over SiO_2-supported molybdenum oxide are well established by isotopic substitution and kinetic measurements in this dissertation. It consists of two stages: ethanol adsorption through an equilibrated step to form ethoxide intermediates, and either of two rate-determining steps, α-hydrogen elimination to produce acetaldehyde and β-hydrogen elimination to produce ethylene. Based on the finding of a non-uniform surface by *in situ* laser Raman spectroscopy, a rigorous analysis employing Temkin's theory of rates on non-uniform surfaces was carried out. A resulting theoretical rate expression for acetaldehyde formation is in good agreement with the experimentally found power rate law expression (see Chapter 4). The sequence of steps used in this derivation is consistent with the results of the isotopic substitution measurements. The key assumption in this derivation is that there are two types of sites, a Temkin site and a uniform Langmuir site. An example of such a situation has been presented for the case of the hydroisomerization of pentane over supported platinum, but was not solved rigorously.[16]

Even though it is believed, based on the results of the *in situ* laser Raman measurements and kinetic analysis, that a fully oxidized Mo center is necessary for the reaction, direct spectroscopic observation of the oxidation state of molybdenum oxide under reaction conditions is still needed in order to draw a complete picture of the catalytic cycle of the reaction. Laser Raman spectroscopy is not an appropriate technique for this because it is not sensitive to the lower oxidation states of molybdenum oxide. Near edge x-ray absorption spectroscopy combined with a complimentary reaction

chamber is likely the best approach to this problem. The present study does not provide the means of identification of the origin of the oxygen atom in the acetaldehyde molecule. This is another area open to future study. O^{18} isotope substitution in the lattice oxygen atom position may be the best way to resolve the problem.

References:

(1). Noto, Y., Fukuda, K.; Onoshi, T.; and Tamaru, K. *J. Chem. Soc. Faraday Trans. I* **1967**, 77, 2913.

(2). Ekerdt, J. G.; and Bell, A. T. *J. Catal.* **1978**, 48, 111.

(3). Yamasaki, H.; Kobori, Y.; Naito, S.; Onishi, T.; and Tamaru, *J. Chem. Soc. Faraday Trans. I* **1981**, 77, 2913.

(4). Galuszka, J.; Chang, J. R.; and Amenomiya, *Proc. 7th Int. Cong. Catal.*, Seiyama, T. and Tanabe, K. Eds., Part A, p. 529, Kodansha, Tokyo, **1981**.

(5). Tamaru, K. "*Dynamic Heterogeneous Catalysis*", Academic Press, London, **1978**.

(6). Shindo, H.; Egawa, C.; Onishi, T.; and Tamaru, C. *J. Chem. Soc. Faraday Trans. I* **1980**, 76, 280.

(7). Boudart, M.; Egawa, C.; Oyama, S. T.; and Tamaru, K. *J. Chim. Phys.* **1981**, 78, 987.

(8). Takagi, M.; Kawai, T.; Soma, M.; Onishi, T.; and Tamaru, K. *J. Catal.* **1977**, 50, 441.

(9). Topsoe, N.-Y. *Science* **1994**, 265, 1217.

(10). Tolia, A. A.; Williams, C. T.; Takoudis, C. G.; and Weaver, M. J. *J. Phys. Chem.* **1995**, 99, 4599.

(11). Ertl, G. *Science* **1991**, 254, 1750.

(12). Graham, M. D.; Kevrekidis, I. G.; Asakura, K.; Lauterbach, J.; Krischer, K.;

Rotermund, H.-H.; and Ertl, G. *Science* **1994**, 264, 80.

(13). Ono, T, Nakagawa, Y.; Miyata, H.; and Kubokawa, Y. *Bull. Chem. Sco. Jpn.*, **1984**, 57, 1205.

(14). Deo, G.; and Wachs, I. E. *J. Catal.* **1994**, 146, 335-345. Hu, H.; and Wachs, I. E. *J. Phys. Chem.* **1995**, 99, 10911-10922.

(15). Iwasawa, Y.; Nakano, Y.; and Ogasawara, S. *J. Chem. Soc. Faraday Trans. I* **1978**, 74, 2968.

(16). Boudart, M.; and Djéga-Mariadassou, G. "*Kinetics of Heterogeneous Catalytic Reactions*", Princeton University Press, Princeton, New Jersey, **1984**. p.115.